Dissertation

Submitted to the

Combined Faculty of Natural Sciences and Mathematics

of the Ruperto Carola University Heidelberg, Germany

for the degree of

Doctor of Natural Sciences

Presented by

Elham Fakhr, M.Sc.

Born in Tehran, Iran

Oral examination:

01.03.2022

# Identification and characterization of T cell receptors reactive to the $E7_{(11\text{-}19)}$ epitope of HPV-16

**Referees:**

Prof.Dr. Michael Platten
Prof.Dr. Andreas Trumpp

*In memory of my beloved father, Alireza….*

# I. Acknowledgements

This dissertation was accomplished with the contribution of many wonderful people in the period of October 2017 to October 2021 in the "Targeted tumor vaccines Group" headed by Dr. Angel Cid Arregui at the German Cancer Research Center (Deutsches Krebsforschungszentrum (DKFZ)), Heidelberg.

First of all, I am grateful to the German Academic Exchange Service (DAAD) for providing me with a scholarship grant to develop my PhD work, which would not have been possible without the support and excellent guidance of Dr. Angel Cid Arregui, who gave me the opportunity to work in this fascinating topic in his lab. The door to his office was always open (literally) and I am very thankful for our innumerable and fruitful scientific discussions that guided me throughout the project.

I am highly grateful for the valuable scientific advice of Prof. Dr. Michael Platten, Prof. Dr. Andreas Trumpp and Prof. Dr. Frederik Marmé during my thesis advisory committee (TAC) meetings. I am thankful to Prof. Dr. Ralf Bartenschlager for accepting to be the chair of examination commission and also Prof. Dr. Nina Papavasiliou for agreeing to be the member of PhD defense committee.

Furthermore, I would like to thank Isaac Quirós Fernández who kindly collaborated in this project and helped me with the indirect immunofluorescence microscopy and affinity measurements. I really appreciate his scientific endeavors and learned a lot from our scientific discussions. I am also very thankful to Dr. Mansour Poorebrahim and Sofia Libório Passos Ramos who contributed in the *in silico* analysis and I admire their wonderful team work spirit. I would also like to thank Jasmin Rebholz for her constant technical assistance during the last year of my PhD work. A special thanks to Dr. Matthias Bozza who kindly advised me in the cell electroporation and generously provided me with cells.

My greatest thank to my dear husband Amin who constantly motivated me during my PhD, and whose unconditional love and support have paved the path for me. Finally, I am highly grateful to my dear and lovely mother, Parvin, who encouraged me to start this wonderful journey and taught me how to be encouraged and prepared to new adventures in life. All of this was not possible without her love and unconditional support.

# II. Summary

High-risk human Papilloma viruses (HR-HPVs) are the main causative agents of cervical, anal, vulvar, vaginal and penile cancer as well as head and neck cancer. The most prevalent HR-HPV types are HPV16 and HPV18. HPV16 is responsible for about 50% of HPV-related cancers and thus it is a preferred type to study. The HPV16 E7 $_{(11-19)}$ peptide is a well-characterized epitope presented by HLA-A*02:01 molecules on HPV16+ tumor cells. Therefore, it represents a tumor-specific antigen and is an ideal target for Adoptive T cell therapy (ATC) due to its viral source and being absent in healthy tissues. Recently, a proof-of-concept study in metastatic cervical cancer patients has shown that administration of HPV16-specific tumor infiltrating lymphocytes (TILs) expanded *ex vivo* and infused back to the patient induced tumor regression. However, selection and expansion of TILs has some important disadvantages compared to genetically modified T cells.

This project was aimed at identifying HPV16 E7-specific TCRs that could be applied as an effective immunotherapy to cancers caused by this virus. We believe that tumor samples from patients at developing stages of HPV+ cancers might not be optimal for finding HPV-specific TCRs, since their TILs react weakly against the E6/E7 oncoproteins. Furthermore, HPV16-specific cytotoxic T cells can be frequently found in peripheral blood of healthy donors. Therefore, *in vitro* stimulation of $CD8^+$ T cells derived from healthy individuals and subsequent identification of their TCR repertoire could be a better way to obtain efficient TCR candidates for adoptive T cell therapy of HPV16+ cancers.

For an efficient *in vitro* stimulation of T cells, we used a previously constructed and purified recombinant fusion protein composed of an N-terminal fragment of E7 (amino acids 1-30, $E7_{1-30}$) linked to the N terminus of Flt3L. Immature dendritic cells isolated from PBMCs of healthy donors were pre-incubated with the fusion protein and then co-cultured with autologous T cells. E7-reactive CD8+ T cells (IFN- $\gamma^+$, $CD137^+$ and HLA-A2-$E7_{11-19}$-$Tetramer^+$) were isolated. The exact TCR profile of the E7-reactive T cells was determined by single-cell V(D)J sequencing using the 10X Genomics platform. Our results showed that the E7-Flt3L is a functional protein that can efficiently increase the frequency of $CD8^+$ T cells targeting the HLA-A*02:01-restricted

HPV16 $E7_{(11-19)}$ epitope among peripheral lymphocytes of healthy donors. Moreover, our workflow combined tetramer binding and activation of T cells to improve the selection of truly reactive T cells. Three TCR candidates were screened *in vitro*, which showed different patterns of specificity, avidity, and reactivity. Further, we were able to identify several $E7_{(11-19)}$-reactive motifs in the CDR3β region through *in silico* characterization of 22 selected TCRs. Importantly, most of these motifs were enriched in patients who cleared HPV16 infection compared to patients with cervical intraepithelial neoplasia grade 3 (CIN3) or higher. Taken together, our study has established an efficient workflow for the identification of TCRs targeting tumor viral antigens which can be an important step toward TCR discovery.

# III. Zusammensfassung

Humane Papillomaviren mit hohem Risiko (HR-HPVs) sind die Hauptverursacher von Gebärmutterhals-, Anal-, Vulva-, Vaginal- und Peniskrebs sowie von Kopf- und Halskrebs. Die am weitesten verbreiteten HR-HPV-Typen sind HPV16 und HPV18. HPV16 ist für etwa 50 % der HPV-bedingten Krebserkrankungen verantwortlich und wird daher bevorzugt untersucht. Das HPV16 E7 (11-19)-Peptid ist ein gut charakterisiertes Epitop, das von HLA-A*02:01-Molekülen auf HPV16+-Tumorzellen präsentiert wird. Daher stellt es ein tumorspezifisches Antigen dar und ist aufgrund seiner viralen Quelle und seiner Abwesenheit in gesundem Gewebe ein ideales Ziel für die adoptive T-Zelltherapie (ATC). Kürzlich hat eine Machbarkeitsstudie bei Patienten mit metastasiertem Zervixkarzinom gezeigt, im Rahmen welcher die Verabreichung von HPV16-spezifischen tumorinfiltrierenden Lymphozyten (TILs) *ex vivo* expandiert wurde und dem Patienten zurück infundiert wurde, was eine Tumorregression induzierte. Die Selektion und Expansion von TILs hat jedoch einige wichtige Nachteile gegenüber gentechnisch veränderten T-Zellen. Ziel dieses Projekts war es, HPV16-E7-spezifische TCRs zu identifizieren, die als wirksame Immuntherapie gegen durch dieses Virus verursachte Krebserkrankungen eingesetzt werden könnten. Wir nehmen an, dass Tumorproben von Patienten in sich entwickelnden Stadien von HPV + -Krebsen möglicherweise nicht optimal sind, um HPV-spezifische TCRs zu finden, da ihre TILs schwach gegen die E6 / E7-Onkoproteine reagieren. Darüber hinaus finden sich im peripheren Blut gesunder Spender häufig HPV16-spezifische zytotoxische T-Zellen. Daher könnte die *in vitro*-Stimulation von CD8 + -T-Zellen, die von gesunden Individuen stammen, und die anschließende Identifizierung ihres TCR-Repertoires ein besserer Weg sein, um effiziente TCR-Kandidaten für die adoptive T-Zelltherapie von HPV16 + -Krebsen zu erhalten.

Für eine effiziente *in vitro*-Stimulation von T-Zellen haben wir ein zuvor konstruiertes und gereinigtes rekombinantes Fusionsprotein verwendet, das aus einem N-terminalen Fragment von E7 (Aminosäuren 1-30, E71-30) besteht, das mit dem N-Terminus von Flt3L fusioniert ist. Unreife dendritische Zellen, die aus PBMCs gesunder Spender isoliert wurden, wurden mit dem Fusionsprotein vorinkubiert und dann mit autologen T-Zellen co-kultiviert. E7-reaktive CD8+ T-Zellen (IFN-γ+, CD137+ und HLA-A2-E711-19-Tetramer+) wurden isoliert. Das genaue TCR-Profil

der E7-reaktiven T-Zellen wurde durch Einzelzell-V(D)J-Sequenzierung unter Verwendung der 10X Genomics-Plattform bestimmt. Unsere Ergebnisse zeigten, dass E7-Flt3L ein funktionelles Protein ist, das effizient die Häufigkeit von solchen CD8+ T-Zellen erhöhen kann, die auf das HLA-A*02:01-restringierte HPV16 E7(11-19)-Epitop unter peripheren Lymphozyten gesunder Spender abzielen. Darüber hinaus kombinierte unser Arbeitsablauf die Tetramerbindung und die Aktivierung von T-Zellen, um die Selektion wirklich reaktiver T-Zellen zu verbessern. Drei TCR-Kandidaten wurden *in vitro* gescreent, die unterschiedliche Muster von Spezifität, Avidität und Reaktivität zeigten. Darüber hinaus konnten wir mehrere E7(11-19)-reaktive Motive in der CDR3β-Region durch *in silico*-Charakterisierung von 22 ausgewählten TCRs identifizieren. Wichtig ist, dass die meisten dieser Motive bei Patienten mit abgeheilter HPV16-Infektion im Vergleich zu Patienten mit zervikaler intraepithelialer Neoplasie Grad 3 (CIN3) oder höher angereichert waren. Zusammenfassend hat unsere Studie einen effizienten Workflow für die Identifizierung von TCRs etabliert, die auf tumorvirale Antigene abzielen, was ein wichtiger Schritt in Richtung TCR-Entwicklung sein kann.

# IV. Table of contents

# V. List of Figures

# VI. List of Tables

# VII. Abbreviations

| | |
|---|---|
| **ABTS** | 2,2'-Azino-bis (3-ethylbenzothiazoline-6-sulfonic acid) diammonium salt |
| **APCs** | Antigen presenting cells |
| **ATC** | Adoptive T cell therapy |
| **BAM** | Biomolecular anchor molecule |
| **BCR** | B- cell antigen receptor |
| **BSA** | Bovine serum albumin |
| **C** | constant |
| **CAR** | Chimeric antigen receptor |
| **CCR7** | CC chemokine receptor 7 |
| **CDR** | Complementary determining region |
| **CFSE** | Carboxyfluorescein |
| **CIAP** | Calf Intestinal Alkaline Phosphatase |
| **CIN** | High grade cervical intraepithelial |
| **CRISPR/Cas9** | Clustered regularly interspaced short palindromic repeats /Cas9 protein |
| **CTLA-4** | Cytotoxic T-lymphocyte-associated protein 4 |
| **CTLs** | Cytotoxic T cells |
| **CXCR5** | C-X-C motif receptor-5 |
| **D** | Diversity |
| **DCs** | Dendritic cells |
| **DI** | Deionized |
| **DMEM** | Dulbecco's Modified Eagle Medium |
| **DMSO** | Dimethyl sulfoxide |
| **DN** | Double negative |
| **DP** | Double positive |
| **D-PBS** | Dulbecco's phosphate-buffered saline |
| **E** | Early |
| **EDTA** | Ethylenediamine tetra acetic acid |
| **EGF** | Epidermal growth factor |
| **EMA** | European Medicines Agency |
| **ER** | Endoplasmic reticulum |
| **ETP** | Early thymic progenitor |
| **FBS** | Fetal Bovine Serum |
| **FDA** | Food and drug administration |
| **Flt3L** | Tyrosine kinase-3 ligand |
| **GAG** | Glycosaminoglycan |
| **GRAVY** | Grand Average of Hydropathy |
| **H** | Histidine |
| **H2O2** | Hydrogen peroxide |
| **HCl** | Hydrogen chloride |
| **HEVs** | High endothelial venules |

| | |
|---|---|
| **hFlt3** | Human Flt3 |
| **HNSCC** | Head and neck squamous cell carcinoma |
| **HPV** | Human papilloma viruses |
| **HPVST** | HPV-specific T cells |
| **HR** | high-risk |
| **HSIL** | High-grade squamous intraepithelial neoplasia |
| **HSPG** | Heparan sulfate proteoglycan |
| **ICAM-1** | Intracellular adhesion molecule 1 |
| **ICOS** | Inducible costimulatory |
| **IFN** | Interferon |
| **Ig** | Immunoglobulin |
| **IKKε** | IκB kinase ε |
| **IL** | Interleukin |
| **imDCs** | Immature DCs |
| **IRF** | Interferon regulatory factor |
| **ITAMs** | Immunoreceptor-based tyrosine activation motifs |
| **iTreg** | Induced Treg |
| **J** | Joining |
| **KCl** | Potassium chloride |
| **KH2PO4** | Monopotassium phosphate |
| **L** | Late |
| **LCR** | Long control region |
| **LFA** | Leukocyte function antigen |
| **LM** | Listeria monocytogenes |
| **LPS** | Lipopolysaccharides |
| **LR** | Low-risk |
| **LVs** | Lentiviral vectors |
| **MAP** | Mitogen-activated protein |
| **mc** | Murine constant |
| **mcTCR-β** | Murine constant TCR β |
| **mDCs** | Mature DCs |
| **MDSC** | Myeloid derived suppressor cells |
| **Met** | Methionine |
| **MFI** | median fluoresce intensity |
| **MgCl2** | Magnesium chloride |
| **MgSO4** | Magnesium sulfate |
| **MHC** | Major histocompatibility complex |
| **MIP-3alpha** | Macrophage inflammatory protein 3alpha |
| **MOI** | Multiplicity of infection |
| **MPLA** | Monophosphoryl lipid A |
| **MVA** | Modified vaccinia virus Ankara |
| **NaCl** | Sodium chloride |
| **NaN3** | Sodium azide |
| **nTreg** | Natural Treg |
| **P/S** | Penicillin/Streptomycin |
| **PAMPs** | Pathogen-associated molecular pattern molecules |
| **PBMC** | Peripheral blood mononuclear cell |
| **PD-L1** | Programmed death-1 ligand |
| **PFA** | Paraformaldehyde |

| | |
|---|---|
| **PGE2** | Prostaglandin E2 |
| **Phe** | Phenylalanine |
| **PMA** | phorbol 12-myristate 13-acetate |
| **pMHC** | peptide: MHC |
| **POM-1** | Polyoxotungstate 1 |
| **PPRs** | Pattern recognition receptors |
| **PVs** | Papilloma viruses |
| **R** | Arginine |
| **Rag1** | Recombinase activating gene 1 |
| **rhGM-CSF** | Recombinant human Macrophage Colony-Stimulating Factor |
| **SCCO** | Squamous cell carcinomas of the oropharynx |
| **scfv** | single-chain fragment variable |
| **Ser** | Serine |
| **SLP** | Synthetic long peptides |
| **SP** | Single positive |
| **TAA** | Tumor-associated antigens |
| **TALEN** | transcription activator-like effector nuclease |
| **TAM** | Tumor associated macrophages |
| **TAN** | Tumor-associated neutrophils |
| **TAP** | Transporter associated with antigen processing |
| **TBK1** | TANK-binding kinase 1 |
| **TCM** | Central memory T cells |
| **TCR** | T cell receptor |
| **$T_{EM}$** | Effector memory T cells |
| **$T_{FH}$** | T follicular helper cells |
| **TFs** | Transcription factors |
| **TGF β** | Transforming growth factorβ |
| **Th1** | T helper 1 |
| **Thr** | Threonine |
| **TILs** | Tumor infiltrating lymphocytes |
| **TLRs** | Toll-like receptors |
| **TNF** | Tumor necrosis factor |
| **TRAV** | T cell receptor alpha variable |
| **TRBV** | T cell receptor beta variable |
| **Treg** | Regulatory T cells |
| **Tyr** | Tyrosine |
| **UMI** | Unique molecular identifier |
| **Un-Jurkat** | Untransduced Jurkat |
| **V** | Variable |
| **VLPs** | Virus-like particles |
| **ZFNs** | Zinc finger nucleases |

# 1. Introduction

## 1.1 The immune system

The immune system is a complex network of molecules and cells that protect the body from viruses, bacteria, fungi and parasites which can potentially cause disease and malignancies. The immune system has two subsystems: Innate and adaptive immune system. Innate immunity is the first line of defense and comprises physical/chemical barriers, humoral innate immunity and cell-mediated innate immunity. Cells of the innate immune system identify pathogen-associated molecular pattern molecules (PAMPs) via pattern recognition receptors (PPRs). This recognition, which is considered to be non-specific, activates phagocytosis, inflammation, cytokine production and recruitment of other immune cells (1, 2). Importantly, innate immune system is essential for the activation and regulation of adaptive immune responses (3). Adaptive immunity is highly tuned and has evolved to provide a broad range of recognition for self- and non-self- antigens. This immunity is tightly regulated by interaction between antigen presenting cells (APCs), B and T lymphocytes and it leads to a slower but highly specific long-term immunological memory (4). Upon first encounter with a pathogen, memory T and B cells are established which can be quickly activated in the subsequent infections. Both Innate and adaptive immunity include a network of biological processes that protect an organism from potential pathogens.

### 1.1.1 Adaptive Immune system

Adaptive immune response is divided into humoral and cell mediated immunity and highly dependent on APCs. Professional APCs include dendritic cells (DCs), Langerhans cells, macrophages and B cells. B cells recognize and uptake soluble antigens through B- cell antigen receptor (BCR), which are membrane bound Immunoglobulin (Ig), and play a central role in humoral immunity (4). Upon recognition of an antigen, the B cell undergoes clonal expansion and produces effector and memory cells. These effector cells are known as plasmablast and can further differentiate into plasma cells. Plasmablast are short-lived and proliferating cells which produce low affinity antibodies in the early phase of infection. Plasma cells, arose from plasmablasts, are long-lived and non-proliferating cells which secrete high affinity antibodies due to affinity maturation (5). Memory B cells circulate in the blood in a quiescent state and in case of reinfection with the same pathogen, they are activated and form long-lived plasma cells (6).

On the other hand, T lymphocytes are key players of cellular immune response and identify the fragments of antigens, so called epitopes, presented by major histocompatibility complex (MHC) class I/II on the surface of APCs via their T cell receptor (TCR). Following antigen recognition, like B cells, T cells proliferate clonally and further differentiate into effector and memory cells, which provide long-term immunity. Based on the expression of glycoproteins on their surface, T cells are classified into $CD4^+$ and $CD8^+$ T cells (7). $CD4^+$ T cells have mainly a helper role in adaptive immunity, whereas the majority of $CD8^+$ T cells become cytotoxic T cells (CTLs)(8). Lymphocytes and APCs are orchestra leaders of adaptive immune system which provides an efficient and long-lasting immunity against pathogens.

### 1.1.2 Dendritic cells: central regulators of adaptive immune response

APCs are indispensable component of cell-mediated immunity. Among professional APCs, DCs play an important role in effective immune responses (9). This specialized APCs were first discovered in 1970s and they are mainly in the blood, epithelia and lymphoid tissues (10). DCs interplay between innate and adaptive immunity by engulfing pathogens, processing and presenting them as epitopes (11).

DCs present endogenous and exogenous antigens on MHC class I and class II, respectively. They are also capable of cross-presentation which means presenting exogenous antigens on MHC-I and endogenous antigens on MHC-II (12, 13). The ability of DCs to cross present is dependent on their state of activation. DCs can be in two states of immature and mature which exhibit different characteristics. Immature DCs (imDCs) are efficient in antigen acquisition, whereas mature DCs (mDCs) are prominent in cross-presentation (14). Generally, two pathways have been described for antigen cross-presentation through MHC-I: (i) vacuolar pathway and (ii) the cytosolic pathway [Fig. 1]. In the vacuolar pathway, the internalized antigen is degraded by lysosomal proteases and the epitopes are loaded onto MHC-I within endo/lysosomal compartment. Cytosolic pathway, unlike vacuolar, is dependent on proteasome and the antigen peptide transporter (TAP). In this pathway, the antigens are transported to the cytosol and degraded by proteasome which is a sophisticated cytosolic protein complex responsible for processing of antigen. Then, subsequent peptides are transported to endoplasmic reticulum (ER) via TAP, which is a complex protein made up of two subunits TAP1 and TAP2, and loaded onto MHC-I (15, 16) . Further investigations are needed for better understanding of the exact mechanisms underlying cross-presentation (17).

Importantly, DCs can distinguish self-and non-self-antigens according to the detection of PAMPs such as lipopolysaccharides (LPS) of gram-negative bacteria or viral double stranded RNA (dsRNA) (18). DCs express PPRs e.g., toll-like receptors (TLRs) which can recognize PAMPs and activate DCs. Upon PAMPs recognition, DCs mature and trigger proinflammatory response by secretion of cytokines such as Interleukin 1(IL-1), IL-6, IL-12, Tumor necrosis factor (TNF) α and interferon (IFN)α (19).

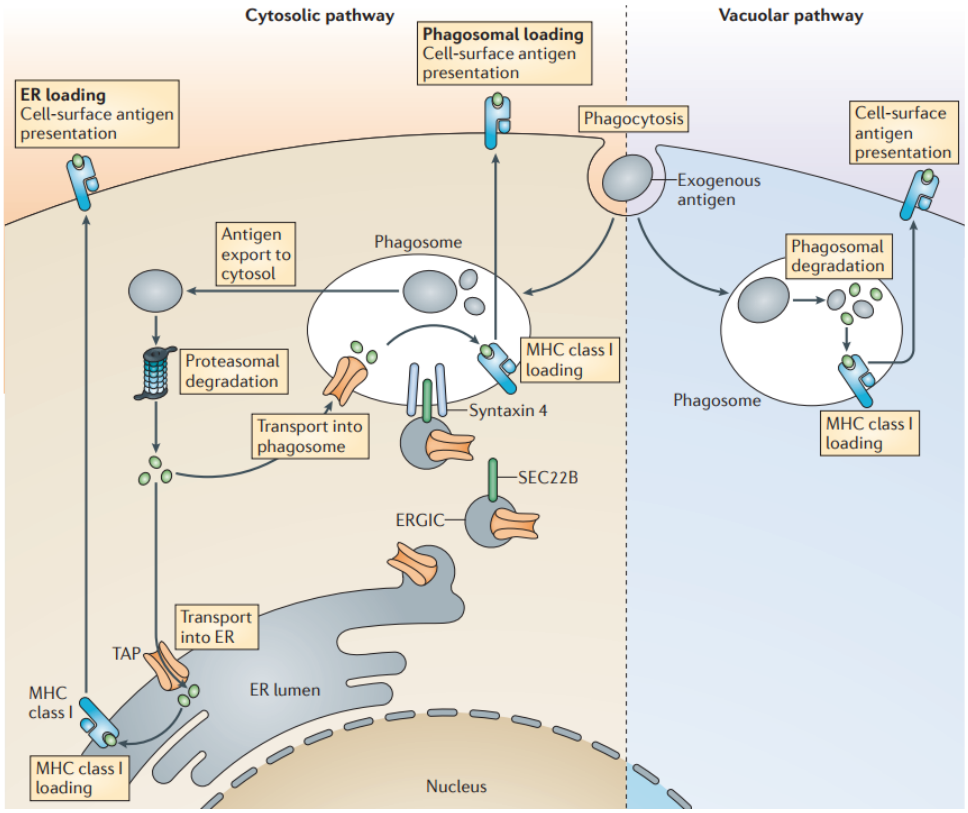


**Figure 1. Intracellular pathways for antigen cross-presentation in dendritic cells.** DCs can cross present the antigens through cytosolic or vacuolar pathway. In the cytosolic pathway, the antigen is exported from phagosome to cytoplasm and processed by proteasome. The fragments of antigens are transported to ER by TAP and loaded on MHC molecules. In the vacuolar pathway, the processing of the antigen and loading on MHC molecule are performed in endo/lysosomal compartment. Taken from (20)

During DCs maturation, MHC and co-stimulatory molecules are upregulated which leads to an efficient antigen presentation and activation of T cells. Costimulatory molecules consist of B7 family (CD80, CD86, inducible costimulatory [ICOS] ligand, programmed death-1 ligand (PD-L1), programmed death-2 ligand (PD-L2), B7-H3, and B7-H4) and TNF family (4-1BB ligand and OX40 ligand) (21, 22). Two members of B7 family, CD80 and CD86, are well defined and studies have highlighted their importance for initiation of antigen-specific immunity (23-25). The expression of CD86 is increased quickly upon cellular activation, whereas the induction of CD80 occurs more slowly. These costimulatory ligands have receptors on T cells including CD28 and cytotoxic T-lymphocyte-associated protein 4 (CTLA-4) which have activator and inhibitor functions, respectively (26). mDCs also express the membrane bound form of CD83, a member of Ig superfamily. CD83 interacts with its ligand on T cells, CD83 (Ligand)L, and also upregulates the expression of MHC-II and CD86 on DCs (27, 28).

Activation of naïve T cells is dependent on receiving three signals mediated by mDCs [Fig.2]. The first signal is generated by the interaction of TCR with the peptide: MHC (pMHC) complex which is accompanied by co-receptors CD4 or CD8. The second signal, called co-stimulatory signal, derived from the binding of costimulatory ligands to their related receptors on T cell surface. Finally, the third signal is delivered by cytokines and induces efficient activation of T cells. It is important to note that the interaction between DCs and T cells is bidirectional and T cells promote DC maturation and enhancing immune response.

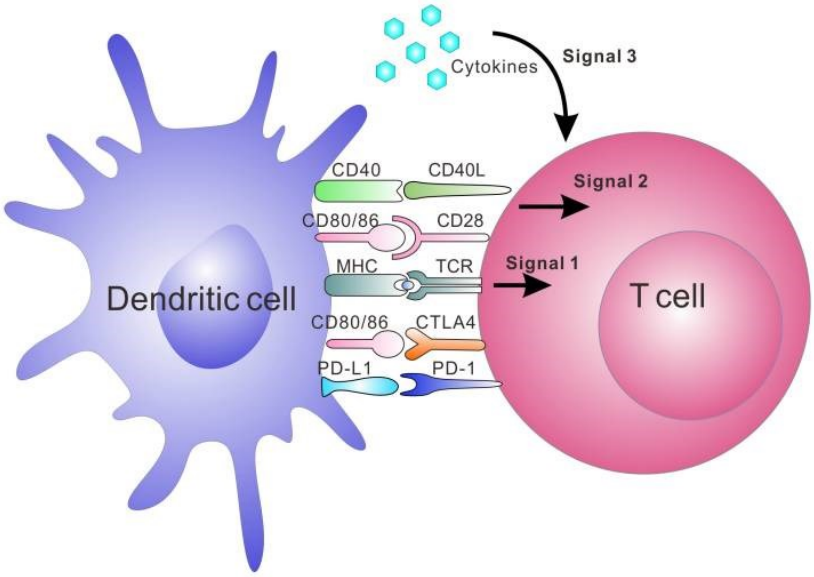


**Figure 2. Dendritic cells trigger the activation of T cells.** Mature dendritic cells activate T cells through three signals. The first signal is mediated by interaction of T cell receptor with peptide: MHC complex. The signal 2 is generated by the binding of costimulatory molecule of dendritic cells with their receptor on T cells. The third signal is promoted by cytokine and result in full activation of T cells. Taken from (29).

Under inflammatory conditions, CD40L is transiently expressed on T cells and interacts with its receptor, CD40, on DCs. This engagement exerts profound effects on DCs including cytokine secretion, expression of costimulatory molecules and promoting cross-presentation (30). DCs can also have inhibitory effect on function and differentiation of T cells and this is mediated by the interaction through PD-L1 on DCs, and PD-1 on T cell (31). DCs can uptake antigens, undergo maturation and present the foreign epitopes to the T cells to initiate cell-mediated immunity.

### 1.1.4 T lymphocytes development

T cells are essential components of cell-mediated adaptive immunity that can recognize antigens through APCs. T lymphocytes have two major lineages according to their TCR chains: α/β T cells and γ/δ T cells (32). The majority of T cells in peripheral blood are α/β T cells and only small proportion, 0.5-10%, express γ/δ TCR. α/β T cells recognize antigenic peptides presented by MHC molecules, however, most of γ/δ T cells can be activated by peptide or non-peptide antigens in MHC-independent manner (33). Compared to γ/δ T cells, α/β T cells are well studied and characterized.

T lymphocytes precursors originate from hematopoietic stem cells in the bone marrow and migrate to the thymus, where they undergo several developmental stages [Fig. 3] (34). These stages are characterized according to the expression of essential membrane molecules such as CD4 and CD8. In the early phases, the thymocyte, a lymphocyte within the thymus, are phenotypically $CD4^-CD8^-$ . i.e., double negative (DN) which can be subdivided into DN1-DN4. In the next steps, the thymocytes develop to $CD4^+$ $CD8^+$ (double positive, DP) and $CD8^+CD4^-CD3^+$ or $CD4^+CD8^-CD3^+$ (single positive, SP), successively. Moreover, migration of T cell progenitors through different anatomical regions in the thymus, may also influence the T cell development and commitment to a specific lineage (34).

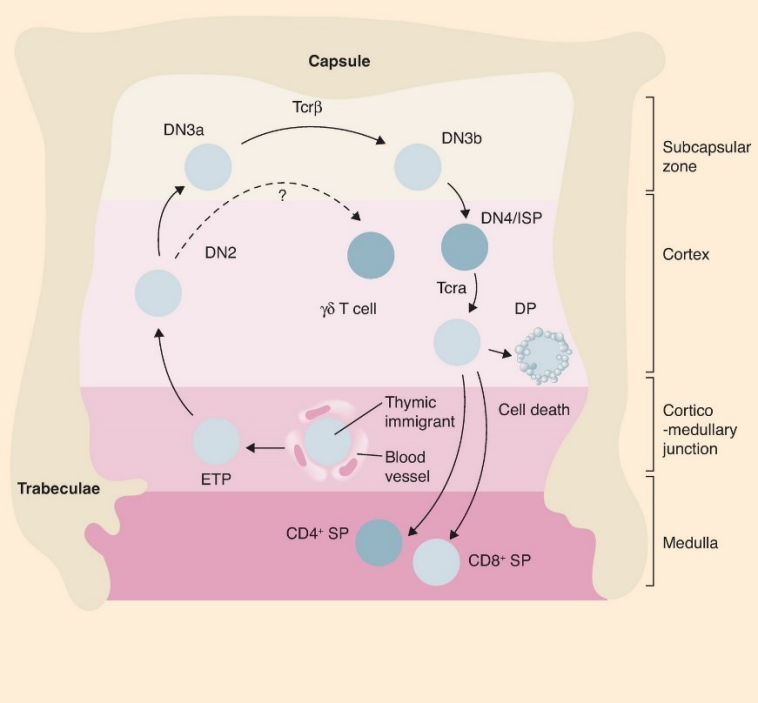


**Figure 3. Development of T cells in thymus. T cell precursors migrate through different regions of thymus during development.** First, progenitors of T cells enter the thymus via blood vessels. The early thymic progenitors (ETP) differentiate to DN subsets, Sp and finally DP cells. Concurrently with the T cell development, they go through TCR α/β gene rearrangements and selection processes. The $CD8^+$ and $CD4^+$ T cells which are functional and not reacting with self-antigens will leave the thymus via blood vessels. Taken from (34).

DN thymocytes are heterogenous cell population which enter the thymus through high endothelial venules (HEVs) and localize in the corticomedullary junction (35). DN1 are classified as the most immature T cell progenitors with a surface phenotype of $CD3^-CD4^-CD8^-CD25^-CD44^+$. A small population of DN1 also express CD117, also known as c-Kit, and they are known as early thymic progenitors (ETP) (36). ETPs move toward the subcapsular zone and generate DN2 cells which are $CD3^-CD4^-CD8^-CD25^+CD44^+$. DN2 cells express genes such as recombinase activating gene 1 (Rag1) and Rag2, CD3 chains and Lck which are important for TCR rearrangement, assembly and signaling (37). During this stage, which is initiated in DN2 and completed in DN3

cells, somatic recombination of TCRβ, TCRγ and TCRδ locus determine the commitment of the thymocytes to αβ or γδ T cell lineages (38, 39). DN3 cells go through cell cycle arrest to ensure successful TCRβ+ or γδ TCR phenotype which rescue the cells from apoptosis. TCRβ+ T cells further develop to $CD4^+CD8^+$ double positive (DP) and they have another arrest in cell cycle leading to rearranging TCRα gene.

TCR rearrangement which is also known as VDJ recombination accounts for huge diversity of TCRs. TCRα and TCRβ chains contain a variable (V) and a constant (C) region (40). T cell receptor alpha variable (TRAV) locus is located on chromosome 14 and consist of V, 70-80 copies and joining (J), 61 copies. Genes encoding T cell receptor beta variable (TRBV) are clustered on chromosome 7 and comprise of V, 52 copies, diversity (D), 2 copies, and J, 13 copies. These copies of the gene segments can rearrange combinatorically in V-J or V-D-J order to produce diverse TCRα and TCRβ chains, respectively. Besides that, non-templated nucleotides can be added or deleted at the joints between gene segments which increase the diversity of VDJ recombination (41). According to high-throughput sequencing, it has been shown that there are around $10^{11}$-$10^{12}$ unique TCRs (42). The most variable parts of V chain are called complementary determining region (CDR) including CDR1, CDR2 and CDR3 which are important for detecting pMHC complex (43). CDR1 tend to interact with peptide and MHC, whereas CDR2 mainly bind to the MHC molecule. CDR3 is the most variable one and is responsible for discrimination of the peptides (44).

Following successful TCR α/β gene rearrangements, DP αβ T cells migrate back to cortico-medullary junctions and go through selection processes. These selections are done based on the interaction of DP cells with pMHC complexes expressed by thymic APCs. First, DP

thymocytes binding to self-pMHC complexes with intermediate affinity, survive and differentiate to SP αβ T cells. This process is known as positive selection and the cells recognizing MHC Ⅰ or MHC Ⅱ complexes differentiate to $CD8^+$ T cells or $CD4^+$ T cells, respectively. In the next step, known as negative selection, the SP thymocytes which interact with high affinity to self-antigens go through apoptosis. Therefore, nonfunctional and autoreactive T cells are eliminated during positive and negative selections (45). Mature T cells will leave the thymus and circulate in the blood to recognize pathogens through APCs.

### 1.1.5 T lymphocytes activation and differentiation

T lymphocytes leaving the thymus are called naïve T cells since they have not recognized their cognate antigen and not been activated. Naïve T cells express homing molecules on their surface including the CC chemokine receptor 7 (CCR7), L-selectin (CD62L) and leukocyte function antigen (LFA)-1 enabling them to bind to adhesion molecules of HEVs. HEVs, specialized post-capillary venules, mediate the migration of lymphocytes to lymph nodes. In the lymph nodes, naïve T cells can interact with their related pMHC molecules presented on APCs and form immunological synapse at their interface. This immunological synapse is composed of TCR: pMHC in company of CD4 or CD8 co receptors, co-stimulatory molecules (e.g., CD28: CD80/CD86) and adhesion molecules such as LFA-1: intracellular adhesion molecule 1 (ICAM-1) for further stabilization of the synapse.

The intracytoplasmic parts of α/β or ϒ/δ chains are too short to propagate any intracellular signal. Therefore, this signal transduction chiefly depends on CD3 complex including six

subdomains 2ε,2 ζ, 1δ,1Ɣ. The cytoplasmic domains of CD3 component have immunoreceptor-based tyrosine activation motifs (ITAMs). Upon TCR-pMHC interaction, Src family kinases phosphorylate the tyrosine of these ITAMs (46). An important tyrosin kinase, called ZAP-70 will be bound to the phosphorylated ITAMs of CD3 ζ. For further activation, there is also a need for the interaction of CD4 (expressed on the surface of helper T cells) or CD8 (expressed on the surface of cytotoxic T cells) with MHC class II or MHC class I, respectively (47). These interactions bring another member of Src family of kinases, LcK, close to CD3 subdomains and activate ZAP-70. Afterwards, ZAP-70 catalyzes the phosphorylation of adaptor proteins such as LAT which in turns increase the transcription factors (TFs) like AP-1, NFAT and NFkB (48). It has been shown that AP-1 and NFkB induce the expression of CD69, a classical early activation marker of lymphocytes (49). Moreover, NFAT and NFkB are involved in the regulation of CD25, which is the alpha chain of IL-2 receptor (50). For optimal activation of naïve T cells, two additional signals through 1) CD28 and 2) receptors of cytokines such as IL-2, IFN-$\alpha$, IL-12, and IL-1 have been also described (51).

Following TCR-pMHC binding and CD28 costimulation, ICOS is expressed on activated T cells. It has been shown that ICOS is important for efficient $CD4^+$ T cell responses through enhancing cytokine secretion and T cell-dependent antibody responses (52). Besides that, interaction of 4-1 BB and OX40, TNF family members, with their ligands on APCs, 4-1 BBL and OX 40L, induce further costimulatory signals. Activated T cells lose the expression of CD62L and CCR7 whereas they upregulate P and E- selectin ligands, integrins (e.g., VLA-1) and inflammatory chemokine receptors (e.g., CXCR3 and CCR5). This changes in adhesion and homing molecules lead to an efficient trafficking of T cells to the inflammation sites (53). On the other hand, the expression

of PD-1 and CTLA-4, which act as immune-attenuators, provide essential negative feedback to restrict the proliferation of T cells.

Based on the cytokines and TFs, activated CD4+ T cells can differentiate into different sub classes: T helper 1 (Th1), Th2, Th9, Th17, T follicular helper cells ($T_{FH}$) and regulatory T cells (Treg). IL-12 and IFN γ are essential cytokines to promote Th1 development and these cells induce an inflammatory response by secreting IL-2, TNFα and IFN γ. On the other hand, Th2 cells, whose differentiation is dependent on IL-2 and IL-4, promote non-inflammatory responses through producing IL-4 and IL-10. Th1 is mainly involved in cell-mediated immunity, however, Th2 induce humoral immune responses, target parasites and contribute to allergic immune reactions (54, 55). Th9 cells, previously classified as a subset of Th2, is a new distinct subset of IL-9 secreting T helper cells which develop in the presence of transforming growth factor (TGF)β and IL-4. It has been shown that Th9 cells mediate allergic reactions and play an important role in counteracting intestinal worm and also tumor growth (56, 57). In the presence of IL-6 and TGFβ, $CD4^+$ T cells differentiate to Th17 cells which are characterized by secretion of IL-17 and IL-22. Th17 cells localize in mucosal interfaces and involved in immune responses targeting pathogenic bacteria and fungi (58). $T_{FH}$ cells, induced by IL-6 and IL -21, express C-X-C motif receptor-5 (CXCR5) and they are in follicular regions of lymphoid tissues mediating immunoglobulin production by B cells (59). Treg cells, mainly have immunosuppressive function, are further divided into two subsets: natural Treg (nTreg) and induced Treg (iTreg). nTregs are a distinct lineage developing in the thymus and expressing FOXP3, CD4 and CD25. However, iTregs arise in peripheral lymphoid organs following antigen priming and TGFβ play a

critical role in their development (60). Tregs are essential for immune central tolerance and their deficiency can cause autoimmune diseases (61).

Upon encountering the cognate antigen, naïve $CD8^+$T cells differentiate into short-lived CTLs which can migrate to sites of inflammation and directly kill infected or malignant cells. In order to generate an efficient cytotoxic response and long-lasting memory $CD8^+$T cells, further co stimulation through the interaction of $CD4^+$ T cells and DCs is needed. In this process, which is called licensing, $CD4^+$ T cells interact with DCs through CD40 L- CD40 binding and licensed matured DCs can efficiently activate $CD8^+$ T cells. CD40 L- CD40 interaction can be also within the direct contact of $CD4^+$ T cells and $CD8^+$ T cells (62). It has been shown that CD40 signaling is essential for maturation of $CD8^+$ T (63). CTLs induce their cytotoxic activity by two pathways in which effector cells directly contact target cells. In the first pathway, CTLs secrete perforin, a membrane-disrupting protein, and granzymes, serine proteases, and it is the main pathway used by CTLs to eliminate transformed or infected cells (64). Perforin facilitates the entry of granzyme into the target cells and it can induce apoptosis through caspase dependent and -independent (65). The second pathway is triggered through the binding of CD59L (FasL), a member of TNF receptor family to Fas which is expressed on target cells. FasL-Fas interaction initiate caspase-dependent apoptosis and it is also important for destroying self-reactive lymphocytes (66).

Following resolving an immune response, about 90 %, of effector $CD4^+$ or and $CD8^+$ T cells are eliminated by apoptosis and only small proportion will survive and form memory T cells (67) . There are two different subsets of memory cells which are classified based on their immediate effector function and expression of different homing receptors. Central memory T cells ($T_{CM}$)

are CD45 R0+ cells expressing CCR7 and CD62L, which are also expressed on naïve T cells, enable them to extravasate through HEVs and migrate to lymphoid tissues. $T_{CM}$ can be activated more quickly compared to naïve T cells due to the upregulation of CD40L and lower dependency on costimulation. Upon TCR engagement, $T_{CM}$ secrete IL-2 and they produce high amount of IL-4 or IFN-γ following differentiation to effector cells. On the other hand, effector memory T cells ($T_{EM}$) express adhesion molecules and chemokine receptors to circulate in non-Lymphoid tissues. Compared to $T_{CM}$, $T_{EM}$ cells have faster effector function and secrete high amount of IL-4, IL-5 and IFN-γ. CD8 $T_{EM}$, especially $T_{EM}$ expressing CD45RA, produce high amount of perforin which increase their cytotoxic activity (68). T cell activation and differentiation is perfectly tuned and they play an important role in combating various pathogens, especially viral infections.

## 1.2 Human Papilloma viruses

Papilloma viruses (PVs) are mainly characterized by their preference to epithelial tissues and genotype-specific host-restriction (69). Among more than 300 identified PVs which have been completely sequenced, there are nearly 200 Human papilloma viruses (HPV). HPVs are a member of *Papillomaviridae* family and fall into five genera, Alpha -, Beta-, Gamma papillomavirus, Mu- and Nu-papillomavirus [Fig. 4] (70). Due to their medical importance, the most extensively studied among them are viruses of the Alpha genus, of which about 30 types infect anogenital and oropharyngeal mucosal epithelia and are further divided into “low-risk” (LR) and “high-risk” (HR) types of which HPV-16 and -18 are the most prevalent according to

their ability to immortalize human keratinocytes and their oncogenic potential (71, 72). Low risk types can cause benign skin and genital warts; however, persistent infection with HR-HPVs is the main causative agent of cervical, vulvar, vaginal, anal, penile and certain head and neck cancers (73-75).

The pathology and site of infection for each HPV type is different. HPV6 has tropism to genital sites; however, HPV 11 has preference for oral sites and can cause recurrent respiratory papillomatosis (70, 76). Moreover, HPV 16 is strongly associated with cervical cancer compared to HPV31 and HPV 35 and it has been also detected in oropharyngeal malignancies (70). These differences in tropism can be explained by the various gene expression controlled by regulatory elements (77).

Correlation between HPV infection and certain types of cancer was postulated already in the 1970s (78). It was later confirmed by detecting HPV DNA with nucleic-acid hybridization experiments and finally by isolation of HPV DNA directly from cervical cancer biopsies (78-81). It is important to note that most of the sexually active people once in their life will be infected by HR-HPVs (82). In most of these cases, immune system cleared HPV infections within 1-2 years (83, 84). However, persistent infection can lead to neoplasia and subsequently malignant tumors. Further understanding of HPVs life cycle and genome as well as immune responses targeting this viral infection are essential for efficient preventive and therapeutic approaches.

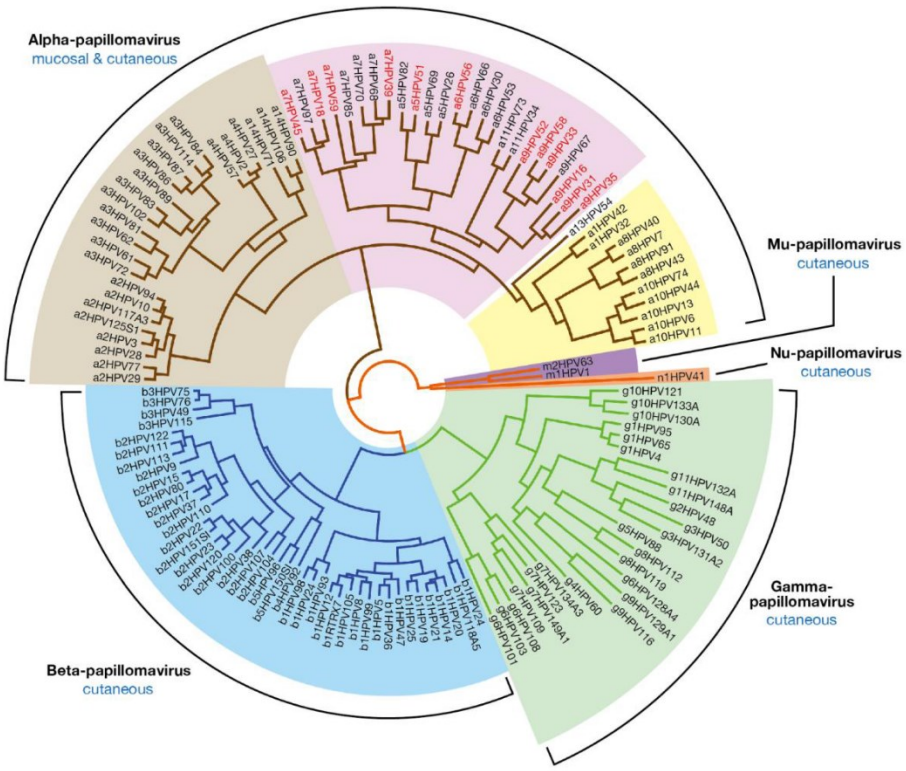


**Figure 4. Human Papillomaviruses are divided into five genera.** The Alpha-papillomaviruses are the most studied genus and are divided into low-risk cutaneous (Brown); high risk (pink) and low- risk mucosal (yellow) according to their oncogenesis. This evolutionary tree is derived by the alignment of early genes, E1 and E2, and late genes, L1 and L2, of HPVs. Taken from (70).

## 1.2.1 HPV genome and viral life cycle

Human papilloma viruses are small (50-60nm diameter), non-enveloped viruses with a circular, double-stranded DNA genome. The genome of HPV viruses is approximately 8 kb and contains 8-9 open reading frames (69). Despite of small size of their genome, HPVs can encode many proteins due to many promoters and alternative splicing (85-87).The HPV genome divided mainly in three regions, long control region (LCR), early (E) and late (L) region [Fig. 5].

LCR, comprising transcription factor binding sites, replication origin, is involved in regulation of viral gene expression. The E regions encode early proteins which are needed for viral replication

and oncogenesis. L regions are responsible for expression of late proteins which are for capsid formation (87). Although E4,E5,E6 and E7 have a great diversity among HPVs, the genes involved in viral replication (E1 and E2) and capsid proteins (L1 and L2) are highly conserved (88).

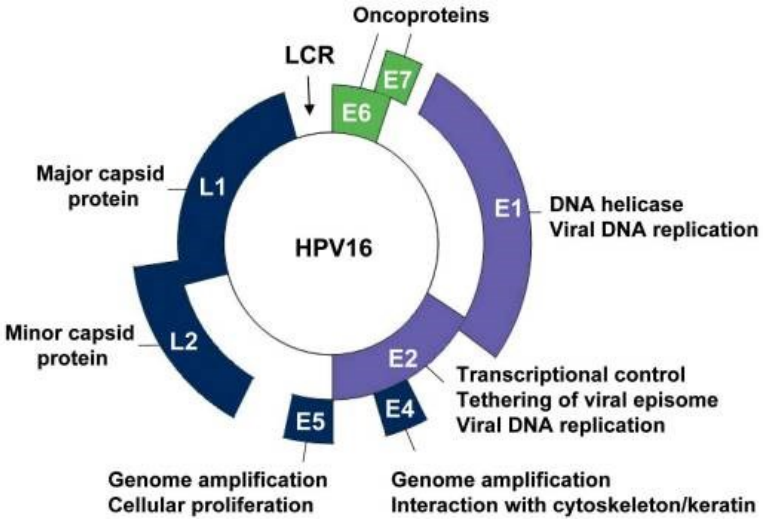


**Figure 5. Schematic representation of double strand circular genome of HPV.** HPV genome is around 8000 base pair and divided in three regions long control region (LCR), early (E) and late (L). The LCR contains regulatory elements, Early genes are involved in viral replication and maintenance, and Late genes accounts for capsid formation. Taken from (89).

Microabrasions make squamous epithelium of mocosa and skin susceptible to HPVs which can infect undifferentiated basal keratinocytes [Fig. 6]. Wound healing and cell proliferation facilitate the episomal maintenance and entry of the virus into the nucleus (90). The entry of HPV is initiated by binding of virions to heparan sulfate proteoglycan (HSPG), a type of glycosaminoglycan (GAG), on exposed basement membrane. This interaction triggers the conformational change in the HPV virions affecting capsid proteins, L1 and L2, and resulted in exposure of L2 amino terminus. This structural change makes the furin convertase recognition site accessible for furin cleavage which is important for HPV entry (69). The exact mechanisms

and molecules involved in internalization of HPVs are not completely understood (91). However, studies have shown that most of HPV types enter the basal cell membrane via a clathrin-dependent endocytosis (92-94). After Infection of basal membrane, E1 and E2 initiate viral DNA replication. E1 plays an important role for episomal maintenance at constant copy number, whereas E2 is important for gene expression and repressing E6 and E7, oncogenes (69). Normally, differentiation occurs upon cell division and moving of cells to upper layers of epithelium. However, HPVs prevent the terminal differentiation in an infected cell to favor their replication. HPVs keep the infected cells in a replicative phase via E5, E6 and E7. (95). E5 proteins , which are short membrane-associated proteins, enhance the activity of mitogen-activated protein (MAP) kinase and stabilize the epidermal growth factor (EGF) receptor (96).

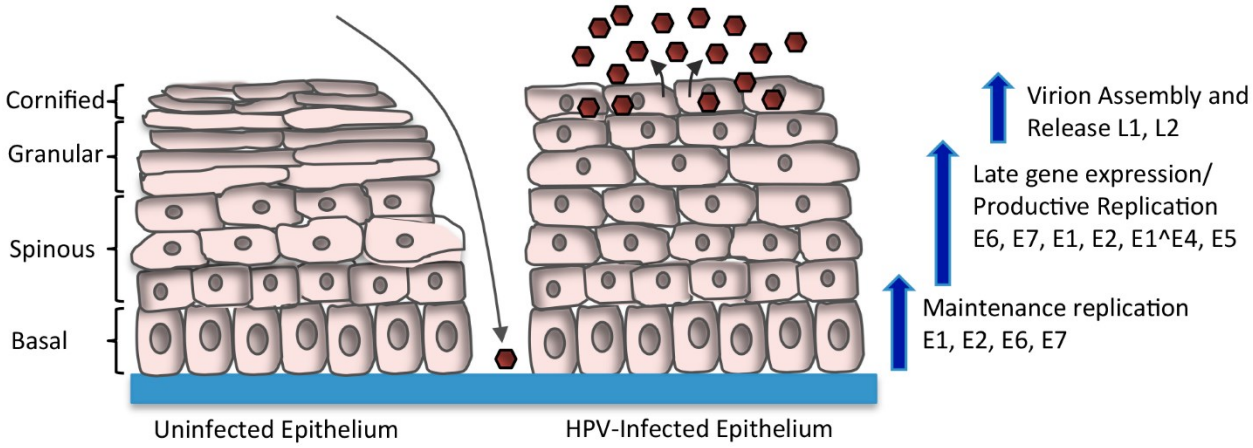


**Figure 6. Life cycle of Human papillomaviruses. HPVs infect undifferentiated basal of Epithelium.** E1, E2, E6 and E7 are important for maintenance of replication in undifferentiated basal cells. Upon differentiation, the late genes are expressed and the viral genome amplified exponentially. The expression of L1 and L2 leads to encapsidation of the replicated genome and virion release. Taken from (97).

Moreover,E6 and E7 mediate further proliferation of the infected cells (98). In HR-HPVs, E6 and E7 are important regulators of cell cycle progression; however, their role in LR-HPVs is not

clearly defined. Random integration of HR-HPV DNA into the host genome and disruption of E2 gene encoding repressor transcription factor for E6 and E7, causes dysregulated expression of these oncogenes and uncontrolled proliferation of infected cells (99, 100). E7 further promotes cell cycle progression by binding to other members of the RB family, e.g. p21, resulting in high CDK2 activity, (101). On the other hand, E6 induces proteasome mediated degradation of p53, leading to impaired DNA damage repair and subsequent accumulation of genetic mutations over the course of persistent infection (102). Finally, E6 can induce telomerase activity by upregulating hTERT expression (103).

In the last step of HPV life cycle, minor coat protein (L2) and major coat protein (L1) are expressed, then they form the capsid and finally result in genome packaging. The mature HPVs are released from terminally differentiated cells by natural shedding of epithelium. It has been proposed that E4 amyloid fibers can contribute to virion release (104). Despite of several investigations, there is still a need for further studies on the life cycle of HPVs to shed light on various proteins and elements involved in the infection and viral proliferation.

### 1.2.2 Immune responses to HPVs

Most of the sexually active individuals, once in their life will be infected with HR-HPVs and in approximately 10% of the cases, HPV can evade the immune system and cause malignant transformation (82-84). The immune system controls HPV infection through innate and adaptive immune responses which are mainly mediated by specific antibodies and effector T cells (83).

However, there is a low humoral immunity against HPV infection in most of the exposed individuals. Moreover, T cell immunity is impaired in patients with high grade cervical intraepithelial (CIN) lesions compared to ones who had cleared the lesions (105). Therefore, HPVs utilize various strategies to evade the immune response.

In early stages of HPV infection in basal membrane, E2 keep early gene expression at low and undetectable levels which hinder effective adaptive immune response. However, immunogenic virions and higher expression of HPV proteins occur in the upper layers of epithelial tissue where the access of immune cells are restricted (86). HPV can further impair the antigen presentation via E6-mediated downregulation of E-cadherin in keratinocytes which interrupt the adhesion of Intraepithelial Langerhans cells (106). It has been also shown that E6 and E7 of HR-HPVs inhibit macrophage inflammatory protein 3alpha (MIP-3alpha) transcription and this avoid the migration of Langerhans precursor cells to inflamed epithelium (107). HPV also counteracts with innate antiviral responses. HPV 16 E6 and E7 can impair the TLR9 signaling, which can recognize unmethylated CpG sequences in viral DNA (108). Moreover, HPV16 can alter the production and signaling of IFN-α, IFN-β and IFN-κ which have antiviral activity. It has been reported that HPV16 E6 oncoprotein can bind to interferon regulatory factor (IRF)3 and interferes with the transcription of IFN-α and IFN-β (109). HPV16 E6 can also epigenetically silence IFN-κ though *de novo* methylation near its transcriptional site (110). Other inflammatory cytokines such as IL-6 and IL-1β can also be decreased by HPV infection (111). Niebler et al., showed that E6 of HR-HPVs can induce proteasomal degradation of pro-IL-1β through E3 ubiquitin ligase E6-Associated protein and p53 (112).

HPVs also have mechanisms to evade from T cell-mediated immunity. HPV can interrupt antigen presentation at different levels and prevent effective function of T cells. It has been shown that the expression of the proteasome subunits PSMB8 and PSMB9 is downregulated in HPV16 infected cells (113). E7 oncoprotein of HPV16 and HPV 18 represses PSMB9 and the promoter of PSMB8 is highly methylated in HPV16 associated cervical cancer (114, 115). HPV can also interrupt the transport of the protein fragments to the ER. In HPV16- positive cervical cancer has been reported that the promoter of TAP1 is hypermethylated and HPV 16 E7 can also inhibit TAP1 transcription (105, 113). Furthermore, HPV16 and HPV18 E7 and HPV16 E5 can impair the expression of MHC I resulting in lower epitope presentation (114, 116). HPV can also affect T cell function through interfering with Th1/Th2 polarization. This can be done by inhibiting Th1, which is important to cell mediated responses, and upregulation of Th2 non inflammatory cytokines such as IL-10 which can downregulate the expression of HLA class I (117). Like other cancers, HPV-associated malignancies create immunosuppressive tumor microenvironment. There are various suppressive immune cells inside the tumor site inhibiting T cell activation and survival such as: myeloid derived suppressor cells (MDSC), Tregs, tumor associated macrophages (TAM) and tumor-associated neutrophils (TAN). These cells produce diverse immune suppressive factors and cytokines like: TGF-β, Prostaglandin E2 (PGE2), reactive ROS, IL-10, and IL4 (118).

In summary, HPV can escape from the immune system through various mechanisms and this allows persistent infection, which can further develop malignant tumors. However, most of these infections are cleared by HPV-specific CD4 and CD8 T cells which highlight the importance

of T- cell immunity in HPV positive cancers. Moreover, the expression of HR-HPV E6 and E7 is upregulated during cancer progression and they are interesting targets for immunotherapy. Therefore, immune directed approaches to trigger T cell responses are promising therapeutic modalities.

## 1.3 Immunotherapy of HPV associated cancers

Persistent infection with HR-HPVs is linked to cervical, anogenital and oropharyngeal cancers. (73). Due to the viral source of these malignancies, the HPV infection can be prevented through prophylactic vaccines. It was shown that virus-like particles (VLPs) made of capsid protein L1, major epitope of HPV virion, are extremely immunogenic and were able to effectively induce neutralizing antibodies (119). Therefore, VLPs were considered as a safe and efficient candidate for preventive HPV vaccines. There are currently three approved prophylactic vaccines: Cervarix®, Gardasil®, Gardasil-9® that can potentially protect the individuals from HPV associated cancers up to 90%. Cervarix® (GlaxoSmithKline) is bivalent, targeting two types of HPVs, and contains VLPs of the most common HR-HPVs, HPV16 and HPV18, and adjuvants which are aluminum hydroxide and monophosphoryl lipid A (MPLA) (120). Gardasil® (Merck) is quadrivalent and prevent infections by HPV16/18 and two LR-HPVs: HPV6 and HPV11 causing genital warts and respiratory papillomatosis, respectively. VLPs of this vaccine are produced in *Saccharomyces cerevisiae* and contains aluminum hydroxyphosphate sulphate as an adjuvant (121). Gardasil-9® (Merck) is a nonacovalent vaccine including VLPs of LR-HPV 6 and 11; HR-HPV16, 18, 31, 33, 45, 52, and 58 and has been approved by Food and drug administration (FDA) and the European Medicines Agency (EMA) (122).

Although regular screening and prophylactic HPV vaccination are expected to significantly decrease the occurrence of cervical as well as other HPV-related cancers, there is still a need for effective therapies to treat advanced HPV-related cancers. Cervical cancer is the fourth common type of cancer and the fourth cause of cancer mortality among women worldwide. Recently, immune directed therapies have shown promising results for the treatment of advanced HPV related cancers (123). Immune checkpoint inhibitors, therapeutic vaccines and adoptive cell therapy are the main immunotherapeutic approaches for HPV positive cancers [Fig. 7].

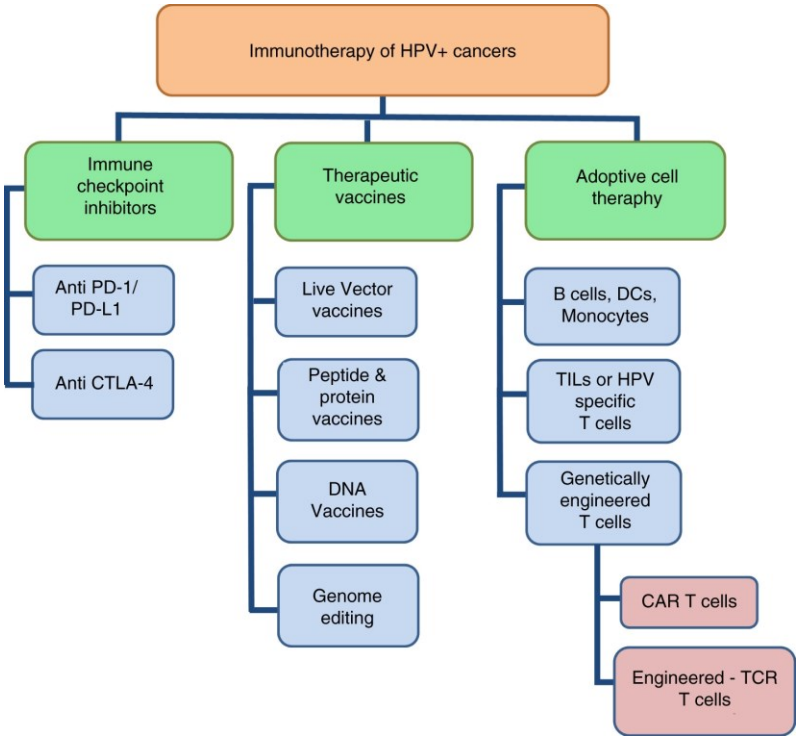


**Figure 7. Immunotherapy of HPV positive cancers.** Immune checkpoint inhibitors, therapeutic vaccines and adoptive cell therapy have been used in clinical studies for immunotherapy of HPV related cancers. Taken from (124).

### 1.3.1 Immune checkpoint inhibitors

Inhibitors targeting PD-1/PD-L1 or CTLA-4, which are negative immune regulators of T cells, have shown encouraging results in several clinical trials. The therapeutic effect of these inhibitors has been studied solely or in combination with chemotherapy, chemoradiation and antiangiogenic drugs. Nivolumab, a fully human antibody targeting PD-1, has shown to be safe but having low anti-tumor activity in recurrent or metastatic cervical cancer patients (NCT02257528) (125). However, it seems to be more effective in metastatic vaginal, vulvar and cervical cancers (NCT02488759)(126). The combination of Nivolumab with chemoradiation (NCT03298893) and chemotherapy is also being evaluated (NCT04282109). Pembrolizumab is another humanized antibody targeting PD-1 that has shown stable anti-tumor activity in metastatic cervical and vulvar cancers in a clinical phase II study (NCT02628067)(127). Moreover, it has shown promising outcomes in PD-L1 positive recurrent or metastatic head and neck squamous cell carcinoma (HNSCC). Pembrolizumab in combination with chemotherapy can be potential immunotherapy for HNSCC (128). AGEN2034 (RebmAB-700) and cemiplimab (REGN2810) are also anti-PD-1 monoclonal antibodies that are being evaluated in cervical cancer patient at clinical phase I/II (NCT03104699) and phase III (NCT03257267), respectively. Durvalumab (NCT02725489) and Atezolizumab (NCT02914470, NCT03556839, NCT02921269) are monoclonal antibodies targeting PD-L1 that are under study at different clinical phases for treating cervical cancer patients.

CTLA-4 is a negative immune regulator and it has been shown that single nucleotide polymorphisms in its promoter is correlated with cervical cancer (129). Initial reports of a phase II clinical study of Ipilimumab, anti-CTLA-4, shows that it is well tolerated in cervical cancer

patients and induce immune activation (NCT01693783) (130).Moreover, it has been reported that the combination of Ipilimumab with chemotherapy and chemoradiation is safe and efficient in advanced cervical cancer patients (NCT01711515) (131). Concurrent administration of tremelimumab, anti-CTLA-4 antibody and durvalumab has also shown to be safe and clinically active in advanced cervical cancer (NCT01975831)(132). There are several ongoing clinical studies to assess the safety and efficiency of immune checkpoint inhibitors for therapy of HPV positive cancers. According to initial outcomes, these inhibitors have more efficiency in combination with chemotherapy and radiotherapy.

### 1.3.2 Therapeutic vaccines

Majority of therapeutic HPV vaccines target HR-HPV 16/18 E6 and E7 oncoproteins (133). Several strategies have been used for the development of theses vaccines including, vectors, peptide/proteins, DNA and genome editing tools. Vector vaccines used a bacterial or viral vectors encoding the HPV oncoproteins and can induce antigen presentation (134). ADXS11-001, an attenuated live *Listeria monocytogenes* (LM) encoding HPV16 E7, has shown promising outcome in HPV positive cancer patients as monotherapy or in combination with chemotherapy or immune checkpoint inhibitor in several clinical studies (NCT01266460, NCT02853604, NCT02002182, NCT01671488, NCT02164461, NCT02291055) (135-139). TG4001 comprises of modified vaccinia virus Ankara (MVA) vectors expressing HPV 16 E6/E7 and IL-2. Initial results of Phase I/II trial shows that TG4001 in combination with avelumab is well tolerated and promote antitumor activity in HPV16 positive cancer patients (NCT03260023) (140). TA-HPV is another vector vaccine including a live recombinant vaccina virus encoding E6/E7 oncogenes of HR-HPV

16/18. It has been reported that simultaneous administration of TA-HPV and pNGVL4a-Sig/E7 (detox)/HSP70 DNA vaccine is safe and efficient in HPV16+ CIN III patients (NCT00788164) (141, 142). Despite of successful clinical results so far, the usage of live vector vaccines can be complicated. The immune system may target these vectors instead of HPV related antigens and they can be potential pathogens in immunocompromised patients (143).

Compared with live vector- based vaccines, peptide and protein vaccines are relatively safe. Peptide vaccines comprise of immunogenic peptides of HPV antigens which are presented on MHC Ⅰ. ISA101 is a peptide vaccine including 12 synthetic long peptides (SLP) of HPV 16 E6 and E7. It was reported that ISA101 augmented the efficiency of nivolumab in HPV positive patients (NCT02426892)(144). Moreover, ISA101 in combination with pegylated interferon (IFN-α IIb) has increased the survival duration in cervical cancer patients which was significantly correlated to vaccine mediated T cell responses (NCT 02128126)(145). PepCan is another peptide vaccine comprise of four HPV16 E6 peptides and it was safe in a phase Ⅰ study in patients with CIN2/3 (NCT01653249)(146). In contract to peptide vaccines, protein vaccines have low immunogenicity and they may not be efficient in inducing CTL responses (147). However, this can be improved by using adjuvants and fusion proteins. TA-CIN is a fusion protein vaccine composed of HPV16 L2/E6/E7 and it is being evaluated in HPV associated cervical cancer patients (NCT02405221). TVGV-1 is another fusion protein composed of peptide sequence of human HPV16 E7 fused to an ER retention signal (KDEL) and the Pseudomonas aeruginosa exotoxin A (PE). It is also combined with GPI-0100 as an adjuvant, which is derived from saponins, and being assessed in a phase II clinical trial in HPV16/18 positive high-grade squamous intraepithelial neoplasia (HSIL) (NCT02576561).

Unlike peptide and protein vaccines, DNA vaccines have sustained cellular gene expression (147). According to different clinical studies, these vaccines are safe but they are poor immunogens (148, 149). Consequently, strategies enhancing the processing and presentation of antigens have improved the immunogenicity of DNA vaccines. GX-188E is a DNA based vaccine encoding HR-HPV 16/18 E6 and E7, plasminogen activator signal sequence and FMS-like tyrosine kinase-3 ligand (Flt3L). It has been recently reported that GX-188E can efficiently induce regression of CIN III (150). VB10.1 is another DNA based vaccine expressing HPV16 E6/E7 fusion, a dimerization domain and an MIP-1α sequence which binds to APCs. It was reported in a recent Phase I/IIa clinical study that VB10.1 is safe and can induce E6/E7 specific $CD8^+$ T cell responses in HPV16 positive CIN II/III patients (151). Moreover, genome editing tools including clustered regularly interspaced short palindromic repeats/Cas9 protein (CRISPR/Cas9), zinc finger nucleases (ZFNs) and transcription activator-like effector nuclease (TALENs) can be promising candidates for targeted therapy of HPV associated cancers. It has been shown that targeting HPV 16/18 E6/E7 oncoprotein by CRISPR/Cas9, TALEN or ZFNs can reduce tumorigenicity *in vitro* and *in vivo* models (152-154). The ultimate purpose of all therapeutic vaccines is to induce an efficient cell-based immune response, thus cell-based therapies can play an important role in immunotherapy of HPV positive cancer.

### 1.3.3 Cell-based therapy

In cell-based therapy of HPV positive cancers, immune cells are isolated from the patients and transduced ex vivo to target or express HPV specific antigen and infused back to the same patient (124). The safety and efficiency of BVAC-C, B cells and monocytes infected with

adenovirus expressing HPV16/18 E6/E7, is studied in patients with HPV type 16 or 18 positive cervical cancers at clinical phase I/II (NCT02866006). Adoptive T cell therapy (ATC) is another approach of cell-based therapy which has been shown to be promising for the treatment of metastatic or recurrent cervical cancer. The first study that explored if ATC might be effective in cervical cancer was performed by Stevanović et al., where 9 patients with HPV-18 or HPV-16 associated metastatic cervical cancer were treated with tumor infiltrating lymphocytes (TILs). They previously received chemotherapy or chemoradiotherapy but were not responding to the treatment. After receiving lymphodepleting conditioning chemotherapy, they received one dose of HPV E6- and E7-reactive TILs and several doses of aldesleukin (IL-2). The treatment was well-tolerated with no severe adverse events related to the cell infusion itself. In 3 out of 9 patients they observed objective tumor response, two long-lasting complete responses and one partial response lasting 3 months. Although the number of patients in this study was small, they could see a positive correlation between HPV reactivity, as determined by IFN-gamma secretion and CD137 upregulation, and tumor response. Moreover, the responding patients showed the presence of reactive T cells in peripheral blood even 2 to 13 months later (155). Ramos *et al.* reported that HPV-specific T cells (HPVST) derived from the HPV positive cancer patients could be efficient for immunotherapy of HPV associated cancers (156). Moreover, it was shown that HPV-TILs can effectively cause tumor regression (NCT01585428) (157). Despite encouraging clinical outcomes, selection and expansion of TILs for ATC has some obstacles and limitations, since these techniques are time consuming and require experienced laboratory staff. Besides that, HPV- reactive T cells cannot be frequently found in all patients. Compared to TILs, production of genetically engineered T cells can be easier to standardize for ACT (158).

Chimeric antigen receptor (CAR) T cells are genetically engineered T cells expressing a single-chain fragment variable (scfv). Their Scfv can detect tumor-associated antigens (TAA) which are expressed on the surface of tumor cells. CAR T cells are MHC independent and utilize CD3ζ and other costimulatory molecules including 4-1BB , CD28 and OX40 as intracellular signaling machinery (124). A Phase I/II study aims to evaluate the safety and efficiency of CAR T cells in immunotherapy of cervical cancer patients whose tumors are positive for TAAs such as GD2, PSMA, Muc1 or mesothelin (NCT03356795).

Engineered TCR T cells are another group of genetically modified T cells which express the desired α/ β chains reactive to a specific epitope. As important oncoproteins of HPV, E6 and E7, are presented by MHC molecules, engineered TCR T cells have an advantage over CAR T cells. Draper et al., identified a TCR targeting $E6_{29-38}$ epitope of HPV16 within the TILs of a metastatic anal cancer patient with an ongoing prolonged disease-free interval. This TCR was retrovirally transduced into the T cells and these engineered TCR T cells showed efficient recognition and killing of HPV 16+ cancer cell lines (159). Based on these findings, the safety and efficiency of this engineered TCR T cells were evaluated in 12 HPV positive cancer patients (NCT02280811).The clinical results showed that administration of E6 TCR T cells caused tumor regression in two out of twelve patients (160). Another TCR T cells reactive to $E6_{29-38}$ epitope of HPV16 has been generated by TCRCure Biopharma Ltd and it is being evaluated in a phase I clinical trial (NCT03578406). Jin et al identified a high affinity TCR targeting $E7_{11-19}$ epitope from cervix-infiltrating lymphocytes of a patient with HPV16+ CIN II/III (161). This engineered TCR T cell was assessed in a phase I/II clinical trial for therapy of metastatic HPV positive cancers (NCT02858310). According to their recent published results, robust tumor regression was

observed in 6 of 12 patients, including 4 of 8 patients suffering anti-PD-1 refractory disease (162). Therefore, cellular therapy, especially engineered TCR T cells can be a promising modality for treatment of HPV associated cancers.

## 1.4 Outline of the thesis

Cell based therapy has the potential to be one of the leading approaches for therapy of HPV positive cancers. There are several ongoing clinical studies to evaluate the efficacy and safety of engineered TCR T cells in HPV associated cancers, However, there is a need for further investigation and characterization of HPV specific TCRs. It has been shown that tumor samples from patients in developing stages of HPV+ cancers might not be optimal for identification of HPV-specific TCRs, since they show weak TIL responses against the E6/E7 oncoprotein (161). It is also important to note that under chronic antigen presentation in tumor tissue, the selective pressure that TILs experience can change the TCR repertoire making the identification of high avidity functional TCRs more difficult. Moreover, HPV16-specific CTLs can rarely be detected in the peripheral blood of HSIL and cervical cancer patients compared to healthy individuals. (118). Consequently, *in vitro* stimulation of T cells from healthy donors, who have not been exposed to HPV antigens constantly for a long time, could provide a much broader range of TCRs having different recognition capabilities, as we have shown recently for SARS-CoV-2 (163).

Several studies have tried to generate CTLs by *in vitro* stimulation of PBMCs extracted from healthy donors or HPV+ cancer patients. It has been shown that the transfer of TCR sequences from CTL clone obtained by *in vitro* stimulation of healthy donor CD4+ T cells with an HPV16 E6 epitope, can be used to generate human CD4+ T helper cells which are specific for HPV16+

tumor cells (164). Schreurs et al. showed that CTLs reactive to HPV16 E7 could be generated by *in vitro* stimulation of low frequency CD8β+ precursors derived from healthy donors. In order to get antigen specific CTL clones, they used double tetramer staining isolation followed by limiting dilution cloning. These clones showed reactivity to a CxCa cell line transformed by HPV16 (165). In another study, E7 specific T cells were generated by *in vitro* stimulation of CD8+ T cells derived from patients with squamous cell carcinomas of the oropharynx (SCCO) and from healthy donors (166). In this study there was no significant difference in the frequencies of *in vitro* stimulated antigen specific T cells of SCCO patients compared to normal donors. These T cells were able to target HPV16 E7- expressing Caski cell line. In both of these studies, the $E7_{11-20}$ was considered as the epitope being presented by HPV16+cancer cell. However, it has been shown that $E7_{11-19}$ is the most conserved epitope among HPV 16 strains (167).

Moreover, previous studies have focused on isolating, by serial dilutions, a single clone of CTL reactive to $E7_{11-19}$ and did not use single cell analysis to get the entire TCR repertoire reactive to $E7_{11-19}$. It has been shown that thousands of different TCRs can recognize an immunodominant epitope and, conversely, that one TCR can recognize thousands of different peptides, which ensures effective immune coverage of all, or nearly all, foreign peptides (168). This suggests that an efficient immunotherapy will not be possible if just one TCR clonotype is used. Therefore, considering $E7_{11-19}$, as the true HLA-A2-restricted epitope and using current advanced single cell analysis platforms for identifying the exact profile of TCRs should provide a wide range of TCRs with different affinities. Efficient protocols for *in vitro* activation and expansion of $E7_{11-19}$ specific T cells are needed to provide larger numbers of T cell clones to be tested as candidates for generation of engineered TCR T cells.

Nilges et al., showed that *in vitro* restimulation with the $E7_{11-19}$ peptide did not increase the tetramer positive T cells in PBMCs from neither healthy donors nor cervical cancer patients (169). However, Tatiana et al., demonstrated that using an E6/E7-p16INK4 fusion protein they could enhance cytotoxic CD8+ T cell priming and the number of tetramer positive cells (170). However, they could not identify E6/E7-specific TCR clonotypes.

The aim of this study was to identify and characterize TCR clonotypes of $CD8^+$ T cells reactive to the $E7_{11-19}$ epitope of HPV-16. In order to do that, we sought to induce efficient maturation of DCs and presentation of the $E7_{11-19}$ epitope using a fusion protein called E7Flt3L that was generated previously in our laboratory (Cid-Arregui, unpublished results, patent application pending). This protein is composed of an N-terminal fragment of E7 ($E7_{1-30}$) linked to the N terminus of Fms-like tyrosine kinase 3 ligand (Flt3L). Flt3L is a cytokine which, upon binding to its receptor, Flt3, induces a functional differentiation of DCs that can stimulate allogeneic T cells and present antigens to helper and cytolytic T cells (171).

Immature moDcs isolated from PBMCs of healthy donors were pre-incubated with the E7Flt3L fusion protein and then co-cultured with autologous T cells. Then, $E7_{11-19}$-reactive CD8+ T cells were sorted and processed by single-cell V(D)J sequencing using the 10X Genomics platform. By this means we identified a number of E7-specific TCRs, which were cloned in lentiviral vectors for expression in the TCR-deficient Jurkat cell line and in primary $CD8^+$ T cells for *in vitro* characterization. Further *In silico* simulations of several candidate TCRs provided valuable information about the interacting motifs within the CDR3 regions which is a step forward in TCR discovery.

# 2. Materials and Methods

## 2.1 Materials

### 2.1.1 Laboratory equipment

| Equipment | Company |
|---|---|
| 4D-Nucleofector™ System with Core, X and Y Unit | *Lonza* |
| Centrifuge (5810R & 5415D) | *Eppendorf* |
| Chromium Controller | *10x Genomics* |
| Confocal microscope (LSM 700) | *Zeiss* |
| Documentation agarose gels | *Azure Biosystems* |
| Electrophoresis chamber for agarose gels | *Bio-Rad* |
| Electrophoresis power supply | *Bio-Rad* |
| Flow cytometer (FACS Canto II™) | *BD Biosciences* |
| FACSAria™ Fusion cell sorter | *BD Biosciences* |
| Fluorescent microscope (ECLIPSE TS 100) | *Nikon* |
| Freezer (-20°C) | *LIEBHERR* |
| Freezer (-80°C) | *Thermo SCIENTIFIC* |
| Ice machine | *HOSHIZAKI* |
| Incubator (37°C) | *MELAG* |
| Incubator (37°C,5% CO2, cell culture) | *Thermo SCIENTIFIC* |
| Laminar flow hood (HeraSafe™) | *Thermo SCIENTIFIC* |
| Ligand Tracer | *Ridgeview Instruments AB* |
| Light microscope | *Zeiss* |
| Liquid nitrogen tank | *Barnstead* |
| Microwave | *Siemens* |
| Nano Drop | *Thermo scientific* |
| Neubauer cell counting chamber (BLAU BRAND) | *Sigma Aldrich* |
| PCR cycler (MJ Research) | *Bio-Rad* |
| pH Meter | *Knick* |
| Pipettes (multi-channel) | *Eppendorf* |
| Pipettes (single channel) | *Gilson* |
| Platform shaker | *Eppendorf* |
| Quadro MACS TM Separator | *Miltenyi Biotec* |
| Quantitative PCR | *Applied Biosystem* |
| Qubit™ fluorometer | *Invitrogen* |
| Refrigerator (4°C) | *LIEBHERR* |
| Scale | *Satorius* |
| Tape Station system | *Agilent technologies* |
| Ultra-centrifuge (Optima XPN) | *BECKMAN COULTER* |

| | |
|---|---|
| **Ultra-centrifuge rotor (SW480 Ti)** | *BECKMAN COULTER* |
| Victor™ X4 2030 Multilabel Reader | *Perkin Elmer* |
| Vortexer (Sprout®) | *Heathrow Scientific* |
| Water bath | *Julabo* |
| Water purification system | *TKA Teknolab A.S.S.I s.r.l.* |

### 2.1.2 Consumables

| Name | Company |
|---|---|
| 96 well qPCR plate | *Starlab* |
| Cell culture flask (25 $cm^2$) | *TPP* |
| Cell culture flask (75 $cm^2$) | *TPP* |
| Cell culture plate (12-well) | *TPP* |
| Cell culture plate (24-well) | *TPP* |
| Cell culture plate (48-well) | *TPP* |
| Cell culture plate (6-well) | *TPP* |
| Cell culture plate (96- well)<br>Flat bottom<br>U bottom | <br>*TPP*<br>*CELLSTAR* |
| Cell Strainer (40µm) | *BD Falcon* |
| Chromium Next GEM Chip G Single Cell Kit, 48 rxns (PN-1000120) | *10x Genomics* |
| ELISA plate | *Merck* |
| FACS tubes (5 ml Polystyrene round-bottom tube) | *Corning* |
| Falcon tubes (15 ml and 50 ml) | *Corning* |
| Filter (low binding protein, 0.45µm) | *Millipore* |
| MACS separation column LS | *Miltenyi Biotec* |
| Microtubes (0.2 ml, 0.5 ml and 2 ml) | *Eppendorf* |
| MultiDish 2×2 | *Ridgeview Instruments AB* |
| Nunc cell culture dish | *Thermo Fischer Scientific* |
| Pipet tips<br>(With filter)<br>(Without filter) | <br>*STARLAB*<br>*nerbeplus* |
| STAR seal Advanced polyolefin Film | *STARLAB* |
| Syringe (10 ml, 20 ml) | *B.Braun* |

### 2.1.3 Biological and chemical reagents

| Name | Company |
|---|---|
| 2,2'-Azino-bis (3-ethylbenzothiazoline-6-sulfonic acid) diammonium salt (ABTS) | *Sigma Aldrich* |
| Agarose | *Roth* |
| Ampicillin | *Sigma Aldrich* |
| Amppure XP beads | *BECKMAN COULTER* |
| Biomolecular anchor molecule (BAM) | *NOF corporation* |
| Boric acid | *Sigma Aldrich* |
| Bovine serum albumin (BSA) | *Merck Millipore* |
| Carboxyfluorescein (CFSE) | *Biolegend* |
| Citric Acid | *Sigma Aldrich* |
| Dasatinib | *Cayman Chemicals* |
| D-Biotin | *Sigma Aldrich* |
| Dimethyl sulfoxide (DMSO) | *Sigma Aldrich* |
| Ethylenediaminetetraacetic acid (EDTA) | *Sigma Aldrich* |
| Fluorophore-conjugated Streptavidin | *Biolegend* |
| Glucose | *Roth* |
| Hydrogen chloride (HCl) | *VWR International* |
| Hydrogen peroxide ($H_2O_2$) | *Sigma Aldrich* |
| Isopropanol | *Sigma Aldrich* |
| Magnesium chloride ($MgCl_2$) | *Merck* |
| Magnesium sulfate ($MgSO_4$) | *Merck* |
| Monopotassium phosphate ($KH_2PO_4$) | *Merck* |
| Mowiol® | *Sigma Aldrich* |
| Oxalic acid dihydrate | *Sigma Aldrich* |
| Paraformaldehyde (PFA) | *Sigma Aldrich* |
| phorbol 12-myristate 13-acetate (PMA) | *Sigma Aldrich* |
| Potassium chloride (KCl) | *Merck* |
| Sodium azide (NaN3) | *Merck* |
| Sodium chloride (NaCl) | *Sigma Aldrich* |
| Tris Base | *Sigma Aldrich* |
| Tri-sodium citrate dihydrate | *Merck* |
| Tryptone | *Sigma Aldrich* |
| Yeast extract | *Sigma Aldrich* |
| Trypan blue stain (0.4%) | *Gibco® by Life technologies* |
| DNA ladder (1Kb) | *Thermo Fisher Scientific* |
| DNA Gel Loading Dye (6x) | *Fermentas* |
| Triton ×100 | *Sigma Aldrich* |
| Fish Gelatin | *Sigma Aldrich* |

### 2.1.4 Cell culture medium and supplements

| Medium | |
|---|---|
| **Name** | **Company** |
| Dulbecco's Modified Eagle Medium (DMEM) GlutaMAX™ | *Gibco® by Life technologies* |
| Dulbecco's phosphate-buffered saline (D-PBS) | *Gibco® by Life technologies* |
| RPMI 1640 with L-glutamine | *Gibco® by Life technologies* |
| RPMI without Phenol Red | *Gibco® by Life technologies* |
| X-VIVO20™ | *Lonza* |
| **Supplement** | |
| **Name** | **Company** |
| CD39 inhibitor polyoxotungstate 1 (POM-1) | *Biolegend* |
| Fetal Bovine Serum (FBS) | *Gibco® by Life technologies* |
| Ficoll-Paque | *Sigma Aldrich* |
| 4-(2-hydroxyethyl)-1-piperazineethanesulfonic acid (HEPES) buffer solution (1M) | *Gibco® by Life technologies* |
| Interleukin 2 (IL-2), recombinant, human | *Biolegend* |
| Interleukin 15 (IL-15), recombinant, human | *Biolegend* |
| Interleukin-4 (IL-4), recombinant, human | *Biolegend* |
| Interleukin-7 (IL-7), recombinant, human | *Biolegend* |
| Penicillin/Streptomycin-Solution (P/S) | *Gibco® by Life technologies* |
| Recombinant human Macrophage Colony-Stimulating Factor (rhGM-CSF) | *Biolegend* |
| TransAct™- T cell expansion- CD3/CD28 stimulation reagent | *Miltenyi Biotec* |
| Trypsin-EDTA solution (0.25%) | *Gibco® by Life technologies* |

### 2.1.5 Commercial Kits

| **Name** | **Company** |
|---|---|
| ALLin™ Mega HS HiFi Mastermix | *highQu* |
| APC conjugation | *Abcam* |
| $CD8^+$ T cell isolation | *Miltenyi Biotec* |
| Chromium Single cell 5' Library Construction kit, 16rxns PN-1000020 kit | *10x Genomics* |
| Chromium Single Cell V(D)J Enrichment kit, Human T cell (PN-1000005) | *10x Genomics* |
| Cyber Green master mix | |

| | |
|---|---|
| Endo free Maxi prep | *QIAGEN* |
| Gibson Assembly® Cloning | *NEW ENGLAND BioLabs* |
| IFN-γ Catch assay | *Miltenyi Biotech* |
| Jetprime® | *Polypus transfection* |
| Maxima First Strand cDNA | *Thermo Fischer Scientific* |
| QIAprep® Spin Miniprep | *QIAGEN* |
| Next GEM single Cell 5" Library and Gel bead Kit V1.1,4 rxns (PN-1000167) | *10x Genomics* |
| P3 Primary Cell 4D-Nucleofector™ | *Lonza* |
| High Pure PCR cleanup kit | *Roche* |
| QIAquick Gel Extraction | *QIAGEN* |
| Qubit™ 1x dsDNA HS Assay | *Thermo Fischer scientific* |
| RNeasy | *QIAGEN* |
| Single Index Kit T Set A (PN-1000213) | *10x Genomics* |
| TapeStation DNA ScreenTape & Reagents | *Agilent technologies* |
| TransDetect PCR Mycoplasma Detection | *TransGen Biotech* |
| Cyber Green Rox qPCR | *Thermo Fischer scientific* |
| Cell Proliferation Reagent WST-1 | *Sigma Aldrich* |

### 2.1.6 Antibodies

| Name | Clone | Host | Company |
|---|---|---|---|
| **Immunofluorescence microscopy** | | | |
| anti calnexin-rabbit | C5C9 | rabbit | *Cell signaling* |
| anti-Rabbit IgG Cy™2 AffiniPure | Polyclonal | donkey | *Jackson ImmunoReseach* |
| **ELISA** | | | |
| anti-human β2-microglobulin HRP-conjugated | 2M2 | mouse | *Biolegend* |
| **Flow cytometry** | | | |
| anti-CD137-PE Dazzle™ 594 | 4B4-1 | mouse | *Biolegend* |
| anti-CD69-APC | FN50 | mouse | *Biolegend* |
| anti-human CD3-APC | OKT3 | mouse | *Biolegend* |
| anti-human CD3-APC/ Cyanine7 | SK7 | mouse | *Biolegend* |
| anti-human CD3-PE | OKT3 | mouse | *Biolegend* |
| anti-human CD8a-FITC | SK1 | mouse | *Biolegend* |
| anti-human-CD8b-APC | REA 715 | Cell line | *Miltenyi Biotec* |

| | | | |
|---|---|---|---|
| anti-human HLA-A2-APC | BB7.2 | mouse | *Biolegend* |
| anti-mouse TCRβ chain-PE/Cyanine7 | H57-597 | armenian hamster | *Biolegend* |

### 2.1.7 Cell lines

| Name | Description | Source | Medium |
|---|---|---|---|
| **Adherent cell lines** | | | |
| Caski | Human, cervix, HPV16 positive, HLA-A2 positive | DKFZ | DMEM, 10%(v/v) FBS,1% P/S |
| HEK293T | Human, Kidney | DKFZ | DMEM, 10%(v/v) FBS,1% P/S |
| PCI-13 | Human, Oral cavity squamous cell carcinoma, HPV16 negative, HLA-A positive | DKFZ | DMEM, 10%(v/v) FBS,1% P/S |
| SiHa | Human, cervix, HPV16 positive, HLA-A2 negative | DKFZ | DMEM, 10%(v/v) FBS,1% P/S |
| UPCI-SCC154 | Human, head and neck squamous cell carcinoma, HPV16 positive, HLA-A2 positive | DKFZ | DMEM, 10%(v/v) FBS,1% P/S |
| **Suspension cell lines** | | | |
| Jurkat 76Δ, CD8αβ$^{+}$ | Human, Lymphoblast | DKFZ | RPMI, 10%(v/v) FBS,1% P/S |
| T2 | Human, Lymphoblast | DKFZ | RPMI, 10%(v/v) FBS,1% P/S |

### 2.1.8 Buffers and solutions

| Name | Components and details | |
|---|---|---|
| **Cell staining and isolation** | | |
| FACS (0.5 L) | BSA | 2.5 g |
| | D-PBS | 500 ml |
| | Filtrate and store | -20°C |
| PBMC Isolation buffer | D-PBS | 500 ml |
| | EDTA | 2 mM |
| | Store | 2-8°C |
| $CD8^+$ T cell Isolation buffer | FACS | 50 ml |
| | EDTA | 2 mM |
| | Store | 2-8°C |
| **Molecular Biology** | | |
| 10x PBS (1L) | NaCl | 80 g |
| | KCl | 2 g |
| | $KH_2PO_4$ | 2 g |
| | $Na_2HPO_4.2H_2O$ | 18.2 g |
| | pH | 7.3 |
| | Store | RT |
| 10x TBE (1L) | Tris base | 108 g |
| | Boric acid | 55 g |
| | EDTA (0.5M) | 40 mL |
| | pH | 8.3 |
| | Store | RT |
| **Flex-T™ tetramer preparation** | | |
| Blocking solution | D-Biotin (50mM) | 1.6 µl |
| | NaN3 10% (w/v) | 6 µl |
| | PBS | 192.4 µl |
| **ELISA** | | |
| 10x Dilution buffer (0.5 L) | NaCl | 29.22 g |
| | Tris base | 30.29 g |
| | BSA | 5 g |
| | Tween-20 | 1 ml |

| | | |
|---|---|---|
| | Deionized (DI) water | 400 ml |
| | pH | 8.0 |
| | Filter, store | 2-8°C |
| 1x Dilution buffer (0.5 L) | 10x Dilution buffer | 50 ml |
| | DI water | 450 ml |
| | Store | 2-8°C |
| 10x Substrate buffer | Citric Acid (0.1M) | 59 ml |
| | Tri-Sodium Citrate dihydrate (0.1 M) | 41 ml |
| | pH | 4.0 |
| | Filter and store | 2-8°C |
| 50x ABTS stock solution (0.1L) | ABTS | 2.195 g |
| | Filtered DI water | 100 ml |
| | Store | 2-8°C |
| 100x Hydrogen peroxide stock solution | $H_2O_2$ (30%) | 1 ml |
| | Filtered DI water | 49 ml |
| | store | 2-8°C |
| Substrate solution | DI water | 10.34 ml |
| | 10x Substrate buffer | 1.2 ml |
| | 50x ABTS solution | 240 µl |
| | 100x Hydrogen peroxide solution | 120 µl |
| Stop buffer | Oxalic acid dihydrate | 2 g |
| | DI water | 100 ml |
| | Store | RT |
| **Immunofluorescence microscopy** | | |
| Blocking solution | BSA | 2% |
| | FBS | 2% |
| | Fish Gelatin | 0.2% |
| | Dissolved in PBS | |
| **Media for Bacterial Cultivation** | | |
| SOB medium (1L) | Tryptone | 20 g |
| | Yeast extract | 5 g |
| | NaCl | 0.58 g |
| | KCl | 0.18 g |
| | MgCl2 | 0.95 g |
| | MgSO4 | 1.20 g |
| | pH | 7.0 |
| SOC medium (1L) | SOB medium | 1L |
| | Glucose | 3.6 g |
| LB-medium (1L) | Tryptone | 10 g |

| | | |
|---|---|---|
| | Nacl | 10 g |
| | Yeast extract | 5 g |
| | pH | 7.0 |
| LB-Agar (1L) | Tryptone | 10 g |
| | NaCl | 10 g |
| | Yeast extract | 5 g |
| | Agar | 15 g |
| | pH | 7.0 |

### 2.1.9 Plasmids

| Name | Company |
|---|---|
| **Lentiviral vector** | |
| PHIV-eGFP | *Addgene* |
| pMD2.G | *Addgene* |
| pCMV delta R8.2 | *Addgene* |

### 2.1.10 Competent bacteria

| Name | Company |
|---|---|
| **Gibson Assembly** | |
| NEB 3-alpha Competent E. coli | *NEW ENGLAND BioLabs* |
| **Transformation** | |
| One Shot™ MAX Efficiency™ DH5α-T1$^R$ Competent Cells | *Thermo Fischer Scientific* |

### 2.1.11 Enzymes for molecular biology

| Name | Company |
|---|---|
| Calf Intestinal Alkaline Phosphatase (CIAP) | *Thermo Fischer Scientific* |
| T4 DNA ligase | *Thermo Fischer Scientific* |
| **Restriction Enzymes** | |

| | |
|---|---|
| BamH1 (10 U/µl) | *Addgene* |
| Xbal (20 U/µl) | *NEW ENGLAND BioLabs* |
| Xmal (Cfr91) (10U/µl) | *Thermo Fischer Scientific* |

### 2.1.12 Peptides

| Name | Source | Region | Amino acid | HLA allele | Company |
|---|---|---|---|---|---|
| Cytomegalovirus pp65 | CMV | 495-503 | NLVPMVATV | HLA-A*02:01 | *ProteoGenix* |
| $E7_{11-19}$ | HPV16 | 11-19 | YMLDLQPET | HLA-A*02:01 | *ProteoGenix* |
| Epstein-Barr nuclear antigen 4 | EBV | 416-424 | IVTDFSVIK | HLA-A11 | *ProteoGenix* |
| HIV-1 pol | HIV | 476-484 | ILKEPVHGV | HLA-A*02:01 | *ProteoGenix* |

### 2.1.13 Software

| Name | Company |
|---|---|
| 7500 Real-Time PCR | *Applied Biosystem* |
| BD FACS Diva software | *BD Biosciences* |
| BioRender | *BioRender* |
| Chromas 2.1.1 | *Technelysium Pty Ltd* |
| EndNote X8 | *Thomas Reuters* |
| FlowJo 10.1 | *TreeStar* |
| GraphPad Prism 8.4.0 | *GraphPad* |
| Loupe™ V(D)J Browser V3.0.0 | *10x Genomics* |
| MS Office 2016 | *Microsoft Corporation* |
| SnapGene® 5.1.5 | *GSL Biotech LLC* |

## 2.2 Methods

### 2.2.1 General cell culture methods

The cell culture was done under sterile conditions in a laminar flow hood. Media and solutions were sterilized and the equipment was disinfected by 70% ethanol prior to usage. The surface of the laminar flow hood was disinfected by UV lamp. All the cells were regularly screened for mycoplasma contamination by Trans Detect PCR Mycoplasma Detection Kit (*TransGen Biotech*).

#### 2.2.1.1 Culturing and passaging of the cells

Adherent and suspension cell lines were cultured in an incubator at 37°C, 5% CO2 with relative humidity of 95%. The cell culture flasks or plates were removed following the second cell passage. The cells were screened regularly under the light microscope to notice any changes in their culture and they were split or frozen upon reaching ≥70% confluency. The adherent cells were treated with 1 ml or 2 ml Trypsin-EDTA (0.05%), phenol red (*Gibco® by Life technologies*), for T25 or T75 cell culture flasks respectively. The cells were incubated with Trypsin at 37°C, 5% CO2 for 1-2 min to be detached. The treated adherent cells were harvested with 4-5 ml of the serum containing culture medium and centrifuged at 400×g for 5 min. Following the removal of supernatant, the cells were resuspended in their appropriate medium (section 2.1.7) and transferred to the suitable culture flask/plate, split for the experiment or proceed for freezing. The adherent cells were kept in culture at density of 0.5-1×$10^6$ cells/ml. The suspension cells were harvested and centrifuged at 400 ×g for 5 min. They were resuspended in fresh culture medium and according to the cell number they were split, used for experiment or frozen. The suspension cell lines were kept in culture at density of 0.5-1×$10^6$ cells/ml.

#### 2.2.1.2 Freezing and thawing of the cells

The cells at confluence of ≥ 70% were processed for freezing. The adherent cells were trypsinized as described in section 2.2.1.1. The suspension cells were also collected and centrifuged with the same condition to remove the old medium and washed with 1x D-PBS (*Gibco® by Life technologies*). The cells were counted by Neubauer cell counting chamber and $1\times10^6$-$1\times10^7$ cells resuspended in 900 µl FBS + 100µl DMSO in a cryotube (DMSO 10%). The cryotubes were kept on ice and placed into Cryo-safe cryogenic cooler at -80°C freezer. On the following day, the tubes were transferred to liquid nitrogen tank for prolonged storage.

For thawing the cells, the temperature of the water bath was set at 37°C and 5 ml pre-warmed culture medium was prepared in 15 ml canonical falcons. The frozen cryotubes were thawed quickly in the water bath and transferred to the respective falcons. The cells were centrifuged at 400×g, 5 min and washed with their culture medium. Afterwards, they were put in appropriate cell culture flask/plate according to the cell number. In the next day, the culture medium was exchanged with fresh medium to eliminate any residual DMSO.

#### 2.2.1.3 Peripheral blood mononuclear cell (PBMC) isolation

PBMCs were isolated by Ficoll-Paque (*Sigma Aldrich*) density gradient centrifugation from Leukopaks of HLA-A*02:01+ healthy donors ordered from blood bank (IKTZ Heidelberg). As the first step, the blood was diluted with 2-4x volume of the buffer (Section 2.1.8) to increase the purity of the PBMCs. Then, 35mL of the diluted cell suspension was layered carefully over 15 ml of Ficoll-Paque in a 50 ml canonical tube and centrifuged at 400×g for 30 min at 20°C in a

swinging bucket rotor without brake. After the centrifugation, the layers were separated in the following order from top to bottom: Plasma, PBMCs, Ficoll, Granulocytes, Erythrocytes. The upper layer was removed and mononuclear cell layer was carefully transferred to a new 50 ml canonical tube. Around 40 ml buffer was added to the cells and centrifuged at 400×g for 10 min at 20°C. In order to remove the platelets, the cells were washed twice with 50 ml buffer and centrifuged at 200 ×g for 10-15 min at 20°C. The purified PBMCs were counted and frozen in several aliquots for further experiments.

#### 2.2.1.4 Generation of hmo-imDCs

The PBMCs were transferred to adherent tissue culture plates and incubated at 37°C, 5% CO2 for 2 h. The non-adherent cells containing the T cells were collected and frozen or kept in culture for further experiments. The adherent cells were cultured in X-VIVO20™ medium which was supplemented with rhGM-CSF (10 ng/ml) and IL-4 (10ng/ml) (*Biolegend*). After 3 days, the medium was supplemented again with the same concentration of cytokines. Following one week of treatment, the hmo-imDCs were ready to be used in the experiments.

#### 2.2.1.5 Flow cytometry

All the sample preparation steps were done on ice and covered from the light. The cells were collected and centrifuged at 300 ×g for 5 min at 4°C. The supernatant was discarded and the cells were washed with pre-chilled FACS buffer (Section 2.1.8) and centrifuged with the same condition. The cells were put on ice and resuspended in 50µl of FACS including the appropriate

dilution of antibodies. Following 30 min incubation on ice and in the dark, the cells were washed twice with FACS buffer to remove any unbound antibodies. In case of multi color staining, some cells of the same kind were stained with each antibody to be used as single staining. Finally, the cells were resuspended in 100µl FACS buffer and proceeded for flow analysis. The BD FACS Canto™ II flow cytometer and cell sorter from DKFZ FACS core facility were used for the measurements and sorting of the cells. During the measurement, the cells were kept on ice in the dark. The voltages were set based on the unstained control and the compensation was done via single staining samples. The flow cytometry data were analyzed by FlowJo™ v10.8.

## 2.2.2 *In silico* and *in vitro* analysis of E7-Flt3L fusion protein

### 2.2.2.1 *In silico* analysis of the fusion protein

Recombinant E7-Flt3L protein was designed and purified previously in our lab (Cid-Arregui et al, unpublished results). The physical properties of the E7-Flt3L fusion protein were calculated by ProtParam tool from Expasy and they were taken as the reference for optimization of all buffers used for protein purification (172). The 3D structure of the fusion protein was predicted by Galaxy TBM server using template-based modeling approach (173). Further refinement of the top-scored model was done via Galaxy Refine server (174). The crystal structure of hFlt3-FL complex was retrieved from PDB database (PDB ID: 3QS9) served as the control. The unwanted and water molecules were deleted from this pdb file and importantly the Flt3 structure was extracted for docking analysis. The refined 3D model of E7-Flt3L and Flt3 was exposed to a flexible protein-protein docking by SwarmDock tool (175). The binding energy ($\Delta G_{interaction}$) of

the top-scored docking complex was calculated by PRODIGY (176) according to the following formula:

$$\Delta G_{interaction} = -0.09459\ ICs_{charged/charged} -0.10007\ ICs_{charged/apolar} +0.19577\ ICs_{polar/polar} -0.22671\ ICs_{polar/apolar} +0.18681\ \%NIS_{apolar} +0.3810\ \%NIS_{charged} -15.9433$$

IC stands for interfacial contacts of two interactors and they are classified according to the polar, apolar and charged properties of the interacting residues. Moreover, a distance threshold of 5.5 Å was considered between heavy atoms. The physico-chemical properties of E7-Flt3L and hFlt3L wild type was also compared using ProtParam.

#### 2.2.2.2 Indirect immunofluorescence microscopy

The E7-Flt3L fusion protein was labeled with the APC conjugation kit (*Abcam*). 10µl of E7-Flt3L (1.3 mg/ml) was mixed gently with 1µl of APC modifier reagent. The cap of the APC conjugation Mix vial was removed and the E7-Flt3L with added APC modifier reagent was pipetted directly onto lyophilized material and resuspend gently. The cap of the vial was closed and incubated in the dark at RT for 3 hours. Then, 1µl of APC Quencher reagent was added to the suspension and mixed gently. The conjugates were ready to use after 30 minutes. PBMCs isolated from one healthy donor were seeded in 96-well plate wells containing glass covers slips and hmo-imDcs were generated as described in section 2.2.1.4. The hmo-imDcs were incubated with E7-Flt3L (5µg/ml) at 37°C for 3h. Then, the cells were washed and fixed with paraformaldehyde 2% for 10 min. The permeabilization of the hmo-imDcs was done by incubation of the cells with triton 0.1% for 5 min. The cells were washed and incubated with blocking solution (Section 2.1.8) for 1

h at RT. Afterwards the cells were incubated with primary antibody C5C9 Rabbit mAB anti-calnexin diluted 1:50 (*Cell Signalling*) overnight at 4 °C to stain the Endoplasmic reticulum (ER). In the following day, the cells were washed and incubated with the secondary antibody Cy™2 AffiniPure Donkey Anti-Rabbit IgG diluted 1:100 (*Jackson Immuno Research*) for 1 h at RT. Then the cells were washed three times with PBS (Section 2.1.8). In order to recognize the nucleus, the cells were stained with DAPI solution (5µg/ml) and mounted by Mowiol® (*Sigma Aldrich*). In one slide the primary antibody skipped to be used as the negative control and the images were taken via confocal microscope Zeiss LSM 700.

#### 2.2.2.3 Incubation of hmo-imDCs with E7-Flt3L

The PBMCs were isolated from three different healthy donors and the hmo-imDCs were generated based on the protocol described in method 2.2.1.4. The hmo-imDCs were incubated with E7-Flt3L at concentration of 1 µg/ml, 5 µg/ml, 10 µg/ml for 18 and 42 hours at 37°C. To analyze the maturation of the hmo-imDCs, the cells were stained with CD11c (FITC), CD80 (PerCp.Cy5.5), CD83 (APC.cy7), CD86 (APC) (*Biolegend*) and processed to flowcytometry analysis. In order to analyze the binding of the E7-Flt3L to its receptor Flt-3 (CD135), the hmo-imDcs were incubated with E7-Flt3L (5 µg/ml) for 30 minutes on ice in the dark. Then, the cells were washed and stained with CD11c (FITC) and CD135 (PE) (*Biolegend*) and the samples were analyzed by flowcytometry.

### 2.2.3 Stimulation and identification of T cells reactive to E7 $_{(11-19)}$ with E7-Flt3L fusion protein

In order to identify the T cells reactive to E7$_{(11-19)}$ epitope, the cells were stimulated with E7-Flt3L fusion protein and analyzed by tetramer staining and IFNγ catch assays, which are described in the following sections. The schematic representation of these steps is depicted in Figure 8.

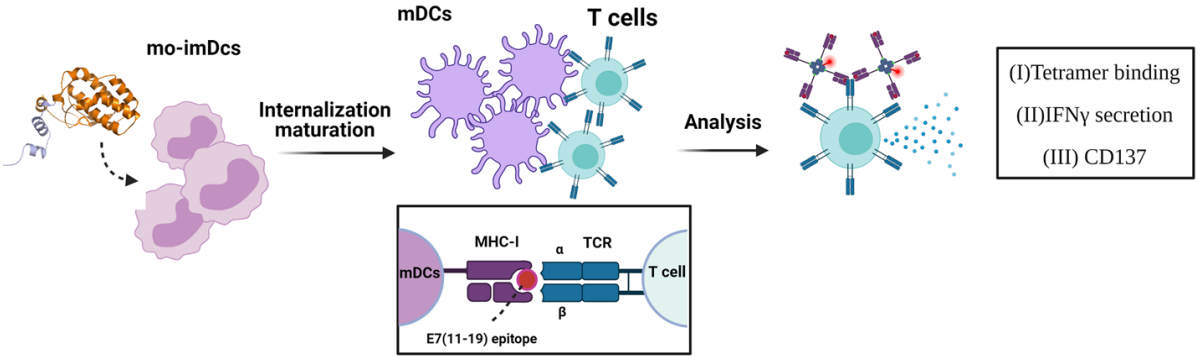


**Figure 8. *In vitro* stimulation of T cells with hmo-imDCs loaded with E7-Flt3L.** The upregulation of activation markers such as CD137, secretion of IFNγ and tetramer binding of the cells were analyzed.

#### 2.2.3.1 Preparation of E7$_{(11-19)}$ loaded Flex-T™ tetramers

The Flex-T technology of Biolegend was used for preparation of E7$_{(11-19)}$ tetramers. The E7$_{(11-19)}$ peptide stock was diluted to 400µM by D-PBS. Then, 20µl of diluted E7$_{(11-19)}$ peptide (400µM) was added to 20µl peptide Flex-T™ monomer UVX (200µg/ml) into a 96 well U bottom plate and mixed well by pipetting up and down. The plate was placed on ice, without lid, and illuminated with UV light (366 nm) for 30 min. Afterwards, the plate was incubated at 37°C for 30 min. 30µl

of the suspension was transferred to a new well and the rest of it was used for peptide exchange analysis by ELISA (Section 2.2.3.2). Then, 3.3µl APC.cy7-streptavidin or APC-streptavidin (0.2mg/ml) (*Biolegend*) was added to the suspension and incubated on ice in the dark for 30 min. To form the tetramers, 2.2µl of blocking solution (Section 2.1.8) was added to the mixture and incubated overnight at 2-8°C or 30 min on ice in the dark. Moreover, the blocking solution can be divided into four portions and added gradually to the monomer mixture by 10 min intervals for more efficient tetramer formation.

**2.2.3.2 Evaluation of peptide exchange on Flex-T™ monomers by ELISA**

Flex-T™ HLA class I ELISA was performed to evaluate the efficiency of peptide exchange. The Epstein-Barr nuclear antigen 4 and Cytomegalovirus pp65 (495-503) peptide were used as negative and positive control, respectively. The peptide exchange was done as described in section 2.2.3.1 and the samples were used for ELISA experiment. The Streptavidin solution was prepared by diluting streptavidin in 1X coating buffer (*Biolegend*) (1: 500) and 100µl of the solution was added to the wells of the ELISA plate. The plate was sealed and incubated overnight at RT. The coating solution was discarded and the plate was washed three times with 300µl 1X wash buffer (*Biolegend*). In order to block the non- specific binding and reduce the background, 300 µl 1X Dilution buffer (Section 2.1.8) was added to the wells and the plate was incubated for 30 min at RT. A small aliquot of peptide exchange reaction was diluted 1400- fold in 1X Dilution buffer, mixed well and 100µl was added to the related wells. 100µl of 1X Dilution buffer was used as the blank control. The plate was sealed and incubated for 1 hour at 37°C.

Afterwards, the wells were washed three times with 300µl 1x wash buffer (*Biolegend*). The concentrated HRP-conjugated anti-human β2-microglobulin antibody (0.2 mg/ml) (*Biolegend*) was diluted to 0.3µg/ml in 1X Dilution buffer and 100µl of it was added to the wells. The plate was incubated again at 37°C for 1 hour and washed three times with 1X wash buffer. The substrate solution was prepared around 10 min prior to use (Section 2.1.8), added to the wells and incubated at RT for 8 min in the dark on a plate shaker at 400-500 rpm. Finally, 50µl of stop solution (Section 2.1.8) was added to each well and the plate was measured on an ELISA reader at 405 nm.

#### 2.2.3.3 IFNγ catch assay and $E7_{(11-19)}$ tetramer staining

The cells were collected and centrifuged at 300 ×g for 5 min at 4°C to remove the medium. Then, they were washed with pre-chilled FACS buffer (Section 2.1.8) and 5µl of IFNγ catch reagent (*Miltenyi Biotech*) was diluted in 20µl FACS buffer and added to the cells. The cells were incubated for 5 min on ice and then 1 ml pre-warmed X-VIVO20™ was added to the samples. The tubes were put on a rotator and incubate at 37°C for 45 min. Afterwards, the cells were washed and the supernatant was discarded. The tetramers were centrifuged at high speed for 1-2 min to sediment the streptavidin residues. The $E7_{(11-19)}$ loaded Flex-T™ tetramers conjugated with APC.Cy7 were diluted in FACS buffer in ratio 1:100, added to the cells and incubated on ice for 30 min in the dark. The cells were washed and stained with CD3 (APC), CD8 (FITC), CD137 (PE-dazzle™ 594) (*Biolegend*) and IFNγ (PE) (*Miltenyi Biotech*) antibodies at

2µg/mL concentration. The samples were incubated on ice for 30 min in the dark. Finally, the samples were washed and measured by flow cytometry analysis by BD FACSCanto™.

#### 2.2.3.4 *In vitro* stimulation of T cells using E7-Flt3L fusion protein

The non-adherent part of the PBMCs Section 2.2.1.4 were cultured in X-VIVO20™ which was supplemented with IL-2 (20 ng/mL) (*Biolegend*) up to one week. The hmo-imDCs were incubated with E7-Flt3L (5µg/ml) for 18 h. In the following day, the non-adherent cells which contained T cells were put in culture with hmo-DCs in ratio of 1:5 (DCs: effector) and incubated for 2, 5 and 12 days. The co-culture medium was X-VIVO20™ supplemented with IL-7 (10 ng/mL) (*Biolegend*) and IL-15 (10 ng/mL) (*Biolegend*). To compare the effect of $E7_{(11-19)}$ peptide with the fusion protein, the hmo-imDCs were also incubated with 10µM of the peptide for 16-18h prior to the co-culture with the T cells. After finishing the incubation time, the cells were collected and subjected to IFNγ-catch assay, tetramer and antibody staining (Section 2.2.3.3).

#### 2.2.3.5 Sorting of the $CD8^+$ T cells reactive to $E7_{(11-19)}$ epitope

T cells from one healthy donor were stimulated using E7-Flt3L (5µg/ml) for 12 days as described in section 2.2.3.4 and around 4774 cells $CD3^+$/ $CD8^+$/ $IFN\gamma^+$/ $E7_{(11-19)}$ $tetramer^+$, were sorted. T cells from two other healthy donors were stimulated with E7-Flt3L (5µg/ml) for 5 days and around 2530 cells $CD3^+$, $CD8^+$, $IFN\gamma^+$/ $CD137^+$/ $E7_{(11-19)}$ $tetramer^+$ were sorted. The sorting of the $CD3^+CD8^+$ T cell was done on a BD FACSAria™ Fusion cell sorter, 80µm Nozzle and 4-way Purity

precision mode. The cells were frozen as described in section 2.2.1.2 and transferred to liquid nitrogen.

## 2.2.4 Single cell V(D)J sequencing and data analysis

The CD8$^+$ T cells which were [IFNγ+-tet+] or [CD137+/IFNγ+/tet+] were sorted and processed for single cell V(D)J sequencing (*10x Genomics*) for identification of TCR repertoire as shown in Figure 9.

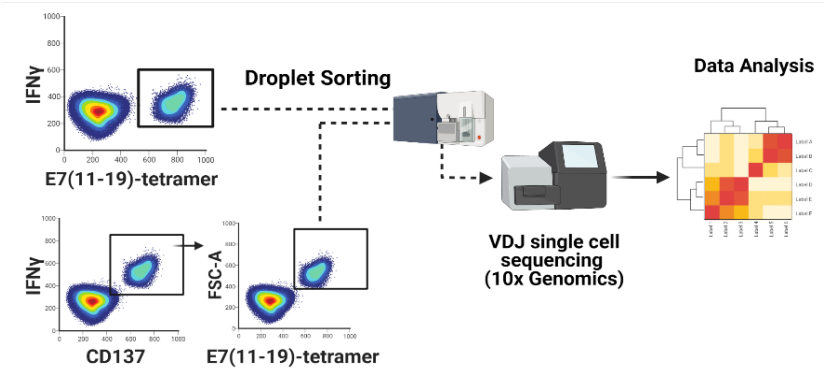


**Figure 9. Droplet sorting of the CD8$^+$ T cells according to the activation markers and tetramer binding.** The sorted cells were processed for single cell V(D)J sample and library preparation. The sequencing data were analyzed to retrieve the TCR repertoire.

### 2.2.4.1 Library preparation and sequencing

The library construction was done according to the Chromium Single Cell V(D)J user guide. All the steps of library preparation were carried out in the single-cell Open Lab (scOpenLab) at DKFZ. The sorted cells were thawed as described in section 2.2.1.2 and resuspended in 31.7µl of Nuclease free water. The cells were subjected to GEM generation and barcoding using

Chromium Next GEM single Cell 5" Library and Gel bead Kit V1.1,4 rxns (PN-1000167). The samples were loaded in the Chromium Next GEM Chip G Single Cell Kit, 48 rxns (PN-1000120) according to the manufacturer recommendation and transferred to the Chromium Controller (*10x Genomics*). Following successful GEM generation, the samples were subjected to GEM-RT cleanup using Dynabeads MyOne SILANE (PN-2000048) provided in the kit. The cDNA of each library was amplified and cleaned-up via Amppure XP beads (*BECKMAN COULTER*). The concentration of the cDNA was measured using Qubit™ 1x dsDNA HS Assay Kit (*Thermo Fischer scientific)* and Qubit™ fluorometer (*fischer scientific)*. The quality control (QC) of the amplified cDNA was done by Agilent TapeStation ScreenTape and Reagents. The average size of the cDNA library of [IFNγ+-tet+] and [CD137+/IFNγ+/tet+] was 1416 bp and 1443 bp, respectively. Then, the cDNA went through target enrichment using Chromium Single Cell V(D)J Enrichment kit, Human T cell (PN-1000005). The enrichment was done in two steps and Human T cell mix 1 (PN-Human 2000008) containing Forward primer (2µM) and Reverse Outer primer (1 µM) was used in the first phase. Following the PCR reaction and cleanup, the target enrichment 2 was performed via Human T cell mix 2(PN- Human 2000009) containing Forward primer (2µM) and Reverse Inner primer (1 µM). After target enrichment, the concentration and QC of the samples were evaluated as described previously. The enriched Library construction was done using the Chromium Single cell 5' Library Construction kit, 16rxns PN-1000020 kit and these steps were followed sequentially according to the manufacturer protocol: Fragmentation, End Repair & tailing, Adaptor Ligation, Post Ligation Cleanup-selection with Amppure XP beads, sample Index PCR, double sided Size selection with Amppure XP beads and finally post library construction QC. The indexing of the libraries was done by Single Index Kit T Set A (PN-1000213). [IFNγ+-tet+]

and [CD137+/IFNγ+/tet+] libraries were indexed by F1 and F2, respectively. The nucleotide content of the indexes is shown in Table 1.

The average size of the libraries was 580 bp and they were multiplexed and submitted to the sequencing core facility at DKFZ. The sequencing was performed using MiSeq reagent Kit V2 and MiSeq ™- System (*Illumina*). The paired End sequencing with read length of 250 bp was done to retrieve the full length TCR sequence.

**Table 1.The nucleotide content of indexes used for indexing the libraries.**

| Name | Nucleotide |
|---|---|
| **IFNγ-tet library** | |
| **SI-GA-F01-a** | GTTGCAGC |
| **SI-GA-F01-b** | TGGAATTA |
| **SI-GA-F01-c** | CAATGGAG |
| **SI-GA-F01-d** | ACCCTCCT |
| **CD137-IFNγ-tet library** | |
| **SI-GA-F02-a** | TTTACATG |
| **SI-GA-F02-b** | TGGAATTA |
| **SI-GA-F02-c** | ACGCGGGT |
| **SI-GA-F02-d** | GAATTCCA |

### 2.2.4.2 Analysis of the single cell sequencing data

The sequencing data were transferred to the project file of our laboratory account in DKFZ large scale data facility (lsdf) by Omics IT and Data Management- Core Facility (ODCF) at DKFZ. The Putty (https://putty.org/) was downloaded to connect to the LSF cluster using the user account to the head node (Host): odcf-lsf01.dkfz.de. The Human reference dataset (GRCH38/Ensemble/10x) was downloaded using wget command:

```
$ wget http://cf.10xgenomics.com/supp/cell-vdj/refdata-cellranger-vdj-GRCh38-alts-ensembl-2.0.0.tar.gz
```

Then the file was untar by this command:

```
$ tar -xzvf file_name.tar.gz
```

and the path of the file was found by:

```
$ Realpath file_name
```

In the terminal, the list of packages was installed using this command:

```
$ module avail
```

Then the cellranger package was loaded:

```
$ module load cellranger/3.0.1.
```

The 10x sequencing data of our library had a specific path in the LSF cluster which was used for data analysis and it was provided by ODCF. The cellranger was run by this command lines:

```
$ cellranger vdj --id=Name of the sample \
            --reference = Path to the cell Ranger V(D)J compatible reference (which
              was found by Realpath command) \
            --fastqs= Path of the FASTQ files\
            --sample= Sample names \
            --localmem=64 (Restricts cellranger to use the specified amount of
              memory Giga bite to execute pipeline stages) \
            --localcores=8 (Restricts cellranger to use the specified number of cores
             to execute pipeline stages
```

The cellranger pipeline was run successfully for both libraries of [IFNγ+-tet+] and [CD137+/IFNγ+/tet+]. The v. loupe file, which was created as one of the outputs of the pipeline, was opened by Loupe™ V(D)J Browser V3.0.0 to visualize the TCR sequences.

## 2.2.5 Expression of candidate TCRs in Jurkat cell line and *in vitro* characterization

### 2.2.5.1 Design of the hybrid murine-human TCR expression cassette

Alpha and Beta variable regions of TCRs targeting HPV16 E7 $_{(11\text{-}19)}$ were selected from our single cell V (D) J sequencing library. In order to improve the efficient expression of transgenic TCRs, two changes in the sequence were applied: (I) Murine constant region was used to generate murine-human hybrid TCR and (II) an additional disulfide bond was introduced by replacing with Cysteines the $Thr^{48}$ on the alpha chain and the $Ser^{57}$ on the Beta chain of the murine constant region. Moreover, a Furin cleavage site, basic amino acids e.g., Arginine and Lysine, a self-cleaving P2A sequence and a strep-tag were also introduced between the alpha chain (alpha variable and alpha murine constant) and beta chain (beta variable and beta murine constant). For efficient cleavage, the Furin cleavage site and P2A were joined with Glysin-Serin spacer. For cloning purposes, two restriction recognition sites XbaI and BamHI were added at 5' and 3' ends of the TCR sequence, respectively. Adding 'ACC' prior to the 5' restriction site of XbaI ensured efficient cleavage. Two termination codons 'TGATAA' were added at 3' of the sequence followed by recognition site of BamHI. Then the coding region was translated by the (https://web.expasy.org/translate/) online tool to confirm the consistency of the protein

sequence. The designed TCR sequence was synthesized by ProteoGenix Inc. The candidate TCRs were named as TCR-EF1-4.

#### 2.2.5.2 Preparation of plasmid vectors for second generation lentiviral vector system

The second-generation system was used for producing Lentiviral vectors (LVs) expressing TCRs. The plasmids consist of the pCMV delta R8.2, pMD2.G and PHIV-eGFP (*Addgene*) which were the packaging, envelope and transfer vectors, respectively. The plasmids were received as bacterial stab and small amounts of them were cultured on agar plates containing 100 µg/ml Ampicillin plate. The precultures (LB containing 50µg/ml Ampicillin) were prepared with one colony of each plasmid, which were grown on the antibiotic agar plates, and inoculated in bigger culture for plasmid preparation. The purification of plasmids was done by Endo free Maxiprep (*QIAGEN*) kit according to the manufacturer protocol. The PHIV-eGFP plasmid was cut with XbaI (*NEW ENGLAND BioLabs)* and BamH1(*Thermo Fischer Scientific)* restriction enzymes. As the enzymes were in Glycerol, the total volume of enzymes was not higher than 10% of the whole reaction (Table 2). The reaction was incubated at 37°C for 1 h and the samples were mixed with 6x loading dye (*Fermentas*) and loaded on a 0.8% agarose gel. As the reference, 3µl of 1kb DNA ladder (*ThermoFisher Scientific*) was used. The gel was run for 60 min at 80 volts. The linearized plasmids were cut and purified from the gel using QIAquick Gel Extraction kit (*QIAGEN*).

**Table 2. Restriction enzyme reaction for digestion of PHIV-eGFP plasmid.**

| reagents | Amount |
|---|---|
| Plasmid PHIV-eGFP | 3µg |
| XbaI (20 U/µl) | 2 µl |
| Bam H1 (10 U/µl) | 2 µl |
| Buffer Tango 1x | 12 µl |
| Nuclease free water | To reach final volume of 50 µl |

As the next step, the phosphate groups of the linearized plasmids were removed CIAP (*ThermoFisher Scientific*). The reaction was set up as described in Table 3 and incubated at 37°C for 30 min. The enzyme was inactivated by heating the sample at 85°C for 10 min. The linearized phosphatase treated PHIV-eGFP plasmid was purified using High Pure PCR cleanup kit (*Roche*). The plasmids were labeled and stored in a -20°C freezer.

**Table 3. The phosphatase reaction on linearized PHIV-eGFP plasmid.**

| reagents | Amount |
|---|---|
| Linearized Plasmid PHIV-eGFP | 2 µg |
| CiAP buffer (10x) | 10 µl |
| CiAP (1U/µl) | 1 µl |
| Nuclease free water | To reach final volume of 100 µl |

### 2.2.5.3 Cloning of the candidate TCRs into the LV transfer vector

The lyophilized pure plasmid of PUC18-TCR-EF1 to EF4 candidates were dissolved in 10µl molecular biology water (0.5 µg/µl). The DH5α chemically component strain E. coli (*Invitrogen*) was used for the transformation. 0.5µl of dissolved DNA TCR were mixed gently with 5µl of DH5α and incubated on ice for 10 minutes. Then the reaction was put in the preheated water bath at 42° for 30s and the cells were immediately transferred on ice for 2 minutes. Afterwards 100µl of prewarmed SOC medium (Section 2.1.8) was added to the cells and incubated at 37°C

for 1 hour at 300 rpm. Spread 50µl of transformation solution to the pre-warmed LB-agar plates (Section 2.1.8) containing 50µg/mL Ampicillin and incubated overnight at 37°C. From the colonies on each plate, the precultures (LB containing 50µg/ml Ampicillin) were prepared by inoculating one colony of each TCR candidate in bigger cultures and incubated overnight at 37°C hour at 190–rpm for plasmid preparation. The purification of plasmids was done using a Midiprep (*QIAGEN*) kit according to the manufacturer protocol. The PUC18-TCR EF1-4 went through restriction enzyme reaction by XbaI and BamH1 and electrophoresis as described in section 2.2.5.2. The inserts were cut and purified from the gel using QIAquick Gel Extraction kit (*QIAGEN*) and mixed with the linearized, phosphatase treated PHIV-eGFP in the molar ratio 1:1. The required amount of each TCR insert was calculated by this formula:

**Required insert (ng) = mass of vector (ng) × ratio of insert/vector × bp insert/bp vector**

The T4 ligase and its buffer (*ThermoFisher Scientific)* were added following the pipetting scheme in Table 4 and incubated at 14°C overnight.

**Table 4. The ligation of TCR candidates in PHIV-eGFP plasmid.**

| reagents | Amount |
|---|---|
| Vector (PHIV-eGFP) | 1 µl |
| Inset (TCR EF1-4) | 1 µl |
| T4 Ligase buffer | 1 µl |
| T4 DNA ligase | 1 µl |
| Nuclease free water | To reach final volume of 10 µl |

One µl of the reaction was used for the transformation of DH5α stain and cultured on Ampicillin agar plate. A successfully transformed colony went through pre-culture, culture and Endofree Maxiprep as described in section 2.2.5.2. The plasmids were sent to Eurofins Genomics for

sequencing and the integrity of pHIV-eGFP-TCR-EF1, PHIV-eGFP-TCR-EF2, PHIV-eGFP-TCR-EF3 were confirmed, however, the position of TRBV and TRAV in PHIV-eGFP-TCR-EF4 was inverted due to a problem in the original sequence. The transfer vectors containing the candidate TCRs were named as PHIV-eGFP-TCR-EF1, PHIV-eGFP-TCR-EF2, PHIV-eGFP-TCR-EF3 and they were stored at -20°C freezer.

#### 2.2.5.3.1 Cloning of TCR-EF4 in PHIV-eGFP vector by Gibson assembly® cloning

The primers for Gibson assembly® cloning were designed by NEBuilder® Assembly Tool (https://nebuilder.neb.com/#!/) to generate the sequence of pHIV-eGFP as depicted in Figure 10. The sequences of the primers are shown in Table. Appendix.1.


**Figure 10. Schematic representation of PHIV-eGFP-TCR-EF4.** The XbaI and XmaI recognition sites (RS) were introduced to the sequence by Gibson assembly®.

The PUC-18-TCR-EF4 was used as the template for generation of gene segments by PCR. The reactions were set up as described in Table 5.

**Table 5. The PCR reaction for generation of gene segments of TCR-EF4.**

| reagents | Amount |
|---|---|
| PUC18-TCR-EF4 | 10 ng |
| Forward primer (10 µM) | 2.5 µl (0.5 µM) |
| Reverse primer (10 µM) | 2.5 µl (0.5 µM) |
| Nuclease free H2O | 19 µl |
| ALLin™ Mega HS HiFi Mastermix (*highQu*), 2X. | 25 µl |
| Final volume | 50µl |

The PCR condition is shown in Table 6 and it was run with all four pairs of primers.

**Table 6. The PCR condition for generation of gene segments of TCR-EF4.**

| Temperature | Time | |
|---|---|---|
| 98 °C | 30 sec | |
| 98 °C | 10 sec | **35 cycles** |
| 67 °C | 30 sec | |
| 72 °C | 45 sec | |
| 72 °C | 5 min | |
| 4 °C | ∞ | |

Following the PCR reactions, electrophoresis was done to confirm the correct amplification of the gene fragments and the PCR products were purified using High Pure PCR cleanup kit (*Roche*). The PHIV-eGFP plasmid was linearized by XbaI (20 U/µl) and XmaI (Cfr91) (10 U/µl) (*Thermo Fischer Scientific*) restriction enzymes by following the protocol described in section 2.2.5.2. The purified linearized plasmid and four gene segments were mixed according to the Table 7.

**Table 7. The mixture of vector and gene segments of TCR-EF4 for Gibson Assembly®.**

| Gene segments | Amount (µl) | Pmole (range: 0.2-1 Pmole) | Size (bp) |
|---|---|---|---|
| PHIV-eGFP (150 ng/µl) | 1.3 | 0.04 | 7686 |
| BV-EF4 (20 ng/µl) | 0.85 | 0.08 | 324 |
| BC-EF4 (20 ng/µl) | 1.7 | 0.08 | 640 |
| AV-EF4 (20 ng/µl) | 1.1 | 0.08 | 414 |
| AC-EF4 (20 ng/µl) | 1.2 | 0.08 | 451 |
| Total | 6.15 | 0.36 | |

The total amount of the fragments was mixed with 10µl of Gibson Assembly Master Mix (2X) and reached the total volume of 20µl by adding DI H2O which was provided in the kit. The positive control (10µl) was also used based on the manufacture recommendation. The sample was incubated at 50°C for 1 h in the thermocycler. Then, 2µl of the assembly reaction was used for transformation of NEB 3-alpha Competent E. coli which was provided in the kit. The same steps described in method 2.5.3 were followed for transformation and plasmid preparation. The sequencing confirmed the integrity of pHIV-eGFP-TCR-EF4 and the plasmid was stored at -20°C freezer.

#### 2.2.5.3.1.1 Addition of the signal peptide to TCR-EF4 sequence

Based on the reference TRBV2 sequence in the VDJ Loupe, the deleted part of the sequence harboring XbaI recognition site at both ends were ordered. The signal peptide sequence was cut by XbaI restriction enzyme and ligated to the PHIV-eGFP-TCR-EF4 vector. The integrity of the sequence was confirmed by sequencing the samples at Eurofins Genomics.

#### 2.2.5.4 Production of LVs expressing candidate TCRs

The procedures of lentivirus production were performed according to the rules and regulations of Biosafety level2 (BSL2). HEK293 T cells ($1\times10^7$) were seeded into each four 75cm$^2$ cell culture flasks one day prior to the transfection. In the following day, the HEK293T cells reached the confluency of ≥80% and the medium was removed and 5 ml fresh medium was slowly added to each flask. According to the Jetprime® manufacturer protocol (*Polypus transfection*), each plasmid should represent at least 10% of the total DNA amount per well/plate and the maximum amount of DNA for 75cm$^2$ cell culture flask was 10µg. The plasmids were mixed in the ratio of 2: 1: 1 (Transfer vector: Packaging vector: envelope vector) and added to 500µl of Jetprime® buffer. The suspension was mixed well and 20µl of Jetprime® reagent was added to it. The mixture was incubated for 10 min at RT and added carefully to the cell culture flask. Following 4h incubation of the HEK 293T cells at 37°C/5% CO2 another 5 ml medium was added to the cells. After 24h, the transfection efficiency was confirmed by fluorescent microscope detecting eGFP signal. The supernatant of the cells was collected after 48h and 72 h, mixed and centrifuged at 400 ×g for 5 min to remove the cell derbies. The supernatant was passed through 0.45µm low binding protein filter *(Millipore)* and transferred to Open Top tubes (*Beckman Coulter*). The tubes were transferred to Ultracentrifuge rotor SW40Ti (*Beckman Coulter*) and run at 75,000 ×g, at 4°C for 2h. The supernatant was removed carefully and the tubes were put upside down onto a paper towel for 2-3 min. To resuspend the LVs, 1ml D-PBS was added to the open top tubes, transferred to 1.5ml Eppendorf tube and centrifuged on a benchtop centrifuge at maximum speed for 1 min. The lentiviruses were aliquoted and stored at -80°C freezer.

#### 2.2.5.4.1 Titration of the LVs based on eGFP expression

In order to titrate the LVs, (1× $10^4$) JurkatΔ76 cell lines were seeded as triplicate in a flat bottom 96 well plate containing 100µl medium. The LVs were added to the cells as triplicates at different dilutions: 1:10, 1:100, 1:500, 1:1000, 1:5000, 1:10000, 1:100000. The plate was incubated at 37°C for 2 days. The cells were collected and centrifuged at 400 ×g for 5 min. The cells were washed and resuspended in 100µl pre-chilled FACS buffer and processed to flow analysis. The transduction was measured by eGFP expression and the titer was calculated by the following Formula:

$$\frac{TU}{mL} = \frac{[\text{Number of cells transduced} \times \text{Percent fluorscent} \times \text{Dilution Factor}]}{(\text{Transduction volume in mL})}$$

#### 2.2.5.5 Transduction of TCR deficient Jurkat cell line with LVs expressing TCRs-EF1-EF4

In one well of a 12 well plate, around 500,000 JurkatΔ76 cell line were seeded. LV of each candidate TCR were added to the cells at MOI (multiplicity of infection) of 1-3 and the cells were incubated at 37°C/5% CO2 for 4 h. Then, another 500µl of fresh medium was added to the cells. The successful transduction of JurkatΔ76 cell line was analyzed by expression of eGFP and staining with murine constant TCR β (mcTCR-β) -PE.cy7. The transduced cells were kept in culture for 1-2 weeks prior to cell sorting. The sorting of the transduced cells was done using 100µm Nozzle and 4-way Purity precision mode in BD FACSAria™ Fusion cell sorter. The sorted cells were expanded and named as Jurkat-EF1, Jurkat-EF2, Jurkat-EF3 and Jurkat-EF4.

### 2.2.5.6 Analysis of the expression of NFAT2 in Jurkat expressing the candidate TCRs

Jurkat expressing the respective candidate TCRs were co-cultured with Caski, SiHa, UPCI-SCC154 and PCI-13 cells at the ratio of Effector to Target (1.5 :1). The cells were incubated at 37°C/5% CO2 for 24h. In the positive control group PMA (20 ng/ml) was added to the TCR engineered Jurkat cell line and one sample of the cell lines was kept untreated to be the negative control. The cells were collected and their RNA was extracted by RNeasy kit (*QIAGEN*). Then the cDNA synthesis was done by Maxima First Strand cDNA kit (*Thermo Fischer Scientific*). The cDNA synthesis was done according to the manufacturer protocol on 80 ng of the RNA. The real-time PCR was done via Cyber Green master mix (*Thermo Fischer Scientific*). The primer sequence of NFAT2 and GAPDH as the reference gene is shown in Table.Appendix.2. The samples were prepared as shown in Table 8.

**Table 8. The Realtime PCR reaction using Cyber Green master mix.**

| Reagents | Amount |
|---|---|
| Master Cyber (2X) | 12.5 µl |
| Primers (R+F) 10 µM | 1 µl |
| cDNA | 2 µl |
| Nuclease free water | 9.5 µl |

The reaction mix was added to the related wells in a 96 well PCR plate (*STARlab*) as triplicates. The Plate was sealed and centrifuged at 200×g for 1 min. The plate was put in the Real time PCR machine (*Applied Biosystem*) and the program shown in (Table 9) was run. The baseline was corrected by (7500 Real-Time PCR Software) and the data were exported as CVS file. The expression of NFAT2 was calculated according to the $2^{\wedge\Delta\Delta Ct}$ (ΔCt experiment -ΔCt Neg.control) formula.

**Table 9. Temperature profile of the real-time PCR reaction.**

| Temperature | Time | |
|---|---|---|
| 50 °C | 2 min | |
| 95 °C | 10 min | |
| 95 °C | 15 sec | **40 cycles** |
| 65 °C | 1 min | |
| **Dissociation** | | |
| 95 °C | 15 sec | |
| 60 °C | 1 min | |
| 95 °C | 15 sec | |
| 60 °C | 15 sec | |

### 2.2.5.7 Analyzing the expression of CD69 in TCR engineered Jurkat cell lines

Cells of the T2 cell line ($1\times10^5$) were seeded in a 96 well U bottom plate in a serum free RPMI medium. The $E7_{(11\text{-}19)}$ and HIV. Pol peptides were added at concentration of 100µM to the T2 cells. The cells were incubated with the peptide at 37°C/5% CO2 for 18h. For analyzing the CD69 expression of Jurkat-EF1 at different concentrations of $E7_{(11\text{-}19)}$, the respective amount of T2 cell lines were incubated with 1, 10 and 100µM of the peptide. The TCR engineered Jurkat cell line and untransduced JurkatΔ76 cell line ($2\times10^5$ cells) were co-cultured with the peptide-loaded T2 cell lines in X-VIVO20™ medium. The cells were pipetted up and down and the final volume of the co-culture was 150µl. The plate was centrifuged at ×200 g for 2 min to increase the cell-cell interaction. The plate was incubated at 37°C/5% CO2 for 20-24h. The cells were collected and centrifuged at 300 ×g for 5 min at 4°C and stained with CD69-APC antibody (*Biolegend*) and processed for flow cytometry measurement and analysis as described in section 2.2.1.5.

### 2.2.5.8 Evaluating the affinity of candidate TCRs to $E7_{(11-19)}$ peptide and HPV16 cancer cell lines

The affinity of the TCR-engineered Jurkat cell lines to the $E7_{(11-19)}$ peptide-HLA-A2 and to the HPV16 cancer cell lines were measured with the Ligand Tracer® (*Ridgeview instruments*). T2 cells ($1\times10^6$ cells) were loaded with $E7_{(11-19)}$ or HIV pol peptide at concentration of 100µM in complete medium and incubated at 37°C/5% CO2 for 16-18h. The MultiDish 2×2 (*Ridgeview instruments*) was treated with 400µl of biomolecular anchor molecule (BAM) (*NOF corporation*) at concentration of 2 mg/ml at the defined position for 40 min at RT. The T2 cell lines were washed with D-PBS and centrifuged at 300 ×g for 5 min. The cells were resuspended in 400µl D-PBS. The BAM was removed without touching the plate and the cells were slowly loaded to the circular position. The T2 cell lines were incubated at RT for 40 min. Then the excess of T2 cells were washed from the MultiDish 2×2 with D-PBS and the plate was filled with 5 ml medium. The schematic representation of the regions loaded with the Peptide-loaded T2 cell lines is shown in Figure 11. The Caski and SiHa cell lines ($1\times10^6$ cells) were seeded in 500 µl of DMEM complete medium on opposite direction on the Nunc cell culture dish (*Thermo Fischer Scientific*) and incubated at 37°C/5% CO2 overnight. On the following day, the remaining of the cells were removed and the plate was washed with D-PBS. The plate was covered with 5 ml DMEM complete medium until measurement.

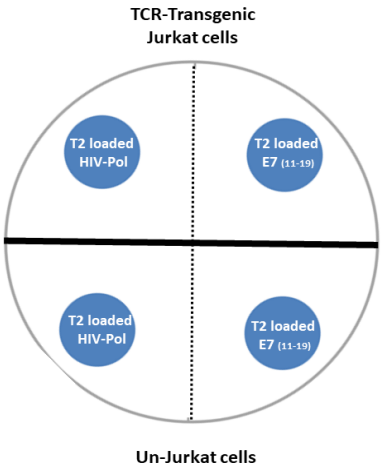


**Figure 11. Schematic representation of MultiDish 2×2 with the T2 cells.** The T2 cell lines were loaded with the $E7_{(11-19)}$ or HIV Pol peptide and seeded in the defined blue position according to the template provided by the manufacturer. The plate was divided into two parts by a rigid border. The transgenic Jurkat cells and Un-Jurkat cell (Untransduced Jurkat cell) were added to the upper and lower part, respectively.

The TCR engineered Jurkat cell lines and untransduced JurkatΔ76 cells, each $5\times10^6$ cells, were stained by 10µM CFSE (*Biolegend*) and 50nM Dasatinib (*Cayman Chemicals*) in 500µl D-PBS. The cells were incubated in the water bath at 37°C for 20 min. Then they were washed two times with D-PBS and centrifuged at 300×g for 5 min. The effector cells were resuspended in 300µl RPMI without phenol red containing 20 mM HEPES. The medium was removed from the plate and 2.5 ml of respective medium was also added to the peptide-loaded T2 cells or HPV16 cancer cell lines. The plate was put in the LigandTracer® in a tilted position and the Detection time of 7s and Delay time of 1s was used for the measurement. The baseline measurement was run for 15-20 min. Afterwards, the stained effector cells were added to the plate. The real-time measurement was run for 1 hour.

## 2.2.6 Expression of candidate TCRs in CD8$^+$ T cells and *in vitro* characterization

### 2.2.6.1 Isolation of CD8$^+$ T cells

Frozen aliquots of PBMCs were thawed as described in section 2.2.1.3 or fresh isolated PBMCs were used for CD8$^+$ T cell isolation with the CD8$^+$ T cell isolation kit, human (*Miltenyi Biotec*). The cells were centrifuged at 300 ×g for 5 min. The supernatant was discarded, resuspended in 1 ml pre-chilled buffer (Section 2.1.8) and the cells were filtrated through 40µm cell strainer (*BD Falcon*) to remove the cell clumps. The cells were centrifuged again and resuspended in the 40 µl of pre-chilled buffer per $10^7$ total cells .10 µl of Biotin-Antibody Cocktail per $10^7$ cells was added to the sample, mixed well and incubated on ice for 5 min. Then, 30 µl of pre-chilled buffer per $10^7$ total cells plus 20 µl of Microbeads Cocktail per $10^7$ cells were added to the tube. The cell suspension was mixed well and put on ice for 10 min. In the meantime, LS column (*Miltenyi Biotec*) was placed in the proper magnet field and washed with 3 ml of buffer. The cells were applied onto the column and the cells in the flow-through, which were enriched CD8$^+$ T cells, were collected in a 15 ml conical falcon. The column was washed with 3 ml buffer to collect any remaining CD8$^+$ T cells. The cells were centrifuged at 300 ×g for 5 min and resuspended in cell culture medium. The CD8$^+$ T cells were counted and they were frozen or kept in culture for experiments.

### 2.2.6.2 Activation and electroporation of CD8$^+$ T cells

Fresh isolated or frozen aliquots of CD8$^+$ T cells were activated prior to electroporation. The P3 Primary cell 4D-Nucleofector™ kit and 4D-Nucleofector system™ (*Lonza*) were used for the

electroporation. $CD8^+$ T cells ($2\times 10^6$) were resuspended in 2 ml X-VIVO20™ containing 20µl TransAct™ (*Milteny biotec*) plus IL-7 (20 ng/ml) and IL-15 (20 ng/ml). The cell suspension was transferred in one well of 24 well plate and incubated at 37°C/5% CO2 for 2 days. Then, the activated $CD8^+$ T cells were washed with D-PBS and centrifuged at 300×g, 5 min at RT. The electroporation master mix was prepared by adding 6µl of supplement to 16.4µl Nucleofector™ solution. Afterwards, the pHIV-eGFP-TCR-EF1-4 (2µg/ml) and electroporation master mix was added to the cells to reach the final volume of 20µl. The cell suspension was mixed well and transferred to one well of 16-well Nucleocuvette™ Strips. The strip was transferred to the machine and the cells were pulsed with the program E0-115 pulse code and solution P3 primary. Then, the strip was incubated at RT for 15 min. The electroporated cells were transferred to one well of 48 well plate containing 1 ml of pre-warmed X-VIVO20™ and incubated at 37°C/5% CO2 for 4-6h. Afterwards, 500µl of the medium was carefully removed and another fresh 500µl X-VIVO20™ containing IL-7 (20 ng/ml) and IL-15 (20 ng/ml) was added. The cells were kept in culture at 37°C/5% CO2 for 2 days. A small aliquot of the cells was used for the staining with anti-mouse TCRβ chain-PE. Cy7(*Biolegend*) and analysis of the expression of eGFP. The samples were processed for flow cytometry measurement and analysis as described in section 2.2.1.5. The successfully electroporated cells were kept in culture for further experiments.

### 2.2.6.3 Measuring the IFNγ secretion in TCR engineered CD8$^+$ T cells in co-culture with peptide loaded T2 cell lines

The protocol described in section 2.2.5.8 was followed with minor changes. T2 cell lines ($4 \times 10^3$ in each well) were loaded with 1, 10 or 100µM of the $E7_{(11-19)}$ peptide in 50 µl serum free RPMI medium and they were incubated at 37°C/5% CO2 for 16-18 h. The CD8$^+$ T cells-EF1-EF3 were counted and according to the percentage of electroporated cells, $16\times10^3$ cells were resuspended in 50µl of X-VIVO20™ containing IL-7 (20 ng/ml), IL-15 (20 ng/ml) and POM1 (20µM). The untransfected CD8$^+$ T cells were used as the negative control. The final volume of the co-culture was 100µl and the effector to target ratio was 4:1. The cells were incubated for 20-24h and subjected to IFNγ- catch assay as described in section 2.2.3.3.

### 2.2.6.4 Analyzing the secretion of IFNγ by TCR engineered T cells after co-culture with target cell lines

The cancer cell lines of Caski, SiHa, UPCI-SCC154 and PCI-13 were seeded ($5\times10^3$ cells) in 96 well flat bottom plate. The transfected CD8$^+$ T cells-EF1-EF3 were added ($5\times10^3$ cells) to the target cell lines. The number of the untransfected CD8$^+$ T cells was adjusted according to the number of transfected cells used for the co-culture. The final volume of the co-culture was 100µl X-VIVO20™ containing IL-7 (20 ng/ml), IL-15 (20 ng/ml) and POM1 (20µM). The cells were incubated for 20-24h and subjected to IFNγ- catch assay as described in method 2.2.3.3.

#### 2.2.6.5 Measuring cell viability by WST-1 assay

The Caski and SiHa cell lines were used for measuring the cell viability by WST-1 assay (*Sigma Aldrich*). Caski, and SiHa were seeded ($5\times10^3$ cells) in 96 well flat bottom plate. The co-culture condition was the same as described in section 2.2.6.4. The effector cells were removed and 90µl X-VIVO20™ containing 10µl WST1 reagent was added to each well. The plate was incubated at 37°C/5% CO2 for 15 min. The plate was measure by plate reader (*Perkin Elmer*) at 450 nm (1.0s) and the reference wavelength of 660 nm (0.1s). The relative lysis of the target cell lines was calculated by the following formula:

$$Relative\ lysis: \frac{[(\text{ Cell line cocultured with UnTcells }) - (\text{ Cell line cocultured with TCR transgenic CD8Tcell})]}{(\text{ Cell line cocultured with TCR transgenic CD8Tcell})}$$

### 2.2.7 *In silico* characterization of TCRs reactive to the E7$_{(11\text{-}19)}$ epitope

#### 2.2.7.1 Predicting the 3D structure of candidate TCRs and performing protein-protein docking

The DNA sequence of TRAV and TRBV of candidate TCRs were retrieved from the V(D)J Loupe (*10x Genomics*). The TCR sequence was designed as TRBV joined to TRAV and The DNA sequences were translated by Expasy (https://web.expasy.org/translate/). The 3D structure of the candidate TCRs was predicted and refined by Galaxy TBM server as described in section 2.2.2.6. The 3D structure of HLA-A*0201 single chain trimer with murine H2K alpha 3 domain and HPV16 E7 $_{(11\text{-}19)}$ was retrieved from the protein data bank (PBD ID: 6E1I). This structure was obtained by X-RAY Diffraction. The water molecules and trans membrane domain of the structure was removed. The refined 3D model of candidate TCRs and structure of HLA-A*0201

single chain trimer was used for the protein-protein docking via Swarmdock tool The interaction of the amino acids in the CDR3β/α with the $E7_{(11-19)}$ peptide was evaluated according to the different conformation predicted by the docking. The conformations with more interactions were considered for calculation of ΔG of interaction by PRODIGY as described in section 2.2.2.6.

#### 2.2.7.2 Comparison of the TCR candidates with the TCRβ repertoire of the Immunoseq database

The TCRβ sequence of TCR repertoire of woman who either cleared or failed to clear an HPV16 infection was analyzed using ImmunosSEQ® ANALYZER (177). The CDR3β of this repertoire were filtered by the interacting domain of TCR candidates derived from the evaluation done in section 2.2.7.1. The frequency of these motifs within the TCR of patients who cleared HPV 16 infection and patients at CIN III was calculated and the ratio of average clonotype frequency of candidate TCRs were compared.

# 3.Results

## 3.1 *In silico* analysis of the binding affinity of the E7-Flt3 ligand to the Flt3 receptor

An E7-Flt3L fusion protein was designed and purified previously (Cid-Arregui et al, unpublished). The interaction of E7-Flt3L with Flt3 was analyzed *in silico* to assess whether the $E7_{(1-30)}$ peptide can affect its binding affinity to Flt3L. This analysis was done by a flexible protein-protein docking by SwarmDock tool and the binding energy was measured by PRODIGY as described in the Methods section. Despite of the slight change in the positioning of fused Flt3L to its receptor, E7-Flt3L had stronger interaction mode compared to wild type Flt3L. The ΔG interaction of human Flt3 (hFlt3) with wild-type Flt3L and E7-Flt3L was -7.3 and -11.2 kcal mol-1, respectively [Fig. 12a &12b]. Moreover, the E7 domain showed a binding tendency to the region of Flt3 responsible for interacting with the ligand. It has been shown that the main binding interface of Flt3 consists of eight amino acids: Histidine (H) 279, Phenylalanine (Phe) 281, Serine (Ser) 301, Threonine (Thr) 302, Tyrosine (Tyr) 303, Arginine (R) 307, Methionine (Met) 309 and R 311 (178). Based on the *in silico* prediction, E7Flt3L interacted with majority (5/8) of these important residues including: H279, F281, T302, Y303 and R307 [Fig. 11c]. Therefore, the $E7_{(1-30)}$ peptide not only did not interfere with the binding of the Flt3L to its receptor, but also it enhanced its binding affinity.

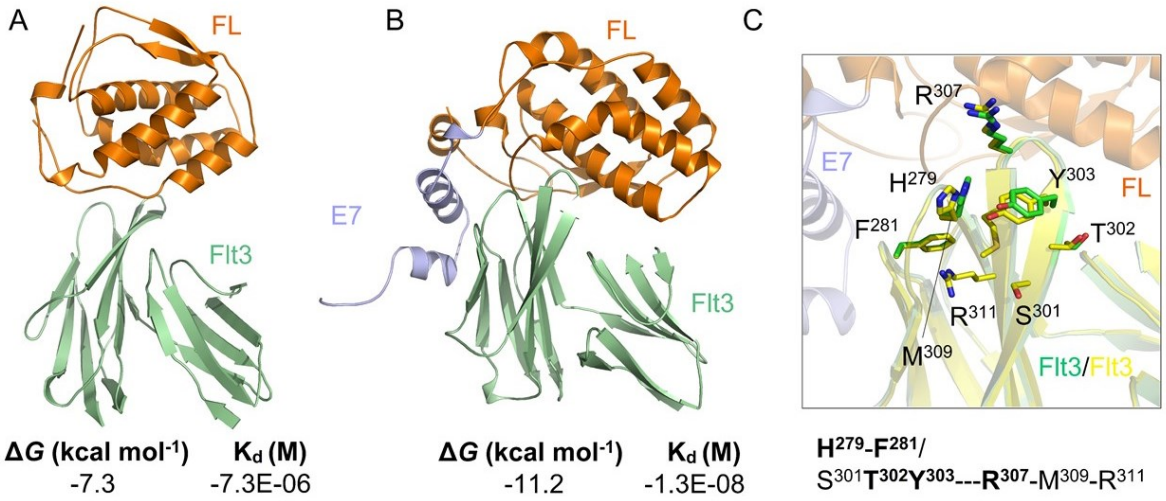


**Figure 12.Comparing the interaction of wild type hFlt3L and E7-Flt3L fusion protein with Flt3 receptor.** (a) The binding of the hFlt3L wild type to Flt3 had a ΔG = -7.3. (b) E7-Flt3L had slight change in the position of interaction with Flt3 and had a ΔG interaction = -11.2. (c) The interacting residues of the binding interface of hFlt3 with E7Flt3L are depicted in bold letters.

The physico-chemical properties of Flt3L and E7-Flt3L was evaluated through ProtParam tool and the results are summarized in [Table 10] (172). The *in vitro* and *in vivo* half-life of both proteins were the same: 30h and >20h, respectively. The GRAVY (Grand Average of Hydropathy) shows the hydrophobicity/hydrophilicity of a protein and calculated as sum of hydropathy values of all the amino acids divided by the number of residues in the sequence (179). The negative GRAVY values indicate that the protein is hydrophilic and the positive values mean that it is hydrophobic (180). Based on the ProtParam analysis, E7-Flt3L is more hydrophilic (GRAVY = -0.487) compared to hFlt3L- wild type (GRAVY= -0.184). Importantly, the instability index of E7-Flt3L was lower which means that the fusion protein is more stable than hFlt3L.

**Table 10. The physico-chemical properties of human Flt3L wild type with E7-Flt3L recombinant protein.**

| Name | PI | half-life *in Vitro* | half-life *in Vivo* | GRAVY* | Instability index |
|---|---|---|---|---|---|
| **hFlt3L- wild type** | 7.56 | 30h | > 20 h | -0.184 | 71.73 |
| **E7-Flt3L- recombinant protein** | 5.62 | 30 h | > 20 h | -0.487 | 62.33 |

***Grand average of hydropathicity**

## 3.2 E7-Flt3L fusion protein can be internalized and induce maturation in human monocyte derived immature DCs

In order to assess the internalization and subcellular localization of E7-Flt3L in the hmo-imDCs, the fusion protein was labeled with an APC and was added to the culture medium. The nucleus and the ER were stained in parallel with DAPI and an anti-calnexin conjugated with Cy™2, respectively [Fig. 13a.I and II]. After 3 hours of incubation, E7-Flt3L-APC was distributed throughout the cytoplasm of hmo-imDCs in small vesicles compatible with a pattern of early/late endosomes and lysosomes [Fig. 13a.III]. Moreover, there was a distribution of the red fluorescence representing E7-Flt3L-APC close to ER (Fig. 13a.IV in green). Following the incubation of hmo-imDCs with the fusion protein, the frequencies of $CD11c^{+}$/ $CD135^{+}$ cells were reduced significantly (p=0.013) suggestive of the internalization of Flt3 upon binding to its ligand [Fig. 13 b &c]. Therefore, the results showed the internalization of the E7-Flt3L by hmo-

imDCs which can lead to degradation of the fusion protein and cross presentation of the $E7_{(11-19)}$ epitope.

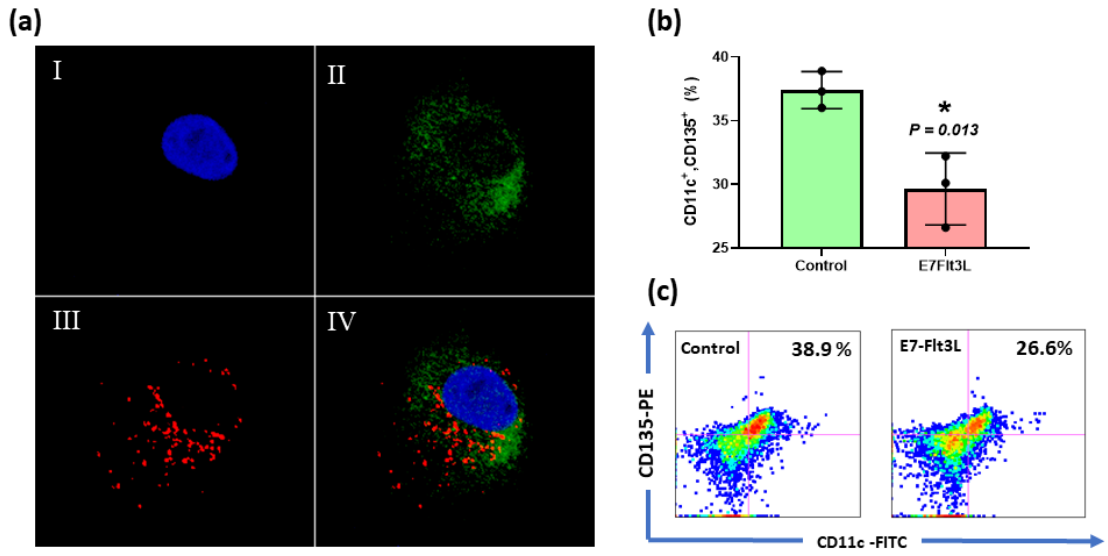


**Figure 13. Internalization and subcellular localization of E7-Flt3L and its effect on Flt3 surface expression. (a.I) the nucleus of hmo-imDCs stained with DAPI show in blue**. (a.II) The ER was stained with anti-calnexin- Cy™2 shown in green. (a.III) The E7-Flt3L fusion protein was labeled with APC and distributed within the cytoplasm. (a.IV) Merged image of the three channels. (b) Percentage of $CD11c^+$, $CD135^+$ upon incubation with E7-Flt3L. (c) Flow cytometry graphs corresponding to (b). The results shown are representative of 3 independent experiments, *$p < 0.05$. Panel (a) shows results obtained in our group by Isaac Quirós-Fernández who collaborated in the project.

Importantly, E7-Flt3L the fusion protein upregulated maturation markers in hmo-imDCs. Following 18h and 42h incubation of hmo-imDCs with different concentration of fusion protein 1, 5 and 10 µg/ml, the population of $CD11c^+$ cells did not change. However, the expression of CD80, CD83 and CD86 was upregulated in $CD11c^+$ cells and this increase, except CD83, was more prominent after 42 hours of incubation [Fig. 14a].

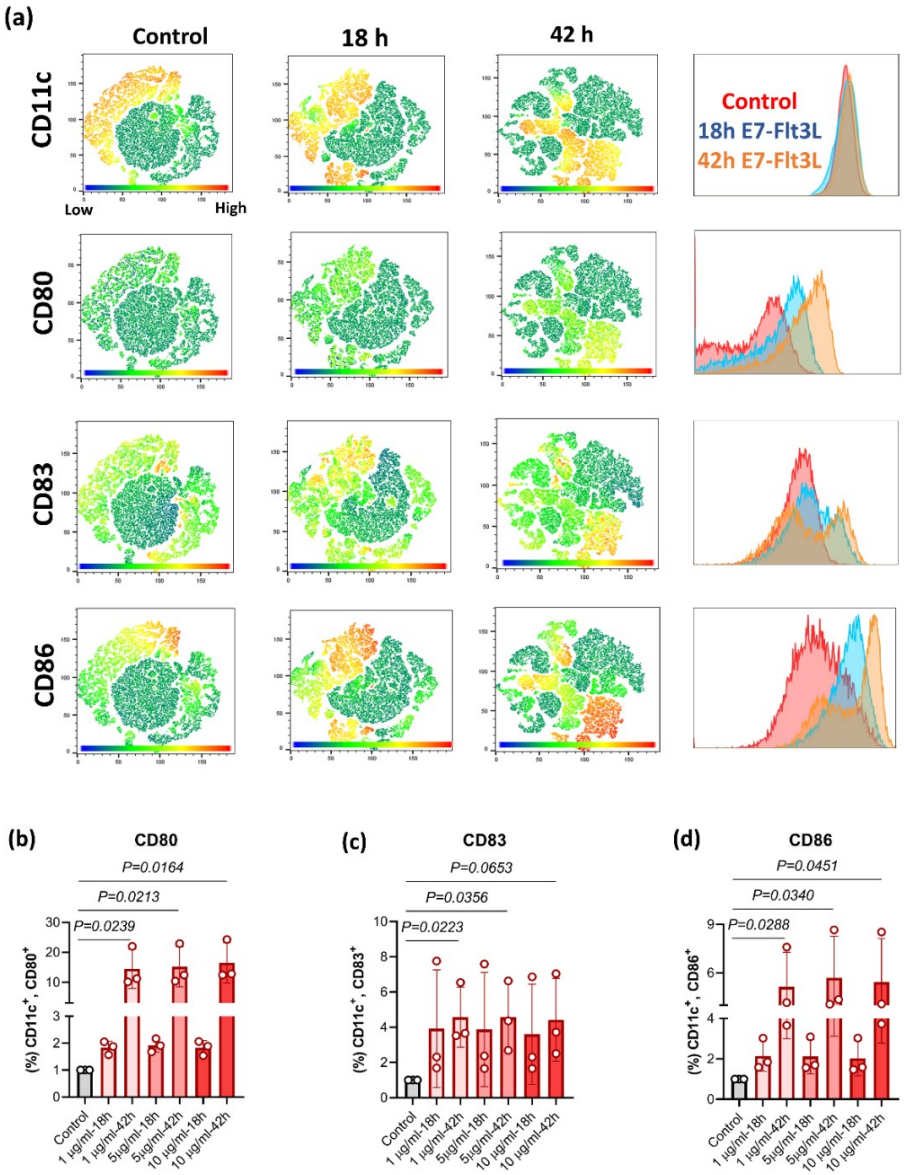


**Figure 14. E7-Flt3L upregulate the maturation markers on hmo-imDcs.** (a) The maturation markers, CD80, CD83 and CD86, were upregulated following 18h and 42h, incubation with different concentrations of E7-Flt3L. The tSNE and flowcytometry analysis of 5µg/ml of E7-Flt3L in one healthy individual is shown as the representative. (b) CD80 showed a significant increase following 18- and 42h of incubation with E7-Flt3L.(c) The percentage of $CD11c^{+}$, $CD83^{+}$ was increased after incubation with the fusion protein. (d) E7-Flt3L, at different concentrations, caused the upregulation of CD86 after 18h and 42h. The percentages corresponding to three different healthy donors are presented and the values were normalized by the control which was untreated hmo-imDCs.

CD80 was upregulated after incubation of hmo-imDcs with either 1µg/ml (p=0.0239), 5 µg/ml (p=0.0213) or 10 µg/ml (p=0.0164) of fusion protein. After 18h and 42h incubation, the percentages of $CD11c^+/CD80^+$ cells were 1.86-fold and 15.39-fold higher than control, respectively [Fig. 14b]. The expression of CD83 was increased following the incubation with E7-Flt3L at different concentration, 1 µg/ml (p=0.0223), 5 µg/ml (p=0.0356) and 10 µg/ml (p=0.0653). However, there was no significant difference in the upregulation of CD83 following the18h (3.8- fold) and 42h (4.5- fold) incubation which showed 3.8-fold and 4.5-fold higher values compared to the control, respectively. The percentage of $CD11c^+/CD86^+$ cells were increased following incubation with 1µg/ml (p=0.0288), 5 µg/ml (p=0.0340), and 10 µg/ml (p=0.0451) of E7-Flt3L. This increase was on average 2-fold after 18h and 5.42-fold after 42h incubation compared to the control [Fig. 14c]. The effect of E7-Flt3L on maturation of the cells was not concentration- dependent since there was no significant difference in upregulation of CD80, CD83 and CD86 following the incubation with 1, 5 and 10 µg/ml of the fusion protein. Based on these results, E7-Flt3L fusion protein can upregulate the costimulatory molecules on hmo-DCs and this is essential for efficient activation of T cells.

## 3.3 E7-Flt3L induced the activation of $CD8^+$ T cells reactive to HLA-A*02:01 restricted HPV16 $E7_{(11-19)}$ epitope in healthy donors

The effect of E7-Flt3L on activation of $CD8^+$ T cells was evaluated through $E7_{(11-19)}$ tetramers binding, secretion of IFN-γ and upregulation of CD137. The $E7_{(11-19)}$ tetramers were prepared

with Flex-T™ technology of Biolegend and the efficient peptide exchanged was confirmed by ELISA [Appendix-Figure.1]. The same gating was applied to all samples to analyze single cell/ live/ $CD3^+$/ $CD8^+$ T cells [Appendix-Figure.2]. Various patterns of $CD8^+$ T cell activation were observed through systematical analysis of 1, 5 and 10 µg/ml of E7-Flt3L at different time points including 2, 5 and 12 days [Fig. 15a]. Following 2 and 12 days of co-culture, E7-Flt3L at concentration of 5 µg/ml increased the percentage of $CD8^+$, E7 $_{(11-19)}$-tetramer$^+$ T cells which were also IFN-$\gamma^+$. E7-Flt3L at concentration of 1 and 10 µg/ml did not increase $CD8^+$/ E7 $_{(11-19)}$-tetramer$^+$ T cells after 2- and 12 days of co-culture. However, there were higher percentage of $E7_{(11-19)}$ tetramer$^+$/ IFN-$\gamma^+$ T cells after 12 days of incubation with 10 µg/ml of E7-Flt3L which can be due to the increased secretion of IFN-γ. E7-Flt3L at concentration of 1 and 5 µg/ml increased the number of $CD8^+$/ E7 $_{(11-19)}$-tetramer$^+$ T cells, whereases 5 µg/ml was optimal in terms of IFN-γ secretion and tetramer binding. E7-Flt3L (10 µg/ml) did not enhance the number of E7 $_{(11-19)}$-tetramer$^+$ T cells but the number of $E7_{(11-19)}$ tetramer$^+$/ IFN-$\gamma^+$ T cells, like 12 days incubation, was higher compared to the control. Therefore, 5 µg/ml of the fusion protein induced an effective activation of $CD8^+$ T cells in different incubation times. Following 5 days of co-culture, the percentage of CD8+/ INF-$\gamma^+$/ $E7_{(11-19)}$ -tetramer$^+$ (0.22± 0.1) was significantly (p=0.03) higher than after 2 days (0.044± 0.012), whereas, there was no significant difference (p=0.08) with 12 days of incubation (0.088± 0.02) [Fig. 15b]. Moreover, incubation with the E7-Flt3L (5 µg/ml) increased the percentage of $CD8^+$/ $CD137^+$/ $E7_{(11-19)}$ -tetramer$^+$ T cells after 2 - (p=0.05), 5 - (p=0.025) and 12 days (0.032) compared to the control [Fig. 15c]. Importantly, upregulation of CD137 following 5 days of co-culture was significantly higher compared to 2- (p=0.05) and 12 days (p=0.04). Besides that, the percentage of $CD8^+$ / INF-$\gamma^+$ T cells was remarkably higher after

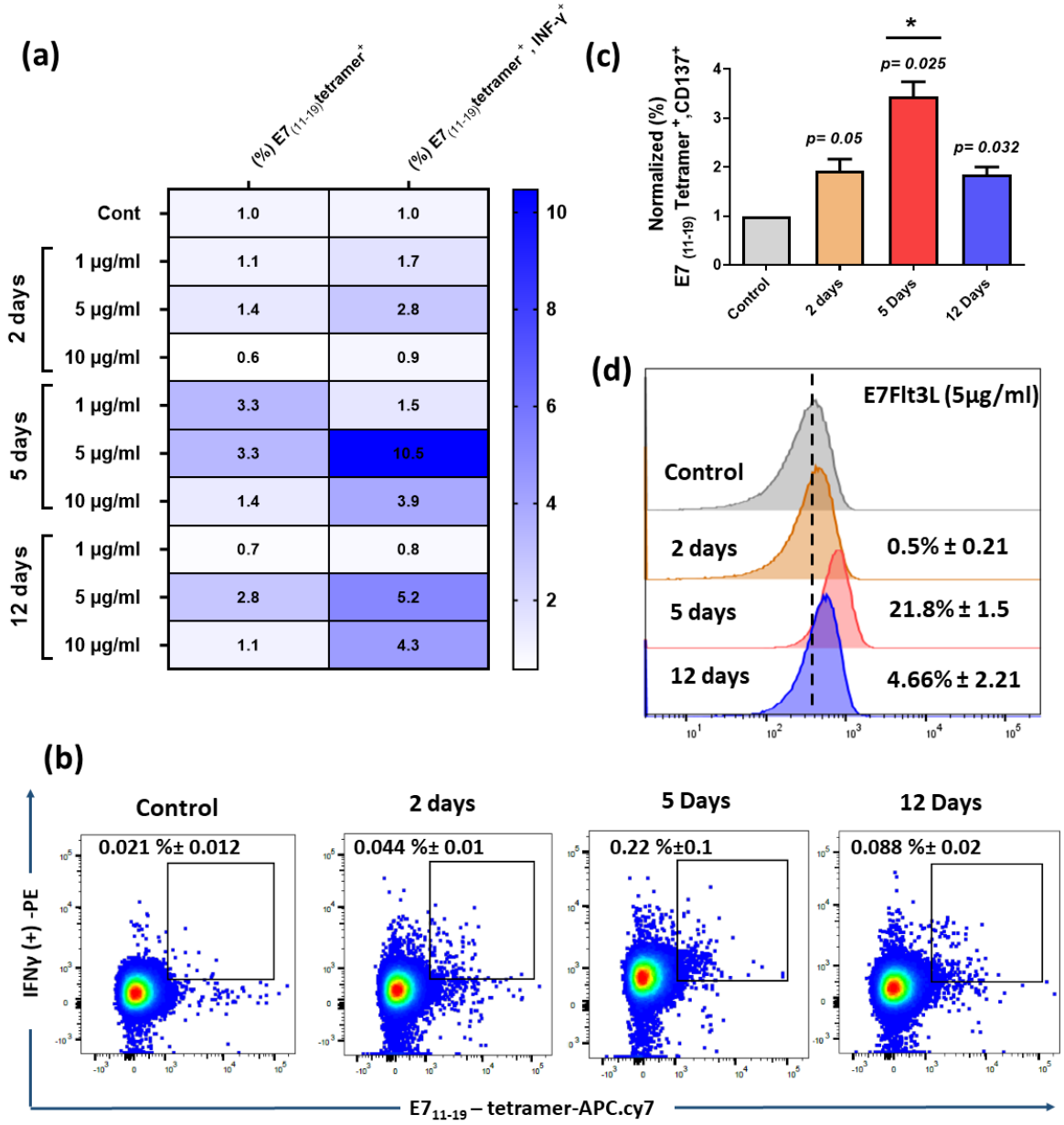


**Figure 15.Analyzing the effect of E7-Flt3L on activation of CD8+ T cells at different concentration and time points.** (a) The percentage of $CD8^+$, E7 $_{(11-19)}$ -$tetramer^+$ and E7 $_{(11-19)}$ -$tetramer^+$/IFN-$\gamma^+$ T cells at three different time points and concentration were normalized by the control and shown as heatmap. (b) The flow cytometry analysis of $CD8^+$ T cells following the incubation with E7-Flt3L (5µg/ml) at day2,5 and 12. (c) The percentage of $CD137^+$/ E7 $_{(11-19)}$ -$tetramer^+$/$CD8^+$ T cells after incubation with E7-Flt3L (5µg/ml) at different time points. (d) The comparison of IFN-$\gamma^+$ T cells following 2,5 and 12 days of incubation with E7-Flt3L (5µg/ml). The results shown are representative of 2 independent experiments.

5 days co-culture [Fig. 15d]. Taken together, E7-Flt3L (5 µg/ml) after 5 and 12 days of incubation can efficiently activate $CD8^+$ T cells. Due to the higher activation of T cells at day 5 of co-culture, we further investigated the effect of E7-Flt3L (5 µg/ml) in three different healthy donors.

According to the tetramer staining results, 5 days co-culture of T cells with hmo-imDCs loaded with E7-Flt3L (5µg/ml) increased the percentage of $CD8^+$/ $E7_{(11-19)}$ -$tetramer^+$ T cells, on average 3.17-fold [Fig. 16a & b].

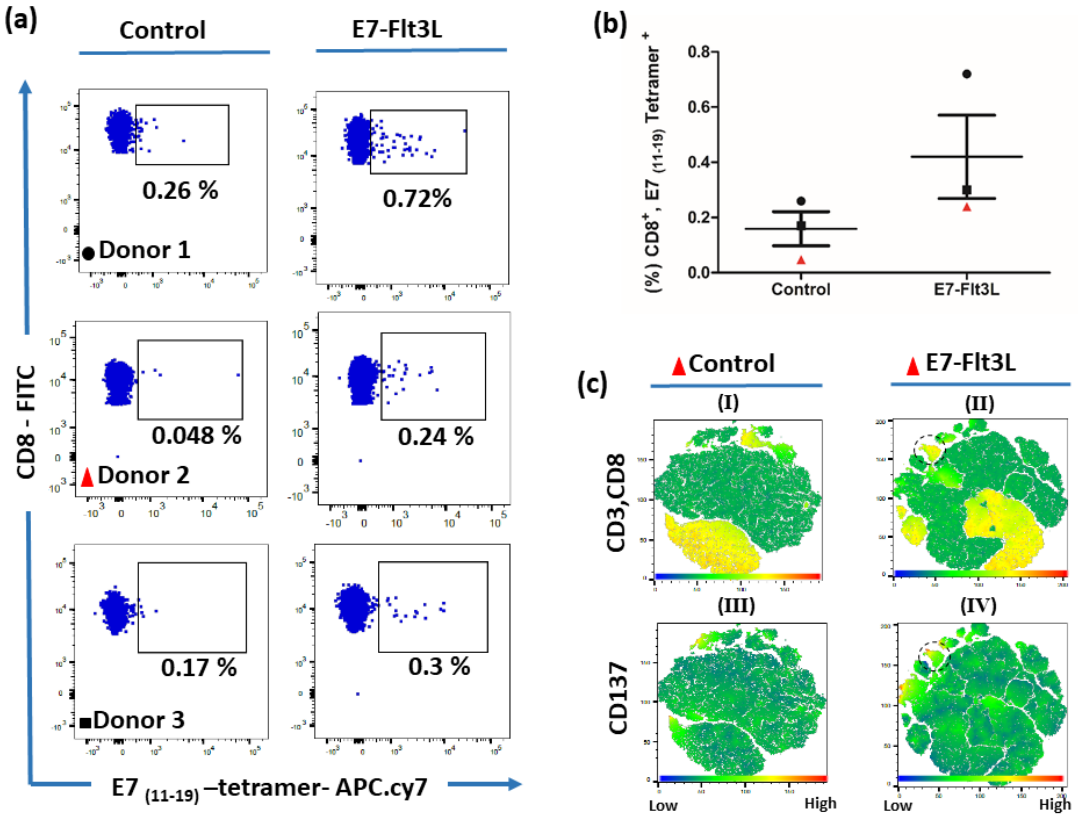


**Figure 16. Comparing the stimulatory effect of E7-Flt3L (5µg/ml) in three different healthy donors**. (a &b) tetramer binding of the CD8+ T cells before and after 5 days stimulation with the fusion protein. (c) tSNE analysis of donor 2 following incubation with the E7-Flt3L.

However, donor2 had a 5-fold increase following stimulation with the fusion protein. The tSNE analysis of the Donor 2 prior and after stimulation showed that the $CD3^+$/ $CD8^+$ T cells proliferated, whereas the same effect was not seen in other healthy donors [Fig. 16c & Appendix-Figure.3]. Interestingly, the small population of $CD3^+$ /$CD8^+$ T cells that has emerged after incubation with E7-Flt3L, were also $E7_{(11-19)}$ -$tetramer^+$/ $CD137^+$ [shown by circle in Fig.16c II & IV].

To further confirm the functionality of fusion protein, the stimulatory effect of E7-Flt3L and $E7_{(11-19)}$ peptide following 2- and 5 days were compared [Fig. 17]. 2- (p=0.028) and 5 days (p=0.001) of incubation with E7-Flt3L increased the percentage of $CD8^+$/ $E7_{(11-19)}$ -$tetramer^+$ T cells, whereas there was no significant change in the tetramer binding following the stimulation with $E7_{(11-19)}$ peptide [Fig. 17a]. Importantly, $E7_{(11-19)}$ peptide did not induce an efficient activation in $CD8^+$ T cells in terms of CD137 upregulation neither after 2 days nor 5 days of incubation. Moreover, the percentage of tetramer binding cells when they were stimulated with the combination of E7-Flt3L(5µg/ml) and $E7_{(11-19)}$ (10µM) was lower compared to the solely incubation of the cells with E7-Flt3L(5µg/ml) [Appendix-Figure.4]. However, the number of $E7_{(11-19)}$ -$tetramer^+$, $CD137^+$ was higher after 2 days of incubation with E7-Flt3L (5µg/ml) and this increase was more prominent after 5 days [Fig. 17 b]. Although following 2 days of incubation with $E7_{(11-19)}$ peptide, the percentage of $E7_{(11-19)}$ -$tetramer^+$/ IFN-$\gamma^+$ T cells did not change, there was a slight increase post 5 days of stimulation. On the other hand, the percentage of $E7_{(11-19)}$ -$tetramer^+$/ IFN-$\gamma^+$ T cells was significantly higher after 2- (p=0.006) and 5 days. (p=0.006) [Fig. 17c].

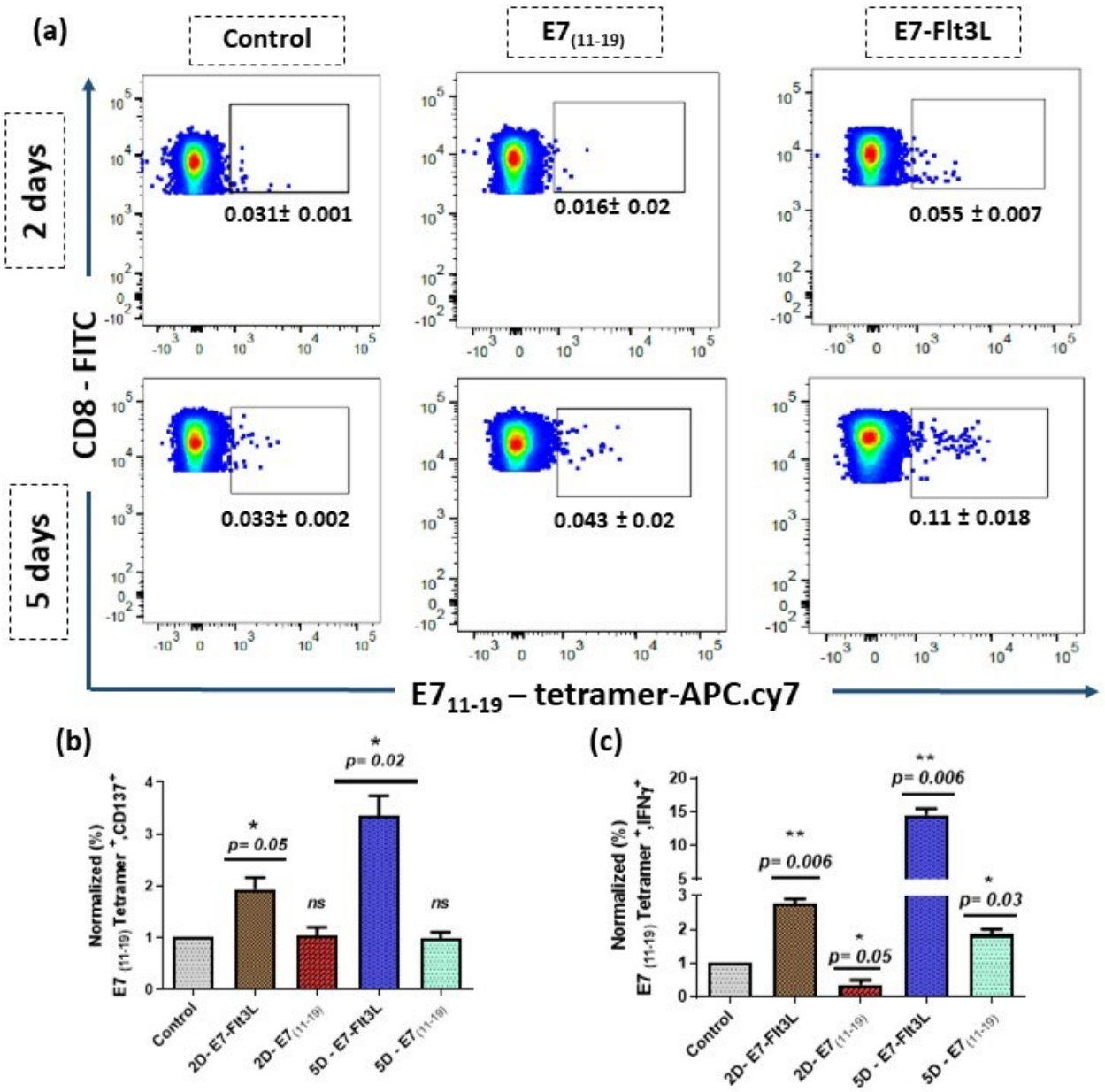


**Figure 17. Comparison of the stimulation of CD8+ T cells with E7-Flt3L and E7(11-19) peptide.** (a) Tetramer binding of $CD8^+$ T cells following incubation with E7-Flt3L (5µg/ml) or E7 (11-19) peptide after 2- and 5 days. (b) Frequencies of E7(11-19) -$tetramer^+$/ $CD137^+$ cells after stimulation with E7-Flt3L (5µg/ml) or E7 (11-19) peptide. The percentages of positives cells were normalized to those of the cells in the control consisting of co-culture without treatment. (c) Normalized percentage of E7 (11-19) -$tetramer^+$/ IFN-$\gamma^+$ cells following incubation with the fusion protein or short peptide. The results shown are representative of 2 independent experiments. The * means p value ≤0.05 and ** indicates p value ≤0.01.

These results indicate that E7-Flt3L is a functional protein that can specifically activate the $CD8^+$ T cells of healthy donors after a short incubation period. Combining the tetramer binding and activation markers can improve the efficient identification of $CD8^+$ T cells reactive to a specific epitope. To this aim, $E7_{(11-19)}$ -reactive $CD8^+$ T cells, which were IFN-$\gamma^+$, $CD137^+$ and $E7_{11-19}$-$Tetramer^+$ (from PBMCs of two healthy donors) or IFN- $\gamma^+$/ $E7_{11-19}$-$Tetramer^+$ (from PBMCs of one healthy donor) were sorted. To determine the exact TCR profile of the $E7_{(11-19)}$ -reactive T cells, we performed single-cell V(D)J sequencing using the 10X Genomics platform.

## 3.4 Identification of the TCR repertoire of $CD8^+$ T cells reactive to the $E7_{(11-19)}$ epitope through single-cell V(D)J sequencing

The VDJ enriched library of 10x was sequenced through MiseqV2-pairedEnd-250 bp to cover the full length of TCR sequence. The Fastq files were analyzed by 10x Cell Ranger pipelines and visualized by 10x Loupe V(D)J browser. The quality of VDJ single cell sequencing was confirmed through web summaries generated by 10x Cell Ranger pipelines. The Barcode rank plot of both libraries had a typical steep drop-off which indicate the good separation of cell-associated barcodes and the barcodes linked to empty GEMs. GEMs containing greater number of transcripts, had also higher number of UMIs [Fig.18a&b]. Another parameter in the cell metrics generated by cell ranger vdj is the Fraction Reads in cells. It shows the fraction of reads including a barcode, which is also called as a cell, that can be mapped to the transcriptome.

According to the 10x genomics guidelines [1], The Fraction Reads in cells should be >70% and this value in the IFNγ-tet and CD137-IFNγ-tet was 95.7% and 92.9%, respectively. The sequencing metrics indicate the successful sequencing by parameters such as Valid barcodes, >75%, and Q30 based in RNA read, ideally >65%. In the IFNγ-tet V(D)J library, the valid barcodes, Q30 bases in RNA Read1 and Q30 bases in RNA read2 were 96.4%, 92% and 88.2%, respectively. The valid barcodes of CD137-IFNγ-tet V(D)J library were 96% and the Q bases in RNA read1 and read2 were 93% and 89.7%, respectively [Fig. 18c].

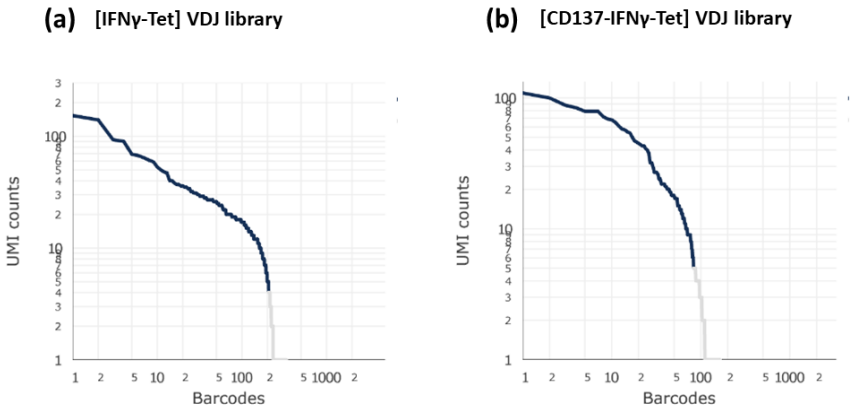


**(c)**

| Library | Fraction Reads (>70%) | Valid barcodes (>75%) | Q30 bases in RNA read 1 (>65%) | Q30 bases in RNA read 2 (>65%) |
|---|---|---|---|---|
| IFNγ-Tet | 95.7% | 96.4% | 92% | 88.2% |
| CD137-IFNγ-Tet | 92.9% | 96% | 93% | 89.7% |

**Figure 18. Barcode rank plot and cell/sequencing metrics of IFNγ-tet and CD137-IFNγ-tet single cell V(D)J libraries.** (a) barcode rank plot of the IFNγ-tet and (b) plot of CD137-IFNγ-tet libraries showed a successful separation of GEMs containing cells and empty ones. (c) Some of the important metrics values which are described in the web summary generated by Cell ranger vdj pipelines**.**

[1] https://support.10xgenomics.com/single-cell-gene-expression/index/doc/technical-note-interpreting-cell-ranger-web-summary-files-for-single-cell-gene-expression-assays

In the IFNγ-tet library,169 paired TCR αβ clonotypes were identified from around 4000 $CD8^+$ T cells. In the other library, CD137-IFNγ-tet, around 2000 cells were initially run through single cell 10x platform, and 69 paired TCR αβ clonotypes were retrieved. In IFNγ-tet, one clonotype had a frequency of 9, nine clonotypes had frequency of 3, eight clonotypes had frequency of 2 and the frequency of the rest of clonotypes was 1 [Fig. 19a].

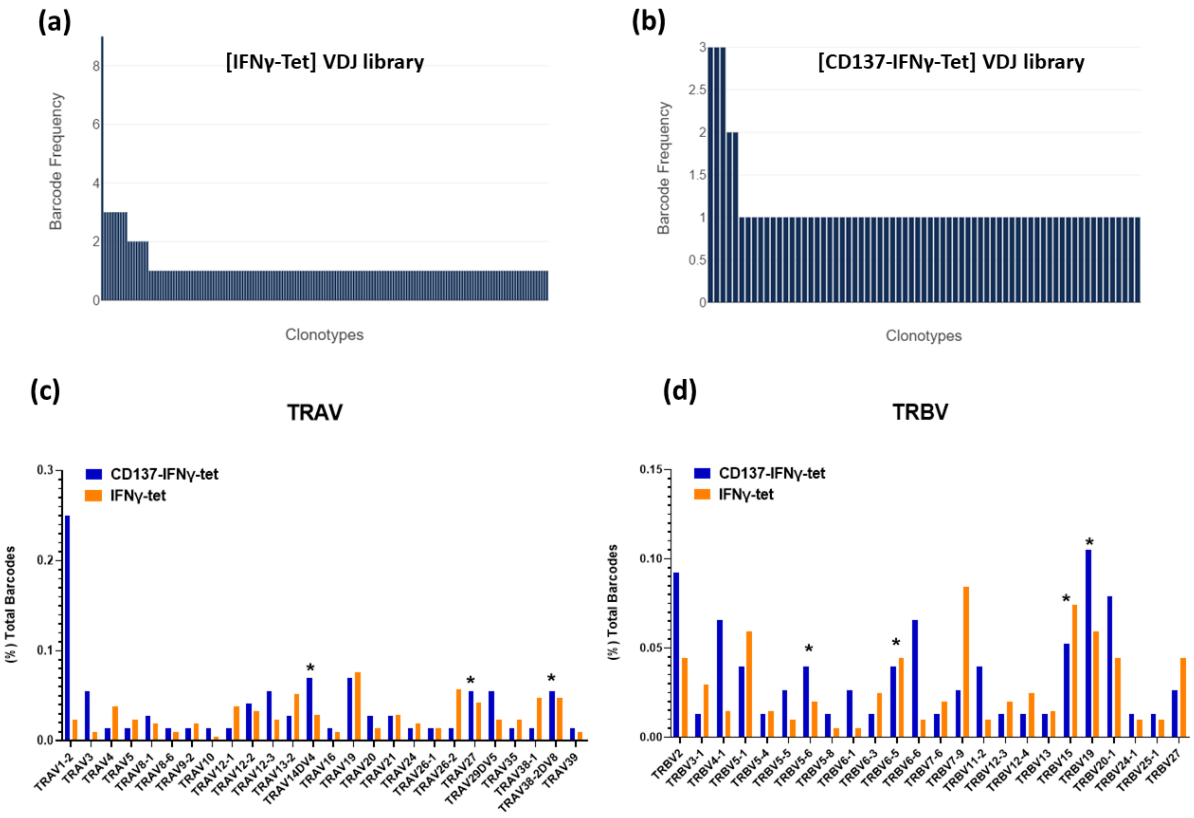


**Figure 19. Frequencies of the identified clonotypes, TRAV and TRBV, in the CD137-IFNγ-tet and IFNγ-tet libraries.** (a) Frequency of clonotypes in the and IFNγ-tet libraries. 18 clonotypes had frequency of ≥2. (b) Frequency of clonotypes in the and CD137-IFNγ-tet. The frequency of 5 clonotypes was ≥2 (c) the TRAV chains shared by both libraries. (d) the TRAV chains shared by the two single cell V(D)J libraries. The TRAV and TRBV chains which are common in top clonotypes are marked with an asterisk.

On the other hand, CD137-IFNγ-tet had three clonotypes with frequency of 3, two clonotypes with frequency of 2 and the rest of clonotypes had frequency of 1 [Fig. 19b]. Although there was no overlap in the clonotypes of both libraries, some clonotypes shared TRBV or TRAV chain. The top clonotypes of both libraries which had frequency ≥ 2 shared three of the TRAV chains including TRAV14DV4, TRAV27 and TRAV38-2DV8 [Fig. 19c]. Four TRBV chains (TRBV5-6, TRBV6-5, TRBV15 and TRBV19) were also shared between the top clonotypes of the two single cell V(D)J libraries [Fig.19d].

## 3.5 Selection of TCR clonotypes for *in vitro* characterization

Four TCR clonotypes, called as EF1, EF2, EF3 and EF4, were selected according to five different criteria [Table 11]. Higher frequency of a clonotype can be an indicative of clonal expansion of a T cell in exposure to an antigen. Therefore, the clonotypes with frequency of ≥2, except for TCR-EF4, were considered. Containing the shared TRAV and TRBV in top clonotypes of two libraries was another selection criterion. Both TCR-EF1 and TCR-EF2 had TRBV15 and TCR-EF3 contained TRAV38-2DV8 and TRBV5-6, however, TCR-EF4 did not contain any of the shared TRAV/TRBV. Median UMI/contig is an indicative of median expression level of each chain per cell and according to 10x recommendation, Median UMI/contig ≥4 is reasonable. Compared to other TCR candidates, TCR-EF4 had a relatively high median UMI/contig value for TRAV and TRBV which were 19 and 20, respectively. Sharing the same TRAV/TRBV with the previously described TCR clonotype reactive to $E7_{(11-19)}$ (E7-TCR) was also considered for efficient selection of

candidate TCRs (161).TCR-EF1 and E7-TCR had both TRAV1-2 and TCR-EF3 shared the same chain of TRBV, TRBV5-6, with E7-TCR.

**Table 11. Criteria for selection of TCRs targeting E7 $_{(11-19)}$ from the V(D) J single cell libraries.**

| Candidates | library | Frequency in the library >2 | Shared TRAV/TRBV in top Clonotypes of both libraries | Median UMI/contig >4 TRA,TRB | Shared TRAV/TRBV with E7 TCR | Similarity with CDR3β of TCR targeting E7(11-20) |
|---|---|---|---|---|---|---|
| TCR-EF1 | [CD137-IFNγ-Tet] | 3 | TRBV15 | [5,10] | TRAV1-2 | No |
| TCR-EF 2 | [IFNγ-Tet] | 9 | TRBV15 | [5,4] | No | NO |
| TCR-EF 3 | [CD137-IFNγ-Tet] | 2 | TRAV382DV8, TRBV5-6 | [5,3.5] | TRBV5-6 | NO |
| TCR-EF 4 | [CD137-IFNγ-Tet] | 1 | NO | [19,20] | NO | Yes |

Moreover, the CDR3β sequence of a described TCR targeting E7$_{(11-20)}$ in the Pathology-associated TCR database (McPAS-TCR database) ,maintained by the Friedman Lab at the Weizmann Institute of Science, shared similarities with the CDR3β of TCR-EF4 (181). Both TCRs had the same three first (CAS) and six last residues (KETQYF). Amino acids located in the middle of TCR-EF4, MGL, shared the same properties (M/L), or were identical (G and L) [Fig. 20].

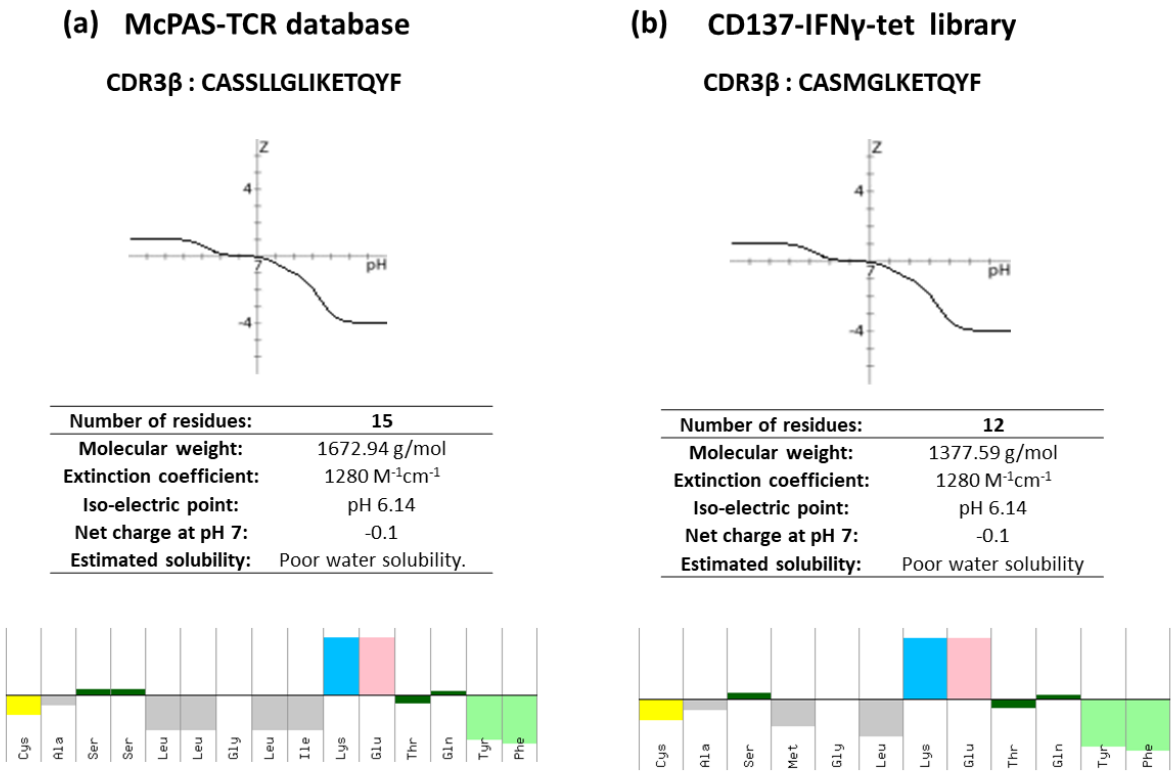


**Figure 20. Comparison of the physicochemical properties of CDR3β of TCR targeting $E7_{(11-20)}$ and TCR-EF4.** (a) Physicochemical properties of the CDR3β of a TCR targeting $E7_{(11-20)}$ which is recorded in the McPAS-TCR database and (b) TCR-EF4 identified in the CD137-IFNγ-tet library. The amino acids were colored based on their properties: Acidic, Aromatic, Basic, Aliphatic, Polar and Cysteine. The amino acids on the top are hydrophilic and the ones in the bottom are hydrophobic. The calculation was done via Peptide property calculator (https://pepcalc.com/).

Following the selection of the candidate TCRs, the expression cassette was designed as described in the Methods section. The schematic designs of the TCR EF1-4 are shown in [Fig. 21] and their full-length DNA sequences are depicted in [Appendix-Figure.5-8].

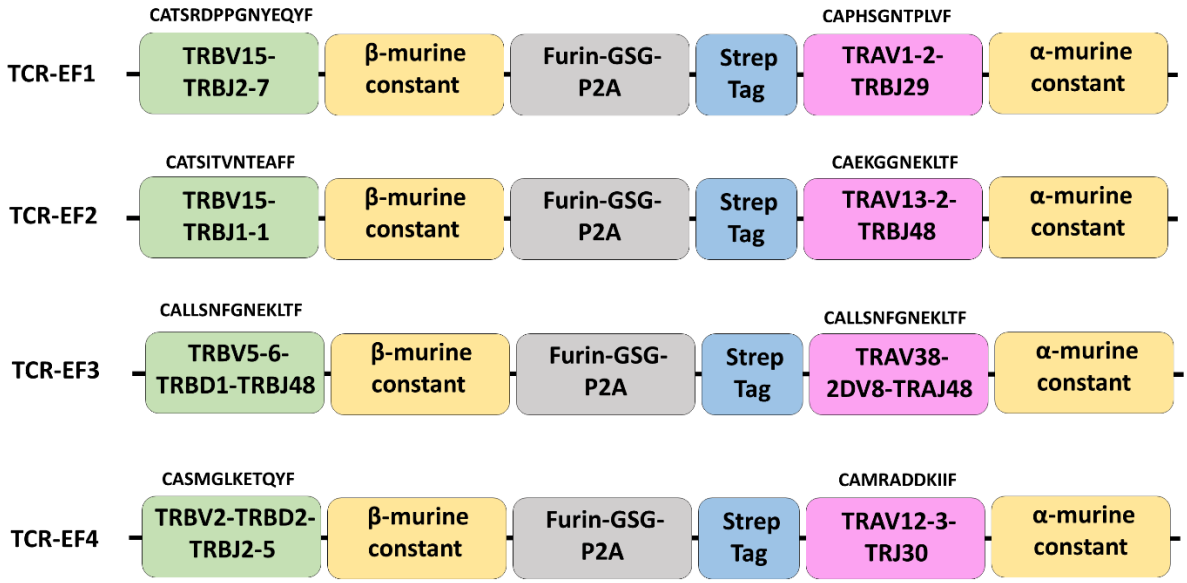


**Figure 21. schematic design of the TCR expression cassette.** The CDR3β and CDR3α peptide sequences are shown above the TRBV and TRAV of each candidate TCR, respectively.

## 3.6 Production of lentiviral vector and expression of candidate TCRs in theJurkatΔ76 cell line

The lentiviral vectors expressing the candidate TCRs were produced in HEK293 T cells, purified and titrated precisely [Fig. 22]. The transfection efficiency of HEK293T cells was determined by the eGFP expression [Fig.22a]. The Jurkat cell lines were transduced with different dilutions of LVs and the titers were calculated based on the formula described in the method section [Fig. 22b]. The LV production protocol was the same for all TCR candidates, however, the titer of LV-TCR-EF1 was higher compared to the other candidates and LV-TCR-EF4 showed the lowest titer

[Fig.22c]. On average the titers of LV-TCR-EF1, EF2, EF3 and EF4 were 15.13 × $10^7$ TU/ ml, 7.85× $10^7$ TU/ ml, 2.67 × $10^7$ TU/ ml and 0.6× $10^7$ TU/ ml, respectively.

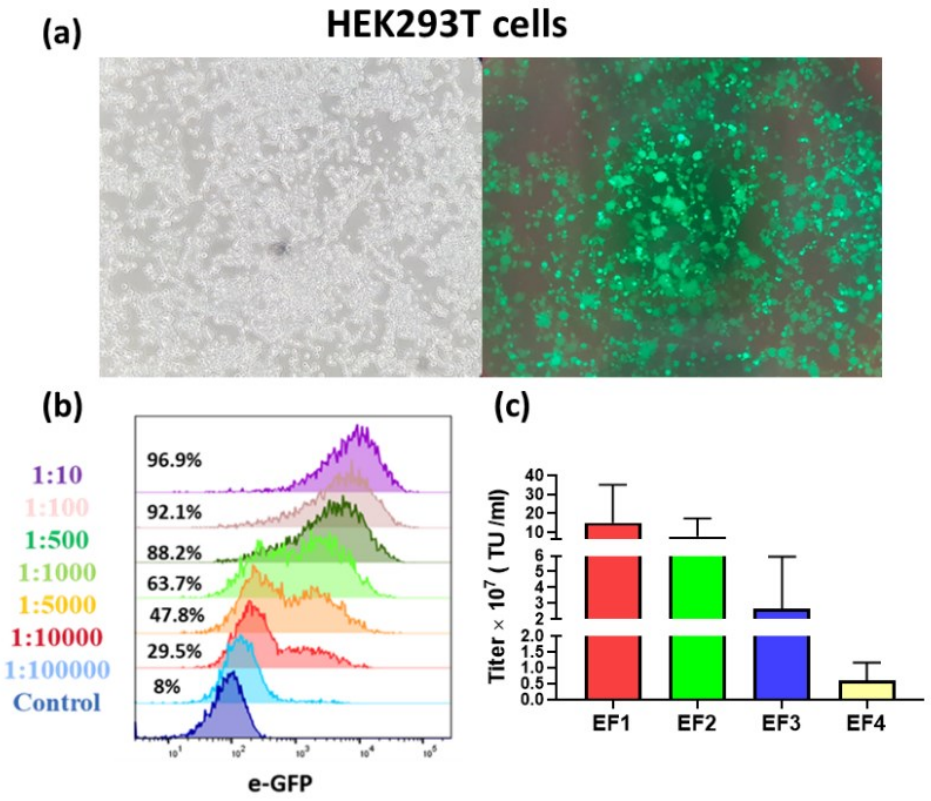


**Figure 22. LV production and titer of LV expressing TCR EF1-4**. (a) HEK 293T cells expressing eGFP 24h post transfection with the LV plasmids. (Nikon ECLIPSE TS100 fluorescence microscope, 10X objective). (b) Transduction of JurkatΔ76 cell line with different dilution of LVs to measure the titer. (c) The average titer of LV expressing candidate TCRs.

The LV expressing candidate TCRs were used for the transduction of TCR deficient JurkatΔ76 cell line which was CD8α$^+$ and CD8β$^+$. Moreover, lack of expression of TCRs was confirmed by CD3 and murine constant (mc) TCRβ staining [Appendix-Figure.9].

This Jurkat cell line was transduced with the LVs of TCRs EF1-4. According to staining of murine constant TCRβ and expression of eGFP, which is encoded by the LV transfer vector, the TCR EF1-

3 were expressed efficiently on the surface of JurkatΔ76 cell line. These transduced Jurkat cells were sorted and called as Jurkat-EF1, Jurkat-EF2 and Jurkat-EF3. Despite of efficient transduction of JurkatΔ76 cell line by LV-EF4, according to eGFP, the expression of TCR-EF4 was not detected [Fig. 23].

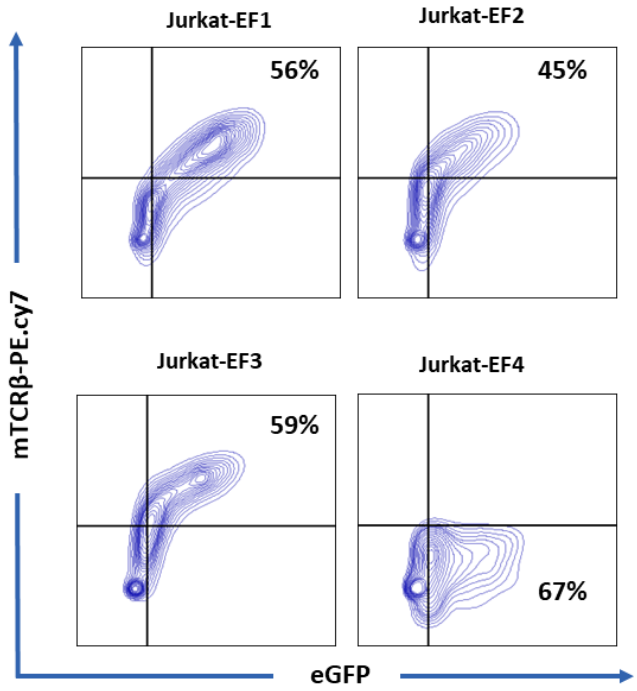


**Figure 23. The expression of candidate TCRs in JurkatΔ76 cell line.** The eGFP signal showed that the JurkatΔ76 cell line was efficiently transduced by the LVs of TCR EF1-4. According to the expression of murine constant TCR β, the TCR EF1-3 were expressed on the surface of JurkatΔ76 cell lines. The expression of murine constant TCR β of TCR-EF4 was not detected on the surface of JurkatΔ76 cell line.

Based on SignalP-5.0 server[2], the presence of signal peptide was predicted in TCR EF1-EF3. However, no signal peptide was detected in the TCR-EF4 sequence which explained why it was not expressed on the surface of JurkatΔ76 cell. The SignalP-5.0 server predicted that the signal

[2] http://www.cbs.dtu.dk/services/SignalP/

peptide of TCR EF1-3 were transported by Sec translocon and cleaved by signal peptidase I with likelihood of ≥ 0.98 (Sec/SPI). The cleavage site of TCR-EF1/EF2 was at position 19 and 20 of the TRBV chain, with probability of 0.6253, and TCR-EF3 had a cleavage site at position 21 and 22, having probability of 0.9385 [Table 12].

**Table 12. prediction of signal peptides in the candidate TCRs EF1-4. This analysis was done by SignalP-5.0 server. The type of signal peptide and position of cleavage site were predicted.**

| Candidate TCRs | Type of signal peptide (SP) | Probability of SP | Cleavage site (CS) | Probability of CS |
|---|---|---|---|---|
| EF1 | Sec/SPI | 0.98 | Pos:19-20. GHG-DA | 0.6253 |
| EF2 | Sec/SPI | 0.98 | pos19-20. GHG-DA | 0.6253 |
| EF3 | Sec/SPI | 0.99 | pos21-22. VDA-GV | 0.9385 |
| EF4 | No signal peptide | ---------- | ---------- | ---------- |
| EF4-repaired | Sec/SPI | 0.96 | pos: 19-20. GLT-EP | 0.5087 |

Based on the data of the Loupe V (D) J browser, 88 bases were inserted in the TRBV2 sequence of the TCR-EF4 which caused the wrong detection of start codon and deletion of signal peptide by the software. This insertion may be due to the sequencing or annotation errors. According to the complete sequence of TRBV2 in reference genome of 10x, the signal peptide was added to the sequence of TCR-EF4. The LV expressing the repaired form of TCR-EF4 was produced and used for transduction of Jurkat cell line. The TCR-EF4 was expressed efficiently on the surface of the cells, however, the cells did not survive [Appendix-Figure.10]. The established cell lines Jurkat-EF1, Jurkat-EF2 and Jurkat-EF3 were used for further *in vitro* characterization.

## 3.7 NFAT2 was upregulated in Jurkat-EF1 and Jurkat-EF2 after co-culture with target cell lines

The NFAT family of proteins consist of five transcription factors: NFAT1, NFAT2, NFAT3, NFAT4 and NFAT5.Among these, NFAT1 and NFAT2 are the most studied ones due to their high expression in T cells. Although NFAT1 is expressed constitutively in normal human T cells, the expression of NFAT2 is induced by activation (182). Therefore, detection of NFAT2 can be sign of T cell activation. The upregulation of NFAT2 was analyzed by real time PCR. In order to detect this upregulation, the TCR engineered Jurkat cell lines were co-cultured with four different cell lines including: Caski ($HPV16^+$, $HLA\text{-}A2^+$), UPCI-SCC154 ($HPV16^+$, $HLA\text{-}A2^+$), SiHa ($HPV16^+$, $HLA\text{-}A2^-$), PCI-13 ($HPV16^-$, $HLA\text{-}A2^-$). The reference control of each group was the effector cells without co-culture. PMA at concentration of 20 ng/ml induced an efficient activation in all Jurkat cell lines, whereas the upregulation of NFAT2 in Jurkat EF1 ($p=0.001$), Jurkat EF2 ($p=0.004$) and Untransduced Jurkat (Un-Jurkat) ($p=0.001$) was more prominent compared to Jurkat-EF3 ($p=0.02$) [Fig. 24]. The real time PCR analysis showed that NFAT-2 was upregulated significantly in Jurkat-EF1 following 24h co-culture with Caski ($p=0.0019$) and UPCI-SCC154 ($p=0.03$). The same upregulation was seen in Jurkat-EF2 in co-culture with Caski ($p=0.0019$) and UPCI-SCC154 ($p=0.04$). However, there was no significant change in the NFAT2 expression of Jurkat-EF3 following co-culture with Caski and UPCI-SCC154. Co-culture of TCR engineered TCR Jurkat and Un-Jurkat cell lines with SiHa and PCI-13 did not change the expression of NFAT2. Based on these results, Jurkat-EF1 and Jurkat-EF2 were efficiently

stimulated by Caski and UPCI-SCC154 target cell lines which are HPV16 positive and expressing HLA-A2 molecule.

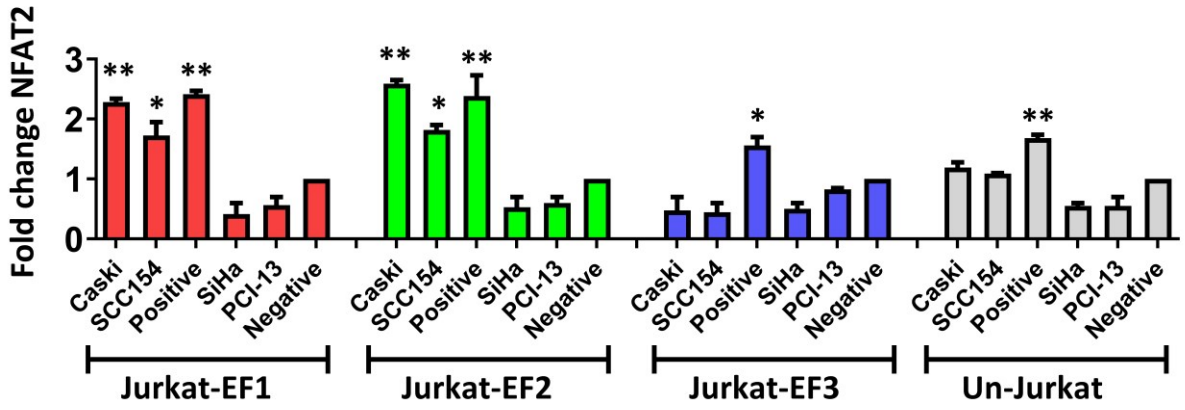


**Figure 24. NFAT2 expression in TCR engineered Jurkat cells after co-culture with target cell lines.** The NFAT2 was upregulated in Jurkat-EF1 in co-culture with Caski and UPCI-SCC154 (p=0.0001). In Jurkat-EF2, the expression of NFAT2 was increased significantly following co-culture with Caski and UPCI-SCC154 (p=0.0004). There was no significant change in the NFAT2 expression of Jurkat-EF3 and Un-Jurkat after co-culture with target cell lines. The expression of NFAT-2 did not change after co-culture of Jurkat-EF1, Jurkat-EF2, Jurkat-EF3 and Un-Jurkat with SiHa, PCI-13. The results shown are representative of 2 independent experiments. Bars are indicative of standard deviations. *, ** and *** represent P values of ≤0.05, ≤ 0.01, ≤0.001, respectively.

## 3.8 Activation of Jurkat-EF1 by T2 cells loaded with the $E7_{(11-19)}$ peptide

The specificity of activation of Jurkat-expressing TCR-EF1, EF2 and EF3 was analyzed in co-culture with T2 cell lines loaded with $E7_{(11-19)}$ peptide or one irrelevant peptide of HIV pol [Fig. 25a]. The results showed that CD69 was upregulated in Jurkat-EF1 in co-culture with $E7_{(11-19)}$ loaded T2 cells compared to irrelevant peptide (p=0.01) or no peptide (p=0.0016). However, there was no difference in the expression of CD69 in Jurkat-EF2 in co-culture with $E7_{(11-19)}$ loaded T2, irrelevant peptide and negative control. HIV pol peptide caused the upregulation of

CD69 in Jurkat-EF2 compared to no peptide control (p=0.03). Although co-culture of Jurkat-EF3 with $E7_{(11-19)}$ loaded T2 cells induced the upregulation of CD69 compared to negative control (p=0.04), there was no significant difference in the expression of CD69 between $E7_{(11-19)}$ and irrelevant peptide. The expression of CD69 did not change in Un-Jurkat after co-culture with peptide loaded T2 cells.

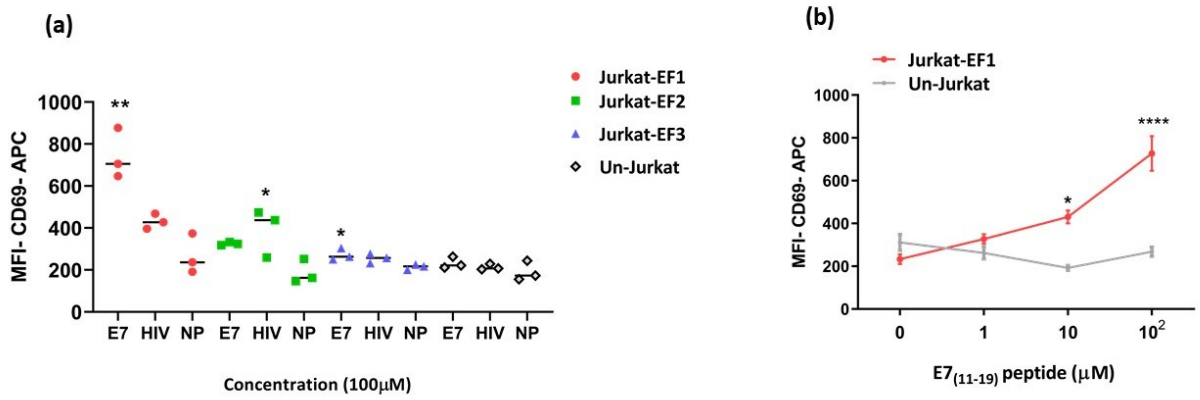


**Figure 25. Expression of CD69 in TCR engineered Jurkat cell lines and Un-Jurkat.** (a) The CD69 was upregulated in Jurkat-EF1 in exposure of $E7_{(11-19)}$ peptide compared to irrelevant peptide and negative control, which is the effector cells without co-culture (p=0.0019). Jurkat-EF2 had higher CD69 expression after co culture with T2 cells loaded with HIV pol peptide or $E7_{(11-19)}$ peptide did not induce CD69 upregulation (p=0.0387). $E7_{(11-19)}$ peptide upregulated the CD69 in Jurkat EF3 compared to negative control (p=0.043). E7, HIV and NP stand for $E7_{(11-19)}$, HIV Pol and no peptide control, respectively. (b) The upregulation of CD69 in Jurkat-EF1 in exposure to different concentration of $E7_{(11-19)}$ peptide (p=0.0010). The results shown are representative of 3 independent experiments. Bars are indicative of standard deviations. *, ** and *** represent P values of ≤0.05, ≤ 0.01, ≤0.001, respectively.

The activation of Jurkat-EF1 after exposure to different concentration of peptides was also analyzed [Fig. 25b]. The results showed that by increasing the concentration of $E7_{(11-19)}$ peptide, there is an ascending trend in the expression of CD69 which was not observed in Un-Jurkat. The

upregulation of CD69 in exposure of 10 (p=0.01) and 100µM (p < 0.0001) was significantly higher compared to Un-Jurkat, however, there was no difference for 1µM of the $E7_{(11-19)}$ peptide. Therefore, Jurkat-EF1 was specifically activated in exposure of $E7_{(11-19)}$ peptide compared to Jurkat-EF2, Jurkat-EF3 and Un-Jurkat. Importantly, the upregulation of CD69 in Jurkat-EF1 is dependent on different concentration of $E7_{(11-19)}$ peptide.

## 3.9 Analysis of the affinity of the candidate TCRs to $E7_{(11-19)}$ tetramer and HPV16 cancer cell lines

The binding of TCR engineered Jurkat cell lines to $E7_{(11-19)}$ tetramer was evaluated [Fig. 26a]. Jurkat-EF1 (p=0.005), Jurkat-EF2 (p=0.0021) and Jurkat-EF2 (p=0.001) bound to $E7_{(11-19)}$ tetramer significantly compared to Untransduced Jurkat. Jurkat-EF1 had higher percentage of $E7_{(11-19)}$ $tetramer^{+}$ cells compared to Jurkat-EF2 (p=0.043), however, there was no significant difference between Jurkat-EF1 and Jurkat-EF3.

The affinity of TCR engineered Jurkat cell lines to $E7_{(11-19)}$ peptide and target cell lines was measured by Ligand tracer®. T2 cells were loaded either with $E7_{(11-19)}$ or HIV Pol peptide and seeded on opposite sides of the Ligand tracer® multi dish. In the case of target cell lines, Caski and SiHa were seeded on opposite sides of the plate. The CFSE labeled Jurkat cells moved to different position of the multi dish/plate by each rotation. Increasing the fluorescence intensity over time indicated the higher binding of the cells to a specific position of the multi dish/plate. The slope related to each part of the multi dish/plate was calculated by linear regression of

fluorescence intensity over time. The coefficient of binding was calculated by dividing the slope of the samples (E7 $_{(11\text{-}19)}$, Caski) by the slope of their controls (HIV pol, SiHa). Therefore, the coefficient of binding defined the tendency of Jurkat cell lines to E7$_{(11\text{-}19)}$ or Caski cell line and higher values means higher affinity.

The results of the binding of labeled TCR engineered Jurkat cell lines to T2 cells showed that Jurkat-EF1 had a significantly higher coefficient of binding compared to Un-Jurkat (p=0.04) However, the coefficient of binding of Jurkat-EF2 and Jurkat-EF3 were not significantly different [Fig. 26b].

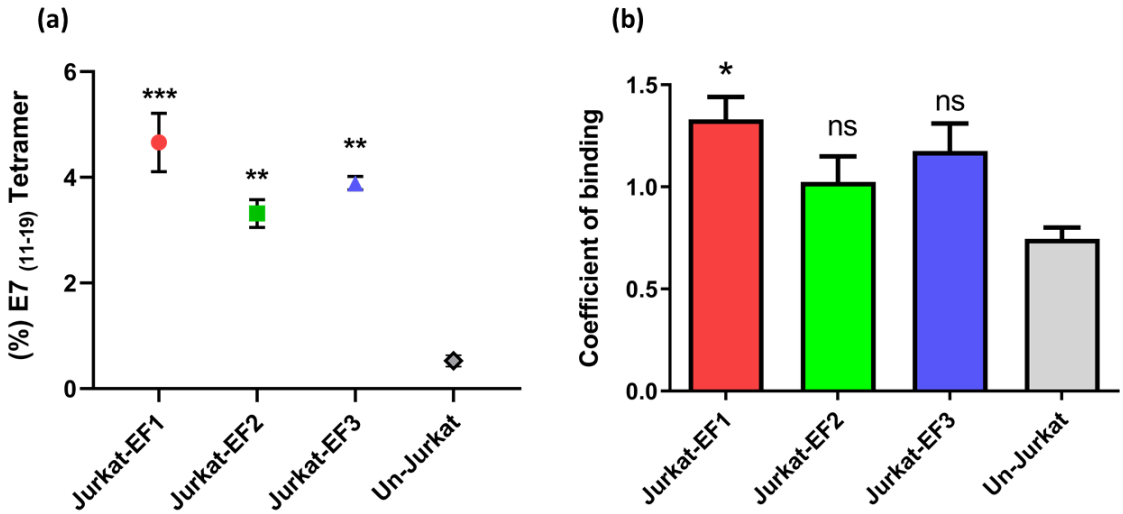


**Figure 26. The percentage of E7$_{(11\text{-}19)}$ tetramer$^+$ and coefficient of binding of TCR engineered Jurkat cell lines.** (a) The percentage of tetramer binding cells in Jurkat cell lines expressing candidate TCRs and Un-Jurkat. Jurkat EF1, EF2 and EF3 had higher tetramer binding cells compared to Un-Jurkat. (p=0.0008). (b) The coefficient of binding of TCR engineered Jurkat cell lines were measured by Ligand Tracer®. Unlike Jurkat-EF2 and Jurkat-EF3, Jurkat-EF1 had a higher coefficient of binding compared to Un-Jurkat. Bars are indicative of standard deviations. The results shown are representative of 2 independent experiments. *, ** and *** represent P values of ≤0.05, ≤ 0.01, ≤0.001, respectively.

On the other hand, binding of the TCR engineered Jurkat cell lines to Caski and SiHa showed different patterns of binding. The binding ratio was calculated by dividing the fluorescence intensity of Caski/ SiHa at each time point and values >1 indicated the higher affinity to Caski compared to SiHa. The results showed that the binding ratio of Jurkat-EF1 was on average 1.42 [Fig. 27a] and Jurkat EF2 and Jurkat EF3 was 1.1 [Fig. 27b&c].

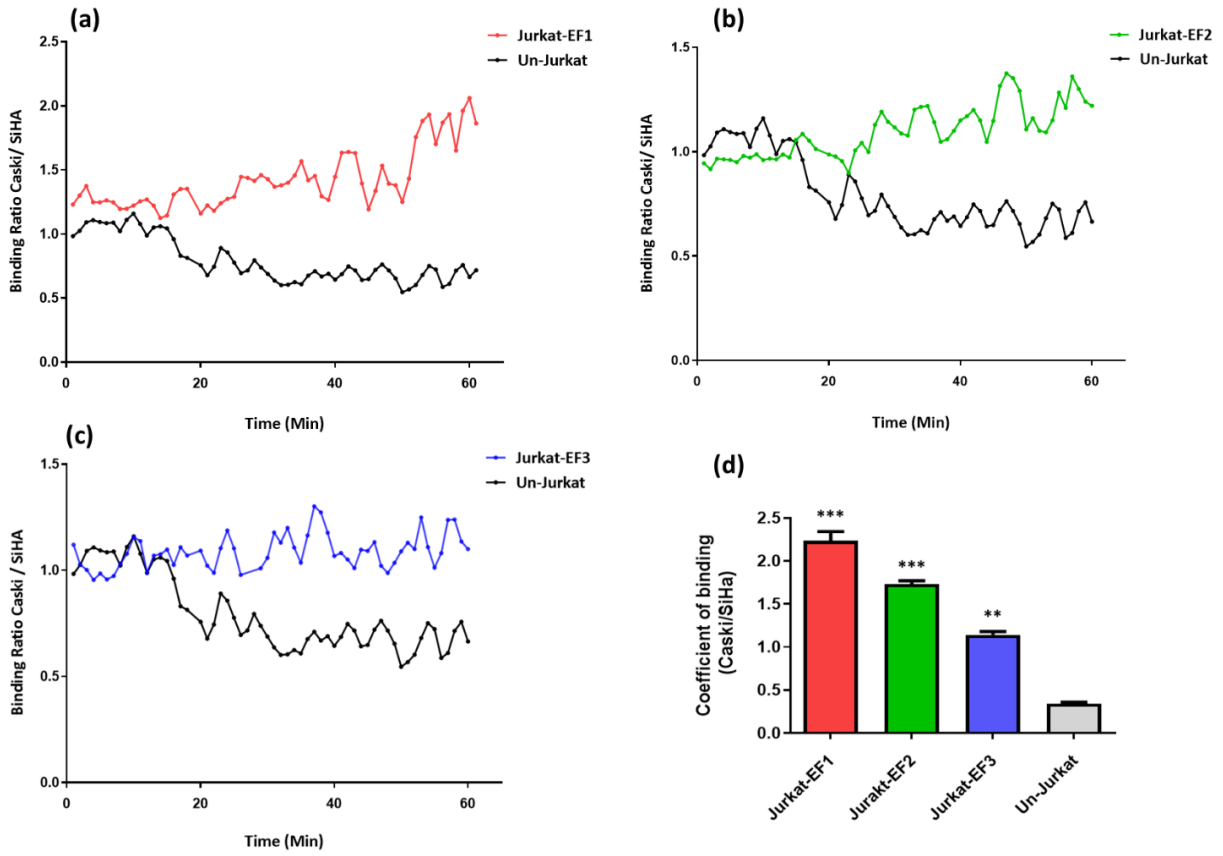


**Figure 27. The binding time course and coefficient of binding of TCR engineered Jurkat cell lines to Caski and SiHa.** (a), (b) and (c) shows the binding ratio of Jurkat-EF1, Jurkat-EF2 and Jurkat-EF3 compared to Un-Jurkat, respectively. (d) The coefficient of binding of TCR engineered Jurkat cell lines were higher compared to Un-Jurkat. The significant differences of TCR engineered Jurkat cell lines compared to Un-Jurkat are shown. Bars are indicative of standard deviations. The results shown are representative of 2 independent experiments. *, ** and *** represent P values of ≤0.05, ≤ 0.01, ≤0.001, respectively.

The binding ratio of Un-Jurkat was on average 0.8 which showed higher affinity of Un-Jurkat cell lines to SiHa compared to Caski. Moreover, the coefficient of binding of all TCR engineered Jurkat cell lines were significantly higher compared to Un-Jurkat ($p < 0.0001$) [Fig. 27d]. The coefficient of binding of Jurkat-EF1 was higher than Un-Jurkat ($p=0.0001$), Jurkat-EF2 ($p=0.01$) and Jurkat-EF3 ($p=0.0007$). The coefficient of binding of Jurkat EF2 had also higher values compared to Un-Jurkat ($p=0.0003$) and Jurkat-EF3 ($p=0.007$). Compared to other Candidate TCRs, Jurkat-EF3 had the lowest coefficient of binding which was significantly higher than Un-Jurkat ($p=0.0025$).

## 3.10 Expression of candidate TCRs in primary CD8$^+$ T cells and functional analysis

The CD8$^+$ T cells expressing eGFP and murine constant TCRβ were called as T cell-EF1, T cell-EF2 and T cell-EF3 and they were used for the functional analysis [Fig. 28].

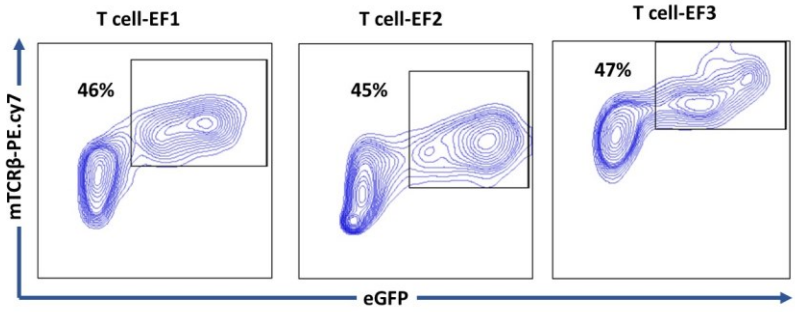


**Figure 28. Expression of TCR EF1-3 in primary CD8$^+$T cells.** The eGFP indicated the CD8$^+$ T cells which were successfully electroporated. The expression of candidate TCRs EF1-3 on CD8$^+$ T cells were confirmed by staining of murine constant TCRβ.

Following co-culture of T cells-EF1 with Caski ($p < 0.0001$) and UPSC-SCC154 ($p < 0.0001$), higher percentage of cells were IFNγ$^+$ compared to Untransfected T cells (Un-T cell) [Fig. 29]. Importantly, more T cells-EF1 were IFNγ$^+$ in co-culture with Caski compared to SiHa ($p=0.004$) and PCI-13 ($p=0.001$). Moreover, the secretion of IFNγ in T cell-EF1 following co culture with UPCI-SCC154 was higher than SiHa ($p=0.0053$) and PCI-13 ($p=0.001$). The IFNγ$^+$ cells of T cell-EF2 were increased significantly after co-culture with target cell lines compared to Un-T cell ($p < 0.0001$). However, there was no significant difference in the IFNγ secretion of T cells-EF2 in co-culture of Caski and UPSC-SCC154 compared to negative control cell lines, SiHa and PCI-13.

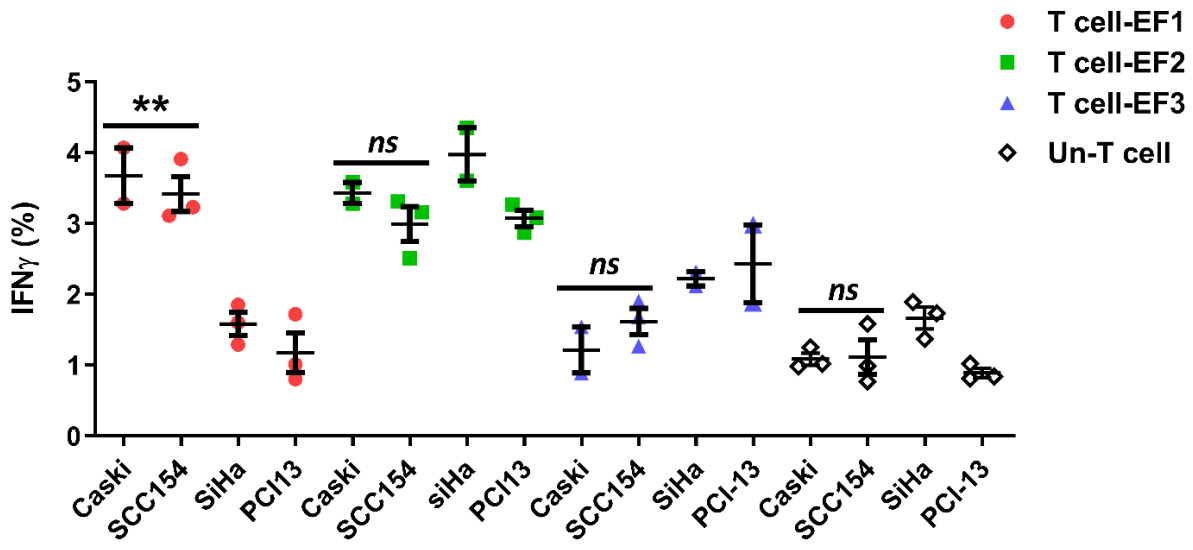


**Figure 29. Secretion of IFNγ by primary CD8$^+$ T cells expressing EF1, EF2 or EF3 after co-culture with target cell lines**. T cells expressing TCR-EF1 showed higher percentage of IFNγ$^+$ cells in co-culture with Caski and UPCI-SCC154 compared to other candidate TCRs. Error bars represent the SEM of 3 technical replicates. ** represent P values of ≤ 0.01.

No difference was detected between the percentage of IFNγ$^+$ cells of T cell-EF3 and Un-T cells in co-culture with Caski, UPCI-SCC154 and SiHa. Importantly, co-culture of T cells-EF3 with Caski

and UPSC-SCC154 did not induce higher IFNγ secretion compared to SiHa and PCI-13. Therefore, T cells expressing TCR-EF1 can specifically became activated in co-culture with HPV16+, HLA-A2+ cell lines, whereas TCR-EF2 and TCR-EF3 did not activate the T cells specifically.

The IFNγ secretion of TCR engineered T cells after exposure to E7 $_{(11-19)}$ epitope was also analyzed. The T2 cell lines were loaded with different concentrations of E7$_{(11-19)}$ peptide and co-cultured with CD8$^{+}$ T cells expressing candidate TCRs. The MFI of IFNγ in T cells-EF1 had an ascending pattern in exposure to increasing concentrations of E7 $_{(11-19)}$ epitope. However, this pattern was not detected in T cells-EF2 and T cells-EF3 [Fig. 30]. T cells-EF1 had higher MFI for IFNγ following co-culture with T2 cells loaded with 10µM (p=0.04) and 100µM (p=0.002) of E7 $_{(11-19)}$ peptide compared to Un-T cells.

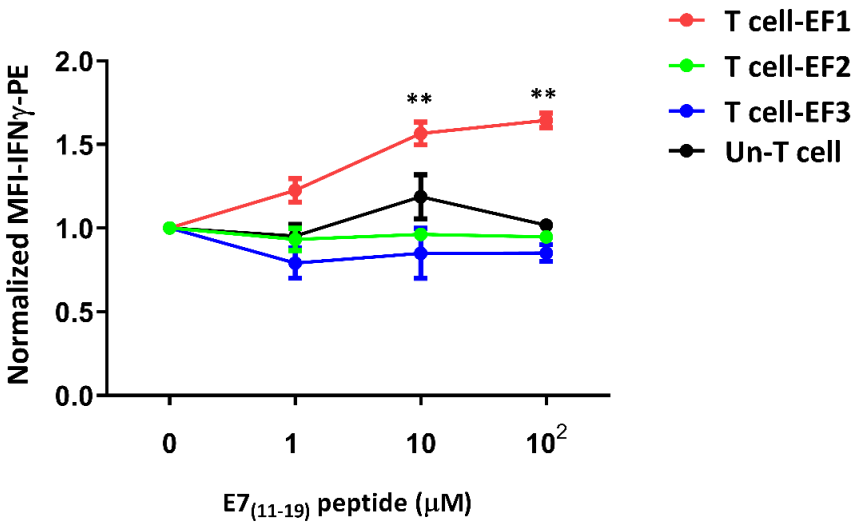


**Figure 30. MFI of IFNγ in TCR engineered CD8$^{+}$ T cells in co-culture with T2 cell lines loaded with different concentrations of E7 $_{(11-19)}$ peptide.** T cells expressing TCR-EF1 showed significantly higher MFI-IFNγ in exposure of 10µM and 100µM of E7 $_{(11-19)}$ peptide. There was no significant difference in the MFI-IFNγ of T cells-EF2 and T cells-EF3 following stimulation with different concentration of E7 $_{(11-19)}$ peptide. Error bars represent the SEM of 3 technical replicates. ** represents P values of ≤ 0.01.

There was no significant difference in MFI- IFNγ of T cells- EF1 following stimulation with 1µM of E7 $_{(11-19)}$ peptide. The MFI- IFNγ of T cells- EF2 and T cells-EF3 did not change in exposure of different concentration of E7 $_{(11-19)}$ epitope compared to Un-T cells.

As the next step, the TCR engineered $CD8^+$ T cells were co-cultured with Caski and SiHa to assess their ability to lyse the cells [Fig. 31]. T cells-EF1 induced significant lysis in Caski cell line compared to SiHa (p=0.0073). Caski and SiHa are both HPV16 positive cell lines, however, SiHa is HLA-A2 negative. This result further highlighted that the activation of TCR-EF1 is dependent on HLA-A2 molecule. There was no significant difference in the relative lysis of Caski and SiHa cell lines following co-culture with T cells-EF2 or T cells-EF3.

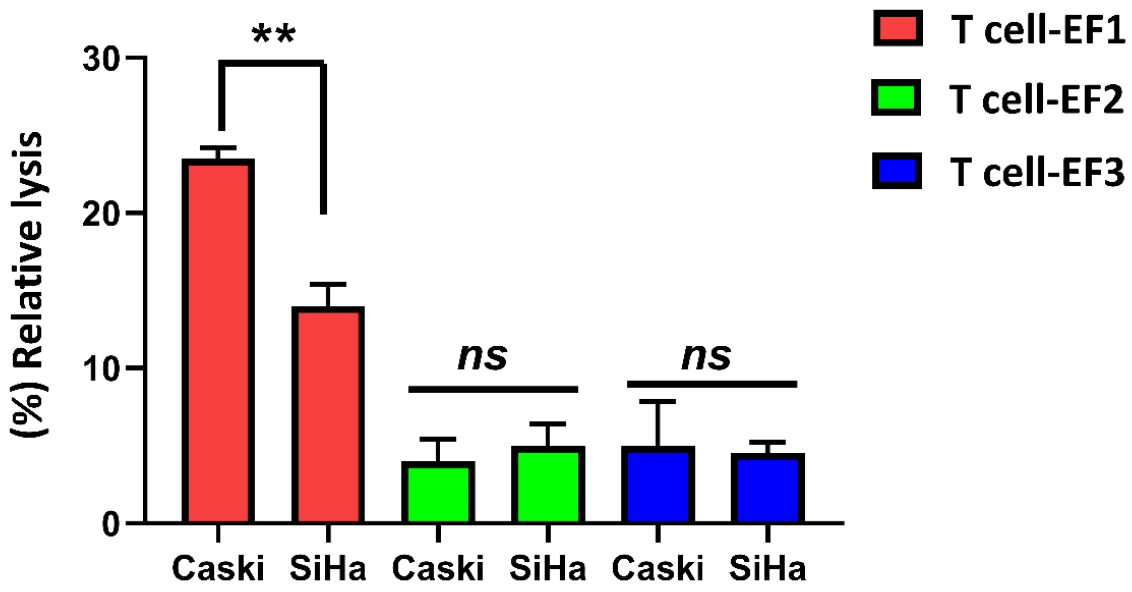


**Figure 31. Relative lysis of HPV16 positive cancer cell lines after co-culture with TCR engineered $CD8^+$ T cells.** T cells-EF1 induced lysis in Caski cell line compared to SiHa. However, there was no significant difference in the relative lysis of the target cell lines following co culture with T cells-EF2 and T cells-EF3. Error bars represent the SEM of 3 technical replicates. ** represent P values of ≤ 0.01.

## 3.11 *In silico* characterization of the four candidate TCRs targeting the E7$_{(11-19)}$ epitope

The interaction of the candidate TCRs with E7 $_{(11-19)}$-HLA-A*02 was assessed *In silico* . The 3D structures of TCR EF1-4 were predicted and refined using the Galaxy web server. Based on the results of SWARM Dock server, the interacting residues of CDR3α/β of each TCR and E7 $_{(11-19)}$ were identified and shown in red [Fig. 32]. The previously described TCR clonotype reactive to E7$_{(11-19)}$ (E7-TCR) was used as Reference control and the TCR targeting-Gag-HIV was considered as negative control. It has been shown that amino acids at position 4,5,6,7 of E7 $_{(11-19)}$ peptide are important for interacting with the CDR3 regions.

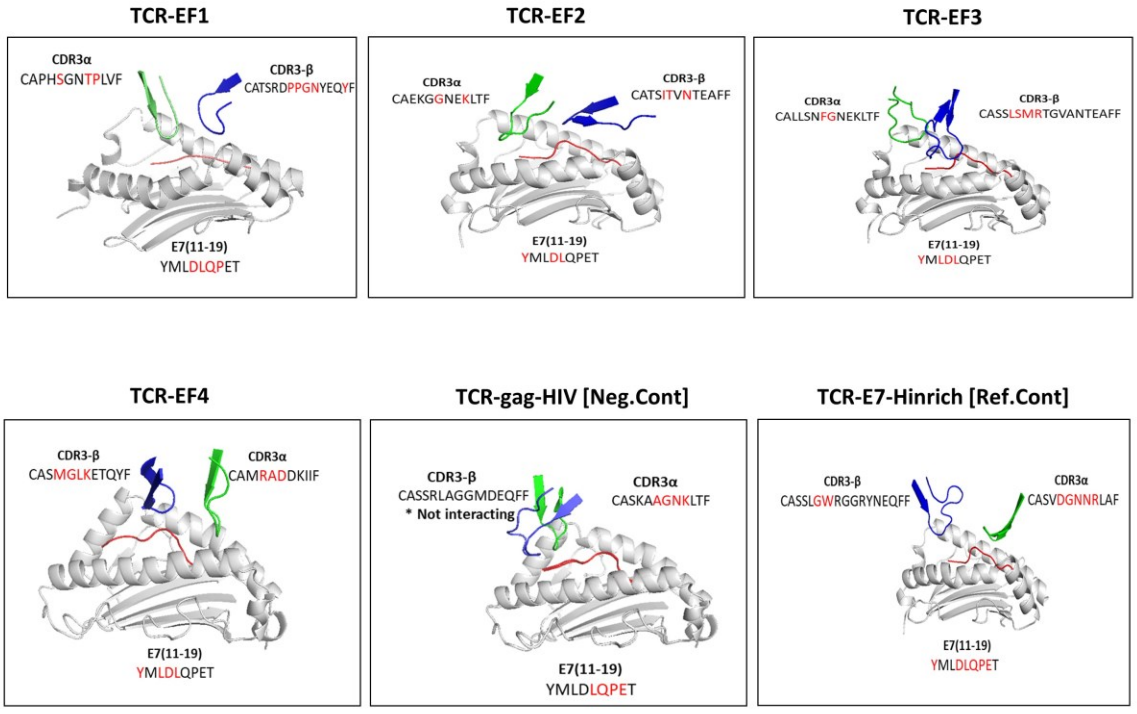


**Figure 32. *In silico* analysis of the interaction of the four candidate TCRs with E7 $_{(11-19)}$- HLA-A*02.** The HLA-A*02 molecule is gray and the E7 $_{(11-19)}$ is in red. The CDR3α and CDR3β chains are shown in green and blue, respectively. The interacting residues are shown in red.

According to the results of *In silico* analysis, TCR-EF1 interacted with all important residues of the E7 $_{(11\text{-}19)}$ peptide. However, TCR- EF2, EF3 and EF4 only interacted with 2 out of 4 essential amino acids of the epitope [Fig. 33a]. Moreover, the ΔG of the interaction between E7 $_{(11\text{-}19)}$- HLA-A*02 and TCR-EF1 was the lowest compared to other candidates, negative and reference control [Fig. 33 b]. The ΔG values for TCR-EF1, EF2, EF3, EF4, negative and reference controls were -13.05, -11.57, -11.90, -11.90, -10.35 and -12.00 respectively.

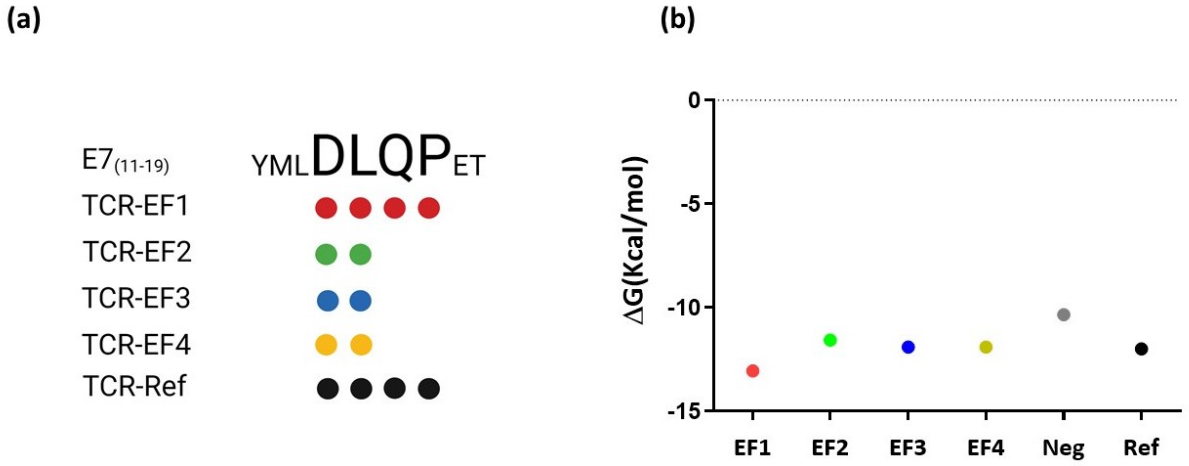


**Figure 33. Interaction of CDR3 regions of candidate TCRs with E7 $_{(11\text{-}19)}$- HLA-A*02.** (a) The essential amino acids for efficient interaction of E7 $_{(11\text{-}19)}$ peptide and CDR3 regions are shown in Bold letters. The interacting amino acids for the TCRs are shown by colorful dots. The CDR3 regions of TCR-EF1 had interactions with all important amino acids of the epitope. (b) The ΔG of the interaction between E7 $_{(11\text{-}19)}$- HLA-A*02 and candidate TCRs. TCR-EF1 has the lowest value.

According to the important interacting residues of the peptide and ΔG values, TCR-EF1 was a better candidate compared to EF2, EF3 and EF4. As the *In silico* analysis was in accordance with *in vitro* results, another eighteen TCR candidates from the [IFNγ-tet] and [CD137-IFNγ-tet] V(D)J libraries were selected for *In silico* characterization. The new candidate TCRs were named as TCR-EF5 to TCR-EF22 and they were chosen based on their frequencies and similarities with CDR3 regions of TCR-EF1. The detailed information of TCR EF5-EF22 is listed in [Appendix.

Table.3]. The *In silico* analysis showed that eight candidate TCRs, TCR EF-7, EF8, EF9, EF13, EF16, EF17, EF18 and EF 20, interacted with all essential amino acids within the E7 $_{(11\text{-}19)}$. The *In silico* simulations of the interaction of these eight candidate TCRs are shown in [Fig. 34] and the other candidate TCRs are depicted in [Appendix-Figure.11].

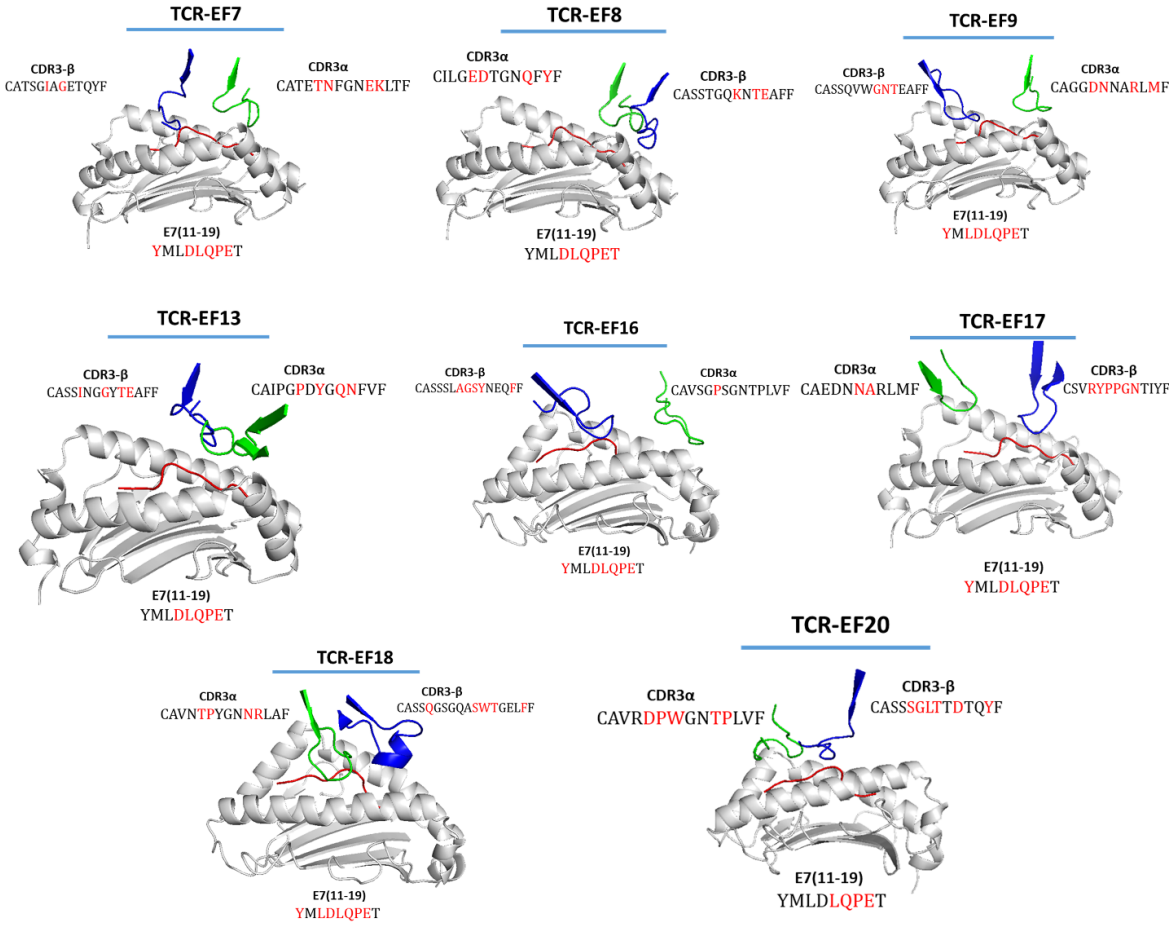


**Figure 34. *In silico* analysis of the interaction of the candidate TCRs with E7 $_{(11\text{-}19)}$- HLA-A*02.** Candidate TCRs TCR EF-7, EF8, EF9, EF13, EF16, EF17, EF18 and EF 20 had interaction with essential amino acids of the epitope at position 4-7. the E7 $_{(11\text{-}19)}$ peptide is shown in red and the HLA-A*02 molecule is in white. The CDR3α and CDR3β chains are shown in green and blue, respectively. The interacting residues are depicted in red.

TCR -EF12 and EF-14 were removed from the analysis because their CDR3α did not interact with the peptide. Interestingly, 6 out of these 8 TCRs had ΔG value of interaction lower than the reference control which was -12.00 kcal/mol [Table.13].

**Table 13. Interaction of identified TCRs with amino acids 4-7 of the E7 $_{(11-19)}$ peptide and the ΔG of their interaction with pMHC complex.** The candidate TCRs shown in red interact with all essential amino acids of the epitope.

| TCR | D | L | Q | P | ΔG (kcal/mol) |
|---|---|---|---|---|---|
| EF-5 | | | | | -13.40 |
| EF-6 | | | | | -13.45 |
| EF-7 | | | | | -11.15 |
| EF-8 | | | | | -13.05 |
| EF-9 | | | | | -12.30 |
| EF-10 | | | | | -12.95 |
| EF-11 | | | | | -14.25 |
| EF-13 | | | | | -14.20 |
| EF-15 | | | | | -12.25 |
| EF-16 | | | | | -11.85 |
| EF-17 | | | | | -12.40 |
| EF-18 | | | | | -14.00 |
| EF-19 | | | | | -13.00 |
| EF-20 | | | | | -14.00 |
| EF-21 | | | | | -12.70 |
| EF-22 | | | | | -13.45 |

## 3.12 Screening of interacting motifs in CDR3β of candidate TCRs in ImmunoSEQ data base

The interacting motifs within the CDR3β of TCR candidates EF1-EF22 were selected [Table 14]. The selected motifs were 5-6 residues and they were not within the three first/last amino acids. Moreover, at least two of the residues of each motif were involved in the interaction with the epitope according to the docking results.

**Table 14. Interacting motifs within the CDR3β sequences of identified TCRs.** The motifs were 5-6 residues and ≥2 of them were involved in the interaction with the $E7_{(11-19)}$ epitope. The interacting residues within CDR3β are shown in red.

| Candidate TCRs | CDR3β | Motifs |
|---|---|---|
| **EF-1** | CATSRDPPGNYEQYF | DPPGN |
| **EF-2** | CATSITVNTEAFF | ITVNT |
| **EF-3** | CASSLSMRTGVANTEAFF | LSMRT |
| **EF-4** | CASMGLKETQYF | MGLKE |
| **EF-5** | CASSVGILTTGQPQHF | VGILT |
| **EF-6** | CASSLIGVSSNNEQFF | IGVSS |
| **EF-7** | CATSGIAGETQYF | GIAGE |
| **EF-8** | CASSTGQKNTEAFF | QKNTE |
| **EF-9** | CASSQVWGNTEAFF | VWGNT |
| **EF-10** | CASSWTKSYEQYF | KSYEQ |
| **EF-11** | CSARGGFDPGELFF | GGFDP |
| **EF-13** | CASSINGGYTEAFF | NGGYTE |
| **EF-15** | CASRIAGATYNEQFF | RIAGA |
| **EF-16** | CASSSLAGSYNEQFF | SLAGSY |
| **EF-17** | CSVRYPPGNTIYF | YPPGN |
| **EF-18** | CASSQGSGQASWTGELFF | ASWTG |
| **EF-19** | CASSYSRGEQFF | YSRGE |
| **EF-20** | CASSSGLTTDTQYF | SGLTT |
| **EF-21** | CATSRDPPGNYEQYF | DPPGN |
| **EF-22** | CASSIGSRGYNEQFF | RGYNE |

The motifs were used for screening of the TCRβ repertoire of 25patients who cleared and 25 patients who were at intraepithelial neoplasia grade 3 (CIN3) or higher, which are in the Immuneaccess® Open Access Database, supplied by Adaptive Biotechnologies Corp (183). The analysis showed that around 70% (12 out of 17) of the motifs were enriched in TCRβ repertoire of the patients who cleared HPV16 infection compared to patients at CIN 3 [Fig. 35].

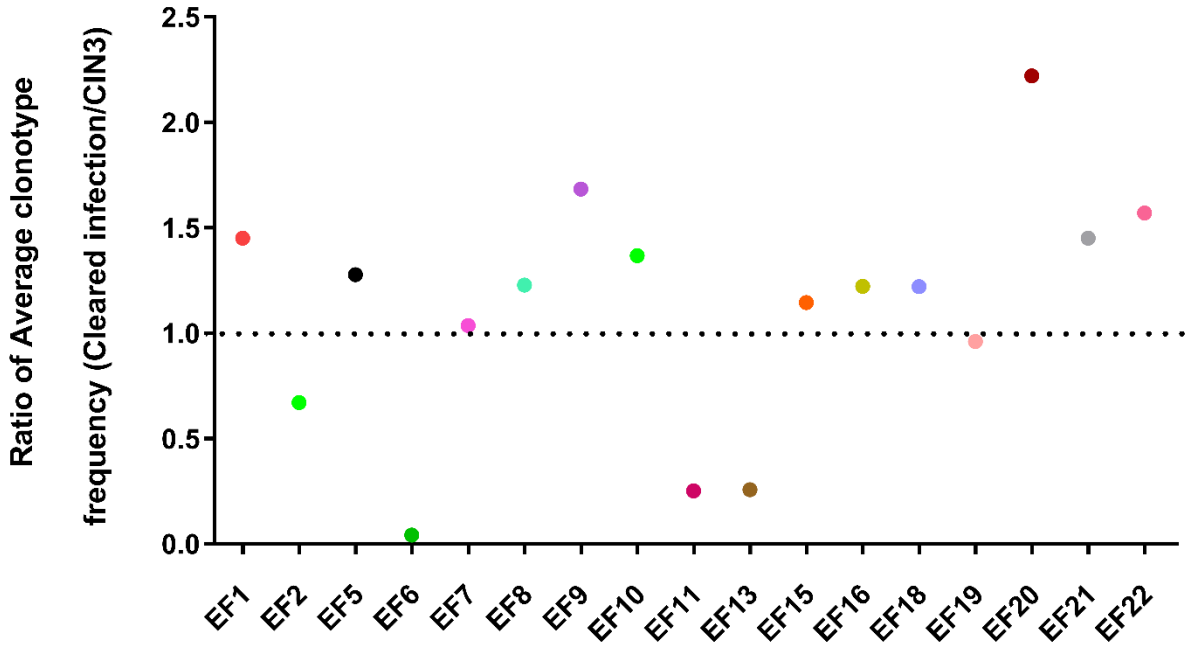


**Figure 35. Ratio of average frequencies of the motifs of identified TCRs in patients who cleared HPV infection versus patients with CIN3**. Most of the motifs identified from candidate TCRs were enriched in patients who cleared HPV infection.

TCRs EF3, EF4 and EF17 were not considered in this analysis because the motifs of TCR-EF3 and EF4 were only found in patients who cleared HPV 16 infection and the motif of TCR-EF17 was only detected in a patient at CIN3 stage. Interestingly, four TCR clonotypes (TCR-EF8, TCR-EF16, TCR EF19, TCR-EF20) were found in total 17 out of 50 patients of the TCRβ repertoire of the

Immunoseq Database [Fig. 36]. TCR-EF8, TCR-EF16 and TCR-EF19, each were found in 2 patients who cleared HPV16 infection and in 2,3 and 4 patients at CIN3 stage, respectively. TCR-EF20 were in 1 patient who cleared the infection and 1 patient at CIN3. The average clonotype frequencies of TCR EF-8, EF-16 and EF-20 were higher in patients who cleared HPV 16 infection. However, the average clonotype frequency of TCR-EF19 was higher in patients at CIN3 stage.

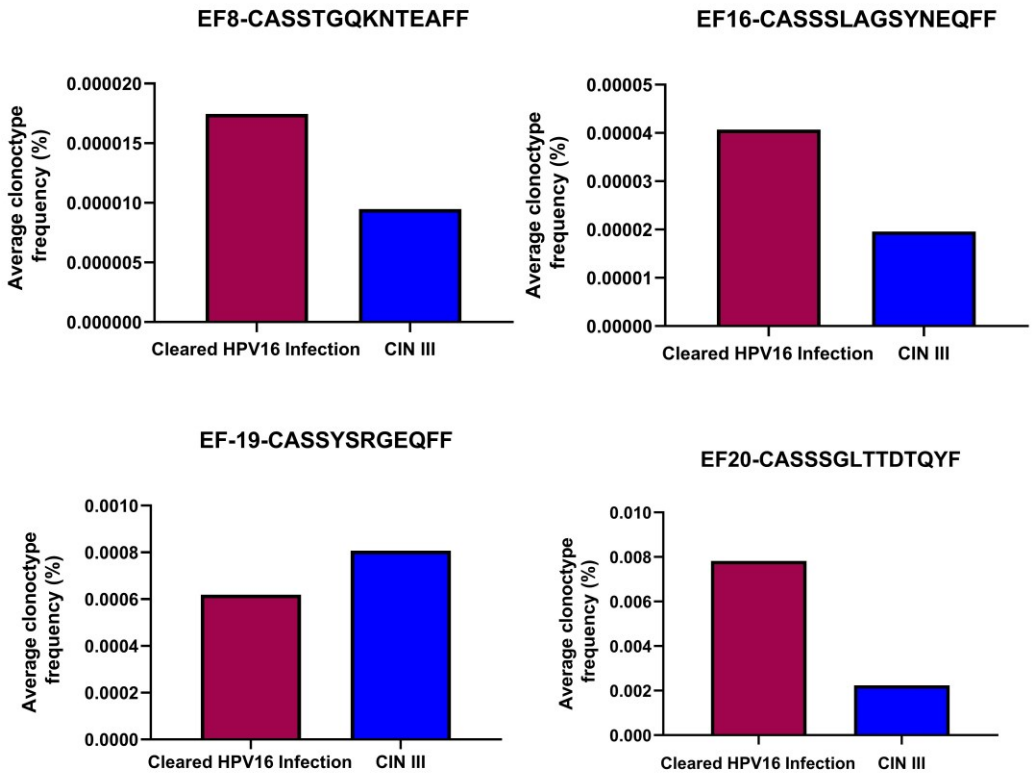


**Figure 36.Four TCR clonotypes (TCR-EF8, TCR-EF16, TCR EF19, TCR-EF20) found in the TCRβ repertoire of the Immunoseq Database.** These clonotypes were found at different frequencies in 17 patients including both individuals with CIN3 or those who cleared HPV 16 infection. Three out of four clonotypes, EF8, EF16 and EF20, had higher average frequencies in patients who cleared HPV 16 infection.

# 4. Discussion

HPV 16 is a causative agent of various types of cancer. The HPV16 E7 oncoprotein is continuously expressed by infected tumor cells and $E7_{(11-19)}$ is a well characterized epitope which is conserved among HPV16 strains. This epitope is presented by HLA-A*02:01 molecules and it is an ideal target for engineered TCR T cell therapy due to its viral source and for being absent in healthy tissues. However, identification of TCRs reactive to the $E7_{(11-19)}$ epitope has been challenging. T cells can recognize the foreign antigens through pMHC molecules on the surface of APCs. The interaction of T cells and APCs has a complex nature and thousands of TCRs can identify an immunodominant epitope and one TCR can interact with thousands of epitopes. This complexity is due to the V(D)J recombination which enhances the recognition power of the adaptive immunity. Besides that, finding an optimal source for selecting the most relevant TCRs is another challenge to be addressed. TILs derived from HPV16+ tumor samples have shown weak responses to the E7 oncoprotein. This can be related to their exhausted phenotype or to chronic antigen presentation which can further alter the avidity profile of TCRs. Therefore, in this study we focused on *in vitro* stimulation of $CD8^+$ T cells from healthy donors who have not been constantly exposed to the antigen to identify a broad range of TCRs with different recognition capabilities. In the first step, the functionality of the E7-Flt3L fusion protein was analyzed *in silico* and *in vitro.* Then, the TCR repertoire of T cells reactive to $E7_{(11-19)}$ was identified by V(D)J single cell sequencing. Three TCR clonotypes were characterized *in vitro* and, at least, one of them showed promising functionality. Further *in silico* analysis of additional TCR clonotypes provided valuable information for TCR discovery.

## 4.1 Efficient workflow for identification of TCRs reactive to $E7_{(11-19)}$

### 4.1.1 E7-Flt3L: a functional fusion protein inducing effective T cell activation through antigen presentation on hmo-DCs

Flt3L is an essential cytokine which can induce functional differentiation of DCs and promote them to be efficient APCs. Following fusion of $E7_{(1-30)}$ to the extracellular domain of Flt3, an important question was whether the $E7_{(1-30)}$ had an impact on the interaction of Flt3L with the Flt3 receptor. According to the *in silico* analysis, addition of $E7_{(1-30)}$ not only does not interfere with the interaction of Flt3L to its receptor but enhanced the ΔG of interaction from -7.3 kcal $mol^{-1}$ to -11.2 kcal $mol^{-1}$, probably due to a synergistic effect of $E7_{(1-30)}$ on the Flt3L-Flt3 complex. Moreover, this addition to Flt3L caused the protein to be more hydrophilic (GRAVY = -0.487) compared to the wild type Flt3L (GRAVY = -0.184). The hydropathy values of 73% amino acids of E7 (22/30) were negative and this can explain the increased hydrophilicity of E7-Flt3L (179). Importantly, the calculation of physico-chemical properties showed that E7-Flt3L fusion protein is more stable than the human wild type Flt3L. It has been shown that certain dipeptides play an essential role in the stability of the proteins (184). The lower instability index of E7-Flt3L indicated that the overall composition of its dipeptides favored the stability. Compared to the fusion protein, human wild type Flt3L had more dipeptides causing instability such as Arginine-Arginine, Proline-Glutamine, Proline-Proline and proline-valine. Therefore, affinity of interaction and stability scores of E7-Flt3L were higher than those of the human wild type Flt3L.

The other point needed to be addressed was the fate of E7-Flt3L fusion protein in hmo-imDCs, which are highly efficient in antigen uptake. Hung et al. showed that the extracellular domain of Flt3L can favor the localization of HPV16 E7 oncoprotein in the ER compartments (185). Compatible with this, our confocal images demonstrated that the E7-Flt3L was localized close to the ER. Furthermore, it has been shown that Flt3L promotes the internalization of Flt3 receptor and the degradation of the internalized receptor can be observed around 20 min after Flt3L-Flt3 interaction (186, 187). In accordance with this, the flow cytometry analysis showed that the percentage of $CD11c^+$, $CD135^+$ DCs have a significant decrease following 30 min incubation of E7-Flt3L with hmo-imDCs. This further validated the binding of E7-Flt3L to its receptor which was predicted *in silico*.

As E7-Flt3L was uptaken by hmo-imDCs, the E7 peptide needed to be processed and cross presented on MHC class I to activate $CD8^+$ T cells. Importantly, it has been shown that Flt3L can promote the antigen uptake and cross-presentation (188). Thus, hmo-imDCs should undergo maturation since mDCs are efficient in antigen presentation and cross-presentation (Section 1.1.2). Kim et al. reported that Flt3L-treatment upregulates CD80,CD83 and CD86 in monocyte derived DCs (mo-DCs) (189). Our results also showed that E7-Flt3L, at different concentrations, significantly increased the expression of CD80, CD83 and CD86 in $CD11c^+$ cells following 18- and 42h incubation. Although, the upregulation of CD80 and CD86 was higher after 18h compared to 42 hours, there was no difference in the expression of CD83 at different time points. This can be explained by the intrinsic properties of hmo-DCs in exposure of stimulants. It has been shown that 48 h incubation of hmo-DCs with LPS did not change the expression of CD83 remarkably compared to 24h (190).

There was no change in the percentage of $CD11c^+$ cells and this further confirmed the FLt3L induced maturation pattern which was described previously (189). Based on our results, E7-Flt3L upregulated the costimulatory molecules on hmo-DCs which is an important prerequisite for efficient antigen presentation and activation of T cells. After confirming the functionality of E7-Flt3L, this fusion protein was used for stimulation of $CD8^+$ T cells derived from healthy donors.

### 4.1.2 Identification of truly E7-reactive T cells by combining tetramer binding and detection of activation markers

The impact of E7-Flt3L fusion protein on the stimulation of $CD8^+$ T cells reactive to $E7_{(11-19)}$ epitope was analyzed systematically. We observed that effect of E7-Flt3L on the percentages of $E7_{(11-19)}$ -tetramer$^+$ $CD8^+$ T cells was dose-dependent. E7-Flt3L at concentration of 5µg/ml induced an efficient activation in the $CD8^+$ T cells compared to other concentrations, 1- and 10 µg/ml. Importantly, E7-Flt3L (5µg/ml) increased the percentage of $CD8^+$ $E7_{(11-19)}$ -tetramer$^+$ T cells which were also IFN-$\gamma^+$ at different time points. One possible explanation can be related to the expression of costimulatory molecules on hmo-imDCs in response to different concentration of E7-Flt3L which can affect antigen presentation and subsequent activation of the T cells. However, our results showed that there was no significant difference in the expression of CD80, CD83 and CD86 on hmo-imDCs in exposure to 1 µg/ml, 5 µg/ml and 10 µg/ml of the fusion protein. It has been already shown that the effect of Flt3L on the functionality of hmo-DCs is dose-dependent (189). In that study, the mo-DCs were treated with

different concentration of Flt3L: 5,10,50,100 and 200 ng/ml. They indicated that mo-DCs generated by 50-100 ng/ml of Flt3L induced a strong stimulation for the proliferation of allogenic T cells. Compatible with these findings, our results demonstrated that E7-Flt3L at its optimal concentration efficiently activated $CD8^+$ T cells. This further supports the functionality of Flt3L in the form of the fusion protein. Furthermore, Drake et al. reported that $CD8^+$ T cells exposed to suboptimal concentrations of antigen had lower tetramer binding and secretion of IFN-γ (191). Our findings also demonstrated that E7-Flt3L (1 µg/ml) was suboptimal concentration and resulted in lower percentage of $CD8^+$ $E7_{(11-19)}$ -$tetramer^+$ IFN-$\gamma^+$ T cells compared to 5 µg/ml. Moreover, a higher concentration of the fusion protein did not augment its stimulatory effect. Following the incubation of the cells with E7-Flt3L (10 µg/ml) at different time points, the percentages of $CD8^+$ $E7_{(11-19)}$ -$tetramer^+$ T cells did not change compared to the control. This can be explained by the fact that higher concentrations of antigen could lead to TCR downregulation and subsequently to lower tetramer binding (192). However, we observed that E7-Flt3L (10 µg/ml) increased the $CD8^+$ $E7_{(11-19)}$ -$tetramer^+$ IFN-$\gamma^+$ T cells and this might be due to the aggregation of the fusion protein at high concentration, which could cause unspecific activation of the $CD8^+$ T cells and secretion of higher amounts of IFN-γ. Further investigations are needed to explain precisely the activation resulting from different concentrations of the fusion protein.

In the next step, the stimulatory effect of E7-Flt3L (5 µg/ml) at different Incubation times was compared. Our results showed that following 5 days of coculture, the percentages of $CD8^+$ $E7_{(11-19)}$ -$tetramer^+$ IFN-$\gamma^+$ T cells was remarkably higher compared to 2- and 12 days. It was shown previously that tetramer binding of T cells was decreased at day 2-3 of stimulation and restored

at day 4 (191). This can explain the lower percentages of $CD8^+$ $E7_{(11-19)}$ -$tetramer^+$ T cells at day 2 compared to day 5. Moreover, the percentages of $CD8^+$ IFN-$\gamma^+$ T cells at 5- and 12-days incubation increased. The lower percentage of the INF-$\gamma^+$ T cells at day 12 compared to day 5 can be related to the exhaustion of the cells due to the chronic stimulation. Further analysis is needed to evaluate the exhaustion markers of $CD8^+$ T cells following 12 days of incubation with E7-Flt3L (5 μg/ml). Besides that, the efficient activation of the $CD8^+$ T cells following stimulation with E7-Flt3L (5 μg/ml) was further confirmed by the upregulation of CD137, a member of TNFR family. It has been shown that high expression of CD137 can be used for identification of antigen-specific $CD8^+$ T cells (193). Our results demonstrated that following stimulation with E7-Flt3L (5 μg/ml), the percentage of $CD8^+$, $CD137^+$, $E7_{(11-19)}$ -$tetramer^+$ T cells was increased at different time points. The upregulation of CD137 was also in accordance with the efficient stimulatory effect of E7-Flt3L (5 μg/ml) on hmo-DCs. Moreover, the percentage of $CD8^+$, $CD137^+$, $E7_{(11-19)}$ -$tetramer^+$ T cells at day 5 was significantly higher compared to other time points which further confirmed the efficient activation of $CD8^+$ T cells following 5 days of stimulation with the fusion protein. The stimulatory effect of E7-Flt3L (5 μg/ml) at day 5 was also consistent among different healthy donors, one of them showing a 5-fold increase of tetramer binding cells. The higher reactivity of Donor2 can be explained by the increased proliferation rate of $CD3^+$ $CD8^+$ $CD137^+$ T cells, which emerged as a small population in the tSNE analysis.

Then, the stimulatory effect of E7-Flt3L (5 μg/ml) was compared with that induced by $E7_{(11-19)}$. The $CD8^+$, $E7_{(11-19)}$ -$tetramer^+$ T cells were decreased following 2 days stimulation with $E7_{(11-19)}$ epitope and restored at day5. This transient loss of tetramer binding phenotype has been

already described after exposure to high concentrations of peptide ($10^{-5}$ M) (191). However, following 2- and 5 days of stimulation of T cells with E7Flt3L (5 µg/ml), the percentage of $CD8^+$, $E7_{(11-19)}$ -tetramer$^+$ T cells were increased. The population of the $CD8^+$T cells reactive to $E7_{(11-19)}$ -tetramer was remarkable at day 5 of stimulation with the fusion protein. Importantly, these tetramer binding cells showed functional phenotype by upregulation of CD137 and secretion of IFN-γ. The higher stimulatory effect of the fusion protein compared to the peptide may be related to the state of the hmo-DCs. In this comparison, hmo-imDCs were loaded with either fusion protein or the $E7_{(11-19)}$ peptide. It has been shown that only hmo-mDCs can be efficiently loaded with exogenous peptide. Therefore, we combined the treatment of the $E7_{(11-19)}$ peptide with E7-Flt3L (5 µg/ml) and the results showed that the stimulatory effect of the combination was still lower than that with the fusion protein only. Another possible explanation can be the fact that stimulation of the T cells with high concentrations of peptide can simulate a chronic infection that could affect the tetramer binding and functionality of the cells. As a result, E7-Flt3L can activate the $CD8^+$ T cells more efficiently compared to the peptide stimulation.

The described *in vitro* stimulation with E7-Flt3L fusion protein was used for identification of $CD8^+$ T cells targeting HLA-A*02:01-restricted HPV16 $E7_{(11-19)}$ epitope in healthy individuals. In accordance with our workflow, Spindler et al. have recently highlighted the fact that analyzing the functionality and tetramer binding is important for efficient selection of T cells (194). The reactive T cells were sorted in the two groups of [IFNγ$^+$-tet$^+$] or [CD137$^+$/IFNγ$^+$/tet$^+$] and were processed for single cell V(D) J sequencing (10x genomics) to decipher the complexity of the TCRs reactive to $E7_{(11-19)}$ epitope.

## 4.2 Selection of candidate TCRs reactive to $E7_{(11-19)}$: finding the needle in the haystack

Following the analysis of the sequencing data, 169 paired TCRαβ clonotypes from the IFNγ-tet library (4000 sorted $CD8^+$ T cells) and 69 paired TCRαβ clonotypes from the CD137- IFNγ-tet library (2000 $CD8^+$ T cells) were retrieved. Compared to the initial input, the numbers of clonotypes identified were low. This can be explained by the quality and viability of the cells prior to the GEM formation. The sorted cells were thawed just before the experiment and cell viability was not measured due to the limited number of cells. Moreover, it is recommended to use fresh samples for the 10x platform and avoid freezing the cells. In our workflow, freezing of the cells was inevitable since we had to pool cells of two different donors for CD137- IFNγ-tet library to reach adequate numbers of cells. Although adding more selection parameters, such as tetramer binding and CD137 can enhance the reliability of the sorted T cells, it can also reduce the number of cells finally available for sequencing which affects downstream analysis.

Different criteria were used for the selection of TCRs for functional analyses. TCR-EF1 and TCR-EF2 were the top selected clonotypes from the [CD137-IFNγ-tet] and [IFNγ-tet] libraries, respectively. The frequency of the TCR clonotypes can be taken as an indirect indicative of its reactivity to a specific antigen. Studies have demonstrated that brief stimulation ,2-24h, of $CD8^+$ T cells with an antigen can lead them to at least 7-10 cell divisions (195-197). Another selection parameter was TCRs sharing the V gene segment in the two libraries or with a known E7-TCR used here as reference. Clustering of the TCR sequences targeting a specific epitope provided evidence of a bias in the usage of certain V-genes and CDR3 amino acid motifs (198, 199).

Moreover, it has been reported that shared TRAV-gene usage accounts for epitope specific responses of $CD4^+$ T cells *in vitro* (200). In accordance with these criteria, we selected our four candidate TCR based on their TRAV/TRBV gene segments and similarity with the CDR3β of a previously published TCR targeting $E7_{(11-20)}$. The median UMI/contig values which were described in the Loupe V(D)J was also used for the selection. Contig is the contiguous sequence of bases produced by de novo assembly. Each first-strand cDNA synthesis from a transcript molecule incorporates a random 10 bp nucleotide sequence called the UMI (unique molecular identifier) which is added during GEM generation. The UMI sequence in each read allows the system to determine which reads came from the same transcript molecule. In other words, the cell barcode distinguishes between cells, and the UMI distinguishes between molecules (for example, RNA fragments) within a cell. Due to the problem that we encountered with the expression of TCR-EF4, it is also advisable to check the signal peptide of the TCR sequence since the Loupe V(D)J can be error prone in distinguishing the right start codon. Therefore, different criteria were used to select four candidate TCRs among 238 different clonotypes for further characterization.

### 4.2.1 Expression of candidate TCRs on Jurkat cell line and $CD8^+$ T cells

In the next step, LVs expressing the selected TCRs were produced and titrated. Interestingly, we observed that the titer of the LVs expressing different candidate TCRs showed variability, and TCR-EF1 had a higher average titer compared to the others. It has been reported that increase in the genome size can reduce the LV titer, however, the size of the candidate TCRs were

relatively similar, around 1.8 kb (201). The difference in the titers of the LVs can be related to the sequences of the TCRs. Due to the different TRAV/ TRBV sequences, the protein structure of the TCRs were not the same and they may result toxic for the HEK293T cells. This toxicity can affect the viability and subsequently the packaging of the LV particles. Further systematical studies are needed to explain the difference in the LV titer of distinct TCRs. The JurkatΔ76 cell line was efficiently transduced with the LVs expressing the TCRs. However, we were not able to efficiently transduce the $CD8^+$ T cells after trying various protocols, e.g., using polybrene, retronectin coated plates. In most of these attempts, the percentages of transduced cells were around 10% (data not shown). It has been shown that stimulation of T cells results in upregulation of low-density lipoprotein receptor (LDLR), which serves as the main receptor for VSV-G-pseudotyped LVs (202). Although in our setting the $CD8^+$ T cells were stimulated with T cell TransAct™ (CD3/CD28 stimulation), IL-7 and IL-15, the transduction efficiency was low. It is possible that the expression of LDLR on the $CD8^+$ T cells was not sufficient for attachment of LV particles. Another explanation for the low transduction efficiency of the $CD8^+$ T cells may be related to antiviral responses. Studies have shown that TANK-binding kinase 1 (TBK1) and IκB kinase ε (IKKε) are regulators of type 1 interferons which play an important role during viral infection (203, 204). Li et al. reported that the inhibition of TBK1/IKKε complex can enhance the LV transduction in T cells (205). Moreover, it has been shown that the transduction efficiency of T cells with TCR reactive to E6 was significantly lower (45-76%) compared to transducing T cells with an E7 TCR (93-99%) (162). Accordingly, we observed variability in the transduction rate of different TCR constructs. Therefore, this study continued with electroporation of the $CD8^+$T cells with the PHIV-eGFP vector containing the selected TCRs for downstream analysis.

## 4.3 Analysis of the functionality and affinity of selected TCRs

In the first step of functional analysis of TCR engineered Jurkat cell lines, the upregulation of NFAT2 in Jurkat-EF1-3 in coculture with HPV16+ cancer cell lines were analyzed. Jurkat-EF1 and Jurkat-EF2 become activated after co-culture with the Caski and UPCI-SCC154 cancer cell lines, both HPV $16^+$ and HLA-$A2^+$. Importantly, coculture with the SiHa cell line, HPV$16^+$ and HLA-$A2^-$, did not induce upregulation of NFAT2 in the Jurkat-EF1 and Jurkat EF2 cells and this further confirmed the HLA-A2 dependency of the activation triggered by TCR EF1 and EF2. There was no upregulation of NFAT2 in Jurkat-EF3 in coculture with any of the cancer cell lines which may be due to its lower affinity compared to other candidates. In the next step the specificity of the interaction of our TCRs with $E7_{(11-19)}$ compared with an irrelevant epitope, pol-HIV, was evaluated. CD69 was upregulated in Jurkat-EF1 after exposure to $E7_{(11-19)}$ epitope on T2 cells compared to the irrelevant peptide and this was compatible with the NFAT2 expression analyses. Importantly, the upregulation of CD69 in Jurkat-EF1 was dependent on the concentration of $E7_{(11-19)}$ peptide. Jurkat-EF2 did not show any increase in expression of CD69 following coculture with the T2 cell lines loaded with the $E7_{(11-19)}$ peptide. However, the MFI of CD69 on Jurkat-EF2 after exposure to the irrelevant peptide was higher compared to the no-peptide control. This may be due to the cross reactivity of the TCR-EF2 with the HIV-Pol peptide. Although NFAT2 was not upregulated in Jurkat-EF3, its expression of CD69 was higher in exposure to the $E7_{(11-19)}$ peptide compared to the irrelevant and no peptide control. The divergence between the NFAT2 and CD69 expression in Jurkat-EF2 and Jurkat EF3 can be related to the transcriptional factors involved in T cell activation pathways. Several studies have shown that CD69 is mainly regulated by AP-1 and NFkB and it is an NFAT-independent gene (49,

206). Therefore, the upregulation of CD69 can be an indirect indicative of expression of AP-1 and NFkB transcription factors. The NFAT2 expression in Jurkat-EF2 was increased upon stimulation by co-culture with target cancer cell lines, but the TCR binding was not sufficient to trigger AP-1 and NFkB transcription factors. Although stimulation of Jurkat-EF3 may induce the activation of AP-1 and NFkB, it could not increase the expression of NFAT-2. Subsequently, TCR-EF1, compared to the other TCRs, provides an efficient signaling to activate the Jurkat cell line. Further in detail analyses are needed to investigate the expression of AP-1 and NFkB in TCR engineered Jurkat cell lines.

The tetramer staining results showed that all selected TCRs were able to bind to the $E7_{(11-19)}$ epitope on HLA-A2 compared to the Untransduced Jurkat, however, the binding affinities of the TCRs were different. Jurkat-EF1 had a higher tendency to binding capacity, which was in accordance with the upregulation of CD69. We were not able to detect any significant binding affinity to $E7_{(11-19)}$ in Jurkat-EF2 and Jurkat-EF3. Further affinity analyses with cancer cell lines demonstrated that all selected TCRs had a higher binding affinity to Caski compared to SiHa. However, the coefficient of binding in Jurkat-EF1 was significantly higher than Jurkat-EF2 and Jurkat-EF3. Analyzing the affinity of candidate TCRs highlighted the fact that the dynamics of TCR-pMHC interaction can regulate the activation of T cells. High affinity TCRs can extend the duration of pMHC:TCR interaction which resulted in efficient recruitment of TCR signaling components. Studies have shown that low potency TCR stimulation prevented the activity of LCK and ZAP-70 leading to attenuation of TCR signals (207, 208). On the other hand, high affinity TCRs can increase the quantity and quality of ZAP-70 catalytic activity which leads to a prolonged activation of downstream signaling cascades (209). In accordance with this, our

results indicated that there is a threshold of affinity for proper activation of T cells. The higher affinity of TCR-EF1 augmented the time of TCR:pMHC interaction and resulted in efficient upregulation of NFAT2 and CD69. Although TCR-EF2 and EF3 showed some level of affinity compared to Un-Jurkat, it was not enough to warrant the duration and quality of TCR signaling. Therefore, we saw a contradictory pattern of activation in Jurkat-EF2 and Jurkat-EF3. Due to the complex nature of TCR interaction, it seems important to combine different activation and affinity analyses to have a comprehensive overview since considering few parameters can be misleading.

In the next step, the secretion of IFNγ in electroporated TCR CD8+ T cells after co culture with four different cancer cell lines was evaluated. The percentages of $IFN\gamma^+$ T cells were higher in T cell-EF1 and EF2 in coculture with Caski and UPCI-SCC 154 compared to untransfected T cells. This can be explained by the regulatory effect of NFAT transcription family members on IFNγ secretion. Studies have shown that IFNγ is a NFAT-dependent gene and the production of this cytokine is mainly regulated by NFAT1 at the level of gene transcription (210, 211). Our Realtime PCR analysis showed that the NFAT2 in Jurkat-EF1 and EF2 was upregulated and that the expression of NFAT2 did not change in Jurkat-EF3. In accordance with this data, T cell-EF1 and T cell-EF2 had higher percentages of $IFN\gamma^+$ compared to T cell-EF3. Compatible with our findings, Pachulec et al. also demonstrated that NFAT2 regulated the production of IFNγ by CTLs. Importantly, they showed that the secretion of IFNγ in NFAT2-deficient CTLs was significantly reduced (212). Therefore, our results further highlighted the role of NFAT2 in the regulation of IFNγ. Importantly, the percentage of $IFN\gamma^+$ cells of T cell-EF1 in coculture with SiHa and PCI-13 did not increase, which showed the specific activation of TCR-EF1. Although the

percentage of IFNγ$^+$ cells of T cell-EF2 in coculture with Caski and UPCI-SCC154 increased, there was no significant difference in the IFNγ$^+$ cells in coculture with SiHa and PCI-13, which served as the negative control. This pattern of IFNγ secretion in T cell-EF2 can be related to the regulatory effect of transcription factors. It has been shown that AP-1, like NFAT, is a crucial transcription factor for efficient regulation of IFNγ (213, 214). As discussed above, the pattern of CD69 expression in Jurkat-EF2 might indicate an insufficient regulatory effect of AP-1. Therefore, the unspecific secretion of IFNγ in T cell-EF2 could be also related to insufficient AP-1 activity. Moreover, the percentage of IFNγ$^+$ cells of T cell-EF3 did not differ from that of untransfected T cells, which can be attributed to the lack of upregulation of NFAT2 in Jurkat-EF3. The sensitivity of T cell-EF1 to the $E7_{(11-19)}$ epitope was further confirmed by the coculture of T cell-EF1 with T2 cell lines loaded with different concentrations of the $E7_{(11-19)}$ peptide. Compatible with expression of CD69 in Jurkat-EF1, the MFI of IFNγ in T cell-EF1 was increased significantly after exposure to 10 and 100µM of peptide. Importantly, the MFI-IFNγ of T cell-EF1 did not change after exposure to 1µM of the $E7_{(11-19)}$ peptide, which indicated that the TCR-EF1 had an intermediate affinity. Interestingly, it has been shown that TCRs with affinities higher than the 10µM threshold did not result in a potent antitumor activity (215). This can be explained by the TCR serial engagement model (216, 217). According to this model, TCRs are needed to be serially engaged with the pMHC molecules on the APC to induce efficient accumulation of intracellular signaling. However, high affinity TCRs having prolonged TCR:pMHC interaction can interrupt the serial engagement of the TCRs. Moreover, very low affinity TCRs can hamper the T cell activation since the pMHC will be considered as non-ligand to avoid self-pMHC recognition. Therefore, short and long lived TCR:pMHC complexes may not be optimal

for T cell function and an intermediate affinity could favor the efficient anti-tumor activity of T cells (218). Besides that, T cell-EF1 induced significantly higher lysis when co-cultured with Caski cells (HPV16+, HLA-A2+) compared to SiHa (HPV16+, HLA-A2-), which further confirmed the HLA-dependent activation of TCR-EF1. Although TCR-EF2 and TCR-EF3 showed some level of activation and affinity, they were not able to lyse the target cancer cell line. Therefore, the TCR-EF1 is a promising candidate to be considered for TCR T cell therapy of HPV associated cancer. Further *in vivo* analysis is needed to pave the way of TCR-EF1 for clinical studies.

## 4.4. *In silico* characterization of candidate TCRs: a step forward in TCR discovery

As identification and selection of reactive TCRs is a challenging step, we used an *in silico* characterization workflow for efficient selection of candidate TCRs. The workflow basically focused on the interaction of the TCR with the $E7_{(11-19)}$ – HLA-A*0201 complex. According to the alanine substitution analysis, Aspartic acid$^{4}$, Leucin$^{5}$, glutamine$^{6}$ and proline$^{7}$ of $E7_{(11-19)}$ peptide are essential for interaction with E7 TCRs (161). The docking results showed that TCR-EF1 interacted with all these four important amino acids. Moreover, the low ΔG of interaction of TCR-EF1 with $E7_{(11-19)}$ – HLA-A*0201 complex demonstrated the higher affinity of TCR-EF1 compared to the other candidates. Interestingly, the *in silico* results were in line with the *in vitro* characterization and confirmed the functionality of TCR-EF1.

The *in silico* analysis was then used for evaluation of further 17 TCRs identified in our study, which were retrieved from both V(D)J libraries [IFNγ-tet] and [CD137-IFNγ-tet]. Interestingly, eight TCRs had predicted interaction with all essential amino acids of $E7_{(11-19)}$. This shows the potential binding of these TCRs to the $E7_{(11-19)}$–HLA-A*0201 complex. Moreover, the ΔG of interaction of 6/8 respective TCRs were lower than the reference TCR which further confirmed their affinity to the $E7_{(11-19)}$ epitope. Importantly, this approach resulted in identification of interacting residues within the CDR3α/β region of the TCRs. In total 22 TCRs were screened and 72% of them had more interacting amino acids in CDR3β compared to CDR3α. Moreover, TCR-EF12 and TCR EF14 did not have any predicted interaction with the peptide within their CDR3α region. Compatible with our findings, Glanville et al. also showed that there was always at least one CDR3β contact but multiple TCRs had no CDR3α interaction. Therefore, it was concluded that the interaction of CDR3β with the peptide is a prerequisite. They did this analysis based on the alignment of amino acids of all reported TCR: pMHC crystal structures (199). Moreover, they also showed that there were stretches of three to five contiguous amino acids (IMGT positions 107-116) in the CDR3 region which were mainly involved in the interaction with the peptide. In line with these findings, we also identified such motifs within CDR3β of candidate TCRs based on the docking results. Intriguingly, most of the motifs were within IMGT position 107-116 of their CDR3 regions and they were not in the three first/last residues. It has been shown that the first and last three amino acids of CDR3 regions are not engaged with the epitope binding (219, 220). To further validate the identified motifs reactive to $E7_{(11-19)}$ epitope, we screened the TCRβ repertoire of patients who recovered from HPV16 infection and of patients with CIN III (177). The results showed that around 70% of the motifs were enriched in

patients who cleared HPV16 infection and this further highlighted the potential role of these TCR candidates in HPV16 associated cancers. TCR-EF9 and TCR EF20 could be also promising candidates for the following reasons: (i) they have interacting amino acids to residues 4-7 of $E7_{(11-19)}$ epitope; (ii) have ΔG of interaction lower than the reference control TCR; (iii) have higher ratio of average clonotype frequency compared to TCR-EF1. Interestingly, the exact same sequences of CDR3β of four clonotypes, TCR-EF8, EF16, EF19 and EF20, were also found in the TCRβ repertoire of the study(177). TCR EF19, unlike other three clonotypes, had higher frequency in CIN III patients. This finding could be explained by the interaction of the TCRs with the essential residues of the $E7_{(11-19)}$ epitope. TCR-EF19 had interaction with residues 4-6, however, TCR-EF8, TCR-EF16 and TCR-EF20 had interaction with all important residues of the $E7_{(11-19)}$ epitope. According to our *in silico* characterization, further $E7_{(11-19)}$ TCRs can be selected for *in vitro* analysis. Moreover, the proposed *in silico* characterization and screening expanded our overview about the interaction of TCRs and the $E7_{(11-19)}$ epitope.

## 4.5 Summary and Outlook

Don Manson argued previously that cross reactivity is an essential feature of T cell repertoire that empowers the immune system and he proposed that a TCR can recognize $10^4$-$10^7$ different pMHC complexes (221). The specificity of the recognition relies on the fact that once a single TCR identifies a specific MHC-restricted epitope, the probability of it to react to another random epitope decreases to $10^{-4}$ (222, 223). Therefore, approaches to identify the TCR repertoire targeting a single epitope can shed light on the complexity of the TCR:pMHC

interaction. To this end, we used E7-Flt3L fusion protein (Cid-Arregui, unpublished results, patent application pending) for efficient stimulation of T cells derived from PBMCs of healthy donors. Our results showed that, compared to the E7 $_{(11-19)}$ epitope, the E7-Flt3L is a functional fusion protein which can efficiently activate $CD8^+$ T cells targeting the HLA-A*02:01 restricted HPV16 E7 $_{(11-19)}$ epitope. Moreover, the combination of tetramer binding and activation markers of T cells improved the reliability of the identification of E7-specific TCRs. E7-reactive $CD8^+$ T cells were V(D)J-sequenced at single cell level and provided valuable information about the TCR repertoire targeting E7 $_{(11-19).}$ Three TCR candidates were screened and they showed different patterns of reactivity and avidity. Based on the *in silico* and *in vitro* analyses, at least one of the TCRs identified here showed promising for adoptive T cell therapy. Moreover, we were able to identify E7$_{(11-19)}$-reactive motifs in the CDR3β region of our selected TCRs, which were mostly enriched in patients who cleared HPV16 infection compared to patients suffering cancer progression. In summary, our study has established an efficient workflow based on PBMCs of healthy donors for the identification of TCRs targeting tumor and viral antigens, which can be of fundamental interest towards TCR discovery, especially for neoepitopes.

# 5. Appendix

**Table. Appendix.1. The set of primers designed by NEBuilder® Assembly Tool for generation of TCR-EF4 gene segments.**

| Name | Primer sequence (5'-3') |
|---|---|
| BV-EF4-FWD | CGGCCGCTGAGTTAACTATTCTAGAATGGGACAGGAAGTGATCTTGCG |
| BV-EF4-Rev | CGCAGATCTTCGAGCACCAGGAGCCGCG |
| BC-Furin-P2A-FWD | CTGGTGCTCGAAGATCTGCGGAACGTGAC |
| BC-Furin-P2A-Rev | ATTTCATCATCTTTTCGAACTGCGGGTG |
| AV-EF4-FWD | GTTCGAAAAGATGATGAAATCCTTGAGAGTTTTAC |
| AV-EF4-Rev | TTCTGGATGTTGGGGAGAATATGAAGTCG |
| AC-EF4-FWD | ATTCTCCCCAACATCCAGAATCCTGAGC |
| AC-EF4-Rev | GGAGAGGGGCGGATCCTAGC*CCGGG*TTATCAGCTGGACCACAG |

**Table. Appendix.2. The sequence of the primers used for real time-PCR analysis**

| Name | Primer sequence (5'-3') |
|---|---|
| NFAT2 - FWD | CTGTGCAAGCCGAATTCTCTGG |
| NFAT2 -REV | ACTGACGTGAACGGGGCTGG |
| GAPDH - FWD | CAAGAGGACAAGAGGAACAGAG |
| GAPDH - REV | CTACATGGCAACTGTGAGGAG |

**Table. Appendix. 3.Selection of TCR candidates EF5-EF22 for in silico characterization.** The candidate TCRs were selected from [IFNγ-tet] and [CD137-IFNγ-tet] V(D)J libraries.

| TCR | CDR3α | CDR3β | Library | Frequency |
|---|---|---|---|---|
| EF-5 | CVVKRDDKIIF | CASSVGILTTGQPQHF | IFNg,tet | 3 |
| EF-6 | CATVLRMDSSYKLIF | CASSLIGVSSNNEQFF | IFNg,tet | 3 |
| EF-7 | CATETNFGNEKLTF | CATSGIAGETQYF | IFNg,tet | 3 |
| EF-8 | CILGEDTGNQFYF | CASSTGQKNTEAFF | IFNg,tet | 3 |
| EF-9 | CAGGDNNARLMF | CASSQVWGNTEAFF | IFNg,tet | 3 |
| EF-10 | CGTEDGGSNYKLTF | CASSWTKSYEQYF | IFNg,tet | 3 |
| EF-11 | CAFGQGAQKLVF | CSARGGFDPGELFF | IFNg,tet | 3 |
| EF-12 | CALSEAGTF | CASSGRQGTTMNTEAFF | CD137,IFNg,Tet | 3 |
| EF-13 | CAIPGPDYGQNFVF | CASSINGGYTEAFF | CD137,IFNg,Tet | 2 |
| EF-14 | CALLSNFGNEKLTF | CASSLSMRTGVANTEAFF | CD137,IFNg,Tet | 2 |
| EF-15 | CALSDPNSGNTPLVF | CASRIAGATYNEQFF | IFNg,tet | 1 |
| EF-16 | CAVSGPSGNTPLVF | CASSSLAGSYNEQFF | IFNg,tet | 1 |
| EF-17 | CAEDNNARLMF | CSVRYPPGNTIYF | IFNg,tet | 1 |
| EF-18 | CAVNTPYGNNRLAF | CASSQGSGQASWTGELFF | CD137,IFNg,Tet | 1 |
| EF-19 | CAVRDPWGNTPLVF | CASSYSRGEQFF | CD137,IFNg,Tet | 1 |
| EF-20 | CAVRDPWGNTPLVF | CASSSGLTTDTQYF | CD137,IFNg,Tet | 1 |
| EF-21 | CAVMDSSYKLIF | CATSRDPPGNYEQYF | CD137,IFNg,Tet | 1 |
| EF-22 | CALNQAGTALIF | CASSIGSRGYNEQFF | IFNg,tet | 1 |

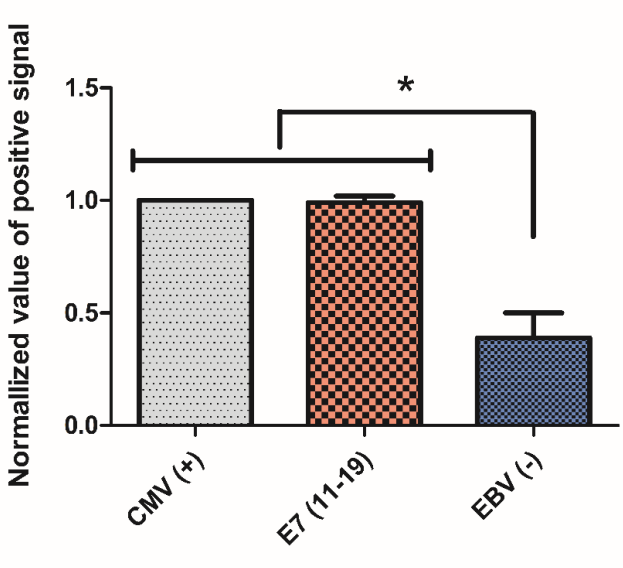


**Appendix-Figure.1. Evaluation of the efficiency of the peptide exchange for preparation of $E7_{(11-19)}$ FlexT-tetramers.** The Flex-T™ monomers UVX (200µg/ml) were mixed with the peptides (400 µM) and illuminated with UV light (366 nm) for 30 min for the peptide exchange. The efficiency of peptide exchange was evaluated by the ELISA. The $E7_{(11-19)}$ epitope was exchanged efficiently compared to the negative control which was Epstein-Barr nuclear antigen 4. The measurements were done by VICTOR™ X Series Multilabel Plate Readers (PerkinElmer) at absorbance 405(1.0s). The signals were normalized based on the positive control which was Cytomegalovirus pp65 (495-503) peptide. Bars are indicative of SD. The results shown are representative of 2 independent experiments. * represents P value < 0.05.

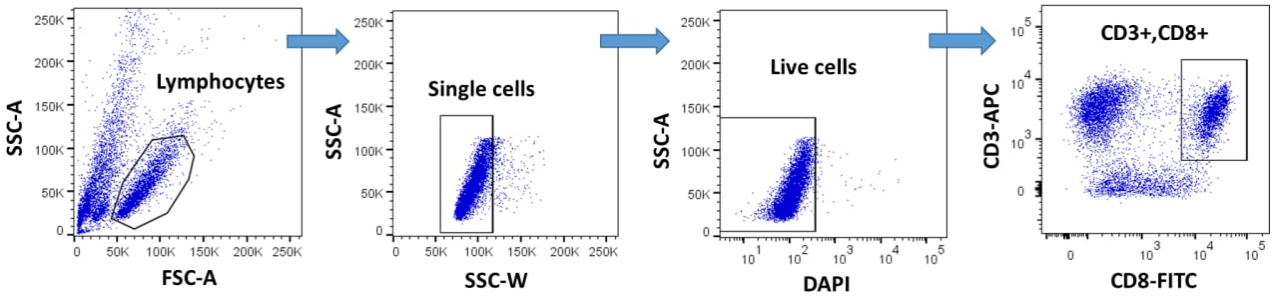


**Appendix-Figure.2. The gating for analysis of single cell/live/ $CD3^+$ /$CD8^+$ T cells.** The Samples were analyzed using a BD FACSCanto™.

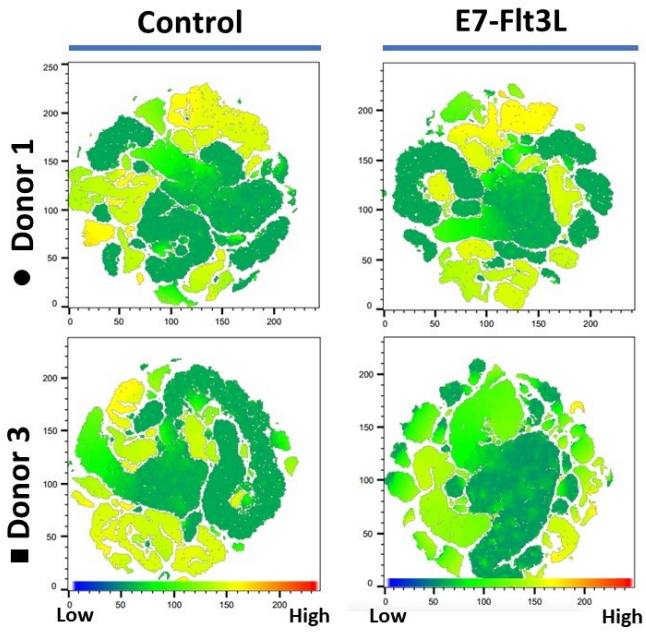


**Appendix-Figure 3. The tSNE analysis of the donor 1 and 3 prior and after stimulation with E7-Flt3L.** There was no significant increase in the $CD3^{+}$/ $CD8^{+}$ T cells following incubation of the cells with E7-Flt3L in Donor 1 and Donor 2.

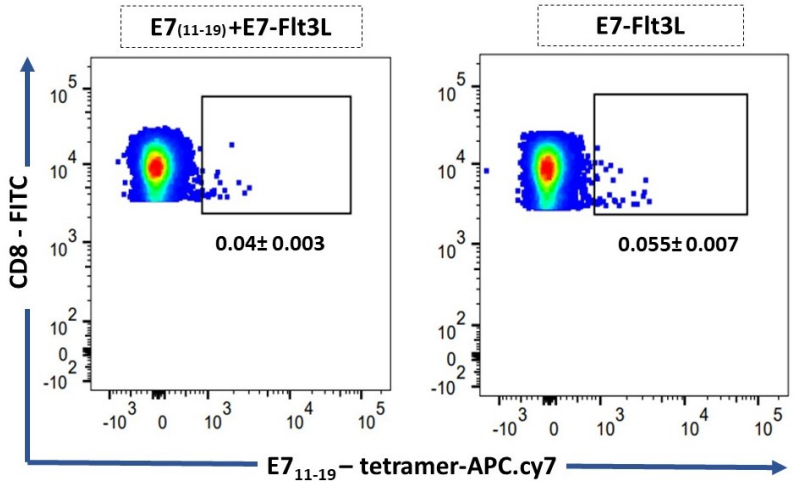


**Appendix-Figure 4. Comparison of the tetramer binding of the $CD8^{+}$ T cells treated with E7-Flt3L or the cocktail of $E7_{(11-19)}$ + E7-Flt3L after 2 days.** The hmo-imDCs were incubated with the mixture of E7-Flt3L(5µg/ml) and $E7_{(11-19)}$ (10µM) and co-culture with T cells. The percentage of E7 $_{(11-19)}$ -$tetramer^{+}$/ $IFN\gamma^{+}$ T cells in the treatment with $E7_{(11-19)}$ + E7-Flt3L were lower compared to the incubation with E7-Flt3L solely.

TCTAGAACCATGGGTCCTGGGCTTCTCCACTGGATGGCCCTTTGTCTCCTTGGAACAGGTCATGGGGATGCCATGG
TCATCCAGAACCCAAGATACCAGGTTACCCAGTTTGGAAAGCCAGTGACCCTGAGTTGTTCTCAGACTTTGAACCAT
AACGTCATGTACTGGTACCAGCAGAAGTCAAGTCAGGCCCCAAAGCTGCTGTTCCACTACTATGACAAAGATTTTA
ACAATGAAGCAGACACCCCTGATAACTTCCAATCCAGGAGGCCGAACACTTCTTTCTGCTTTCTTGACATCCGCTCA
CCAGGCCTGGGGGACGCAGCCATGTACCTGTGTGCCACCAGCAGAGATCCCCCGGGGAATTACGAGCAGTACTTC
GGGCCGGGCACCAGGCTCACGGTCACAGAAGATCTGCGGAACGTGACCCCTCCTAAGGTGTCCCTGTTCGAGCCT
AGCAAGGCCGAGATCGCCAACAAGCAGAAAGCCACACTCGTGTGCCTGGCCAGAGGCTTCTTTCCCGATCACGTG
GAACTGTCTTGGTGGGTCAACGGCAAAGAGGTGCACAGCGGCGTCTGCACAGATCCCCAGGCCTACAAAGAGAGC
AACTACAGCTACTGCCTGAGCAGCAGACTGAGAGTGTCCGCCACCTTCTGGCACAACCCCAGAAACCACTTCAGAT
GCCAGGTGCAGTTTCACGGCCTGAGCGAAGAGGACAAGTGGCCTGAGGGCTCTCCCAAGCCTGTGACACAGAATA
TCTCTGCCGAAGCCTGGGGCAGAGCCGATTGTGGAATTACCAGCGCCAGCTACCAGCAGGGCGTGCTGTCTGCCA
CAATCCTGTACGAGATCCTGCTGGGCAAAGCCACTCTGTACGCCGTGCTGGTGTCTACCCTGGTCGTGATGGCCAT
GGTCAAGCGGAAGAACAGCCGGAAGAGAAGA**GGAAGCGGC**GCCACCAATTTCAGCCTGCTGAAACAGGCTGGC
GACGTGGAAGAGAACCCTGGACCTTGGAGCCACCCGCAGTTCGAAAAGATGTGGGGAGTTTTCCTTCTTTATGTTT
CCATGAAGATGGGAGGCACTACAGGACAAAACATTGACCAGCCCACTGAGATGACAGCTACGGAAGGTGCCATTG
TCCAGATCAACTGCACGTACCAGACATCTGGGTTCAACGGGCTGTTCTGGTACCAGCAACATGCTGGCGAAGCACC
CACATTTCTGTCTTACAATGTTCTGGATGGTTTGGAGGAGAAAGGTCGTTTTTCTTCATTCCTTAGTCGGTCTAAAG
GGTACAGTTACCTCCTTTTGAAGGAGCTCCAGATGAAAGACTCTGCCTCTTACCTCTGTGCTCCCCATTCAGGAAAC
ACACCTCTTGTCTTTGGAAAGGGCACAAGACTTTCTGTGATTGCAAACATCCAGAATCCTGAGCCTGCCGTGTACCA
GCTGAAGGACCCTAGAAGCCAGGACAGCACCCTGTGCCTGTTCACCGACTTCGACAGCCAGATCAACGTGCCCAA
GACCATGGAAAGCGGCACCTTCATCACCGACAAGTGTGTGCTGGACATGAAGGCCATGGACAGCAAGAGCAACG
GCGCCATTGCCTGGTCCAACCAGACCAGCTTCACATGCCAGGACATCTTCAAAGAGACAAACGCCACCTATCCTAG
CAGCGACGTGCCCTGTGATGCCACACTGACCGAGAAGTCCTTCGAGACAGACATGAACCTGAACTTCCAGAACCTG
AGCGTGATGGGCCTGAGAATCCTGCTGCTGAAGGTGGCCGGCTTCAACCTGCTGATGACCCTGAGACTGTGGTCC
AGCTGATAAGGATCC

**Appendix-Figure 5. The full-length sequences of TCR-EF1.** The sequences were inserted in PHIV-eGFP lentiviral transfer vector. The different gene segments are color coded. The TRBV and TRAV chains were separated by Furin p2A and a streptag. The murine constant alpha and beta was used in the TCR sequences. The XbaI and Bam HI recognition sites are shown in blue and the two stop codons in red.

TCTAGAACCATGGGTCCTGGGCTTCTCCACTGGATGGCCCTTTGTCTCCTTGGAACAGGTCATGGGGATGCCATGG
TCATCCAGAACCCAAGATACCAGGTTACCCAGTTTGGAAAGCCAGTGACCCTGAGTTGTTCTCAGACTTTGAACCA
TAACGTCATGTACTGGTACCAGCAGAAGTCAAGTCAGGCCCCAAAGCTGCTGTTCCACTACTATGACAAAGATTTT
AACAATGAAGCAGACACCCCTGATAACTTCCAATCCAGGAGGCCGAACACTTCTTTCTGCTTTCTTGACATCCGCTC
ACCAGGCCTGGGGGACGCAGCCATGTACCTGTGTGCCACCAGCATCACAGTGAACACTGAAGCTTTCTTTGGACA
AGGCACCAGACTCACAGTTGTAGAAGATCTGCGGAACGTGACCCCTCCTAAGGTGTCCCTGTTCGAGCCTAGCAA
GGCCGAGATCGCCAACAAGCAGAAAGCCACACTCGTGTGCCTGGCCAGAGGCTTCTTTCCCGATCACGTGGAACT
GTCTTGGTGGGTCAACGGCAAAGAGGTGCACAGCGGCGTCTGCACAGATCCCCAGGCCTACAAAGAGAGCAACT
ACAGCTACTGCCTGAGCAGCAGACTGAGAGTGTCCGCCACCTTCTGGCACAACCCCAGAAACCACTTCAGATGCCA
GGTGCAGTTTCACGGCCTGAGCGAAGAGGACAAGTGGCCTGAGGGCTCTCCCAAGCCTGTGACACAGAATATCTC
TGCCGAAGCCTGGGGCAGAGCCGATTGTGGAATTACCAGCGCCAGCTACCAGCAGGGCGTGCTGTCTGCCACAAT
CCTGTACGAGATCCTGCTGGGCAAAGCCACTCTGTACGCCGTGCTGGTGTCTACCCTGGTCGTGATGGCCATGGTC
AAGCGGAAGAACAGCCGGAAGAGAAGA**GGAAGCGGC**GCCACCAATTTCAGCCTGCTGAAACAGGCTGGCGACG
TGGAAGAGAACCCTGGACCTTGGAGCCACCCGCAGTTCGAAAAGATGGCAGGCATTCGAGCTTTATTTATGTACTT
GTGGCTGCAGCTGGACTGGGTGAGCAGAGGAGAGAGTGTGGGGCTGCATCTTCCTACCCTGAGTGTCCAGGAGG
GTGACAACTCTATTATCAACTGTGCTTATTCAAACAGCGCCTCAGACTACTTCATTTGGTACAAGCAAGAATCTGGA
AAAGGTCCTCAATTCATTATAGACATTCGTTCAAATATGGACAAAAGGCAAGGCCAAAGAGTCACCGTTTTATTGA
ATAAGACAGTGAAACATCTCTCTCTGCAAATTGCAGCTACTCAACCTGGAGACTCAGCTGTCTACTTTTGTGCAGA
GAAGGGGGGAAATGAGAAATTAACCTTTGGGACTGGAACAAGACTCACCATCATACCCAACATCCAGAATCCTGA
GCCTGCCGTGTACCAGCTGAAGGACCCTAGAAGCCAGGACAGCACCCTGTGCCTGTTCACCGACTTCGACAGCCA
GATCAACGTGCCCAAGACCATGGAAAGCGGCACCTTCATCACCGACAAGTGTGTGCTGGACATGAAGGCCATGGA
CAGCAAGAGCAACGGCGCCATTGCCTGGTCCAACCAGACCAGCTTCACATGCCAGGACATCTTCAAAGAGACAAA
CGCCACCTATCCTAGCAGCGACGTGCCCTGTGATGCCACACTGACCGAGAAGTCCTTCGAGACAGACATGAACCT
GAACTTCCAGAACCTGAGCGTGATGGGCCTGAGAATCCTGCTGCTGAAGGTGGCCGGCTTCAACCTGCTGATGAC
CCTGAGACTGTGGTCCAGCTGATAAGGATCC

**Appendix-Figure 6. The full-length sequences of TCR-EF2.** The sequences were inserted in PHIV-eGFP lentiviral transfer vector. The different gene segments are color coded. The TRBV and TRAV chains were separated by Furin p2A and a streptag. The murine constant alpha and beta was used in the TCR sequences. The XbaI and Bam HI recognition sites are shown in blue and the two stop codons in red.

TCTAGAACCATGGGCCCCGGGCTCCTCTGCTGGGCACTGCTTTGTCTCCTGGGAGCAGGCTTAGTGGACGCTGGAG
TCACCCAAAGTCCCACACACCTGATCAAAACGAGAGGACAGCAAGTGACTCTGAGATGCTCTCCTAAGTCTGGGCA
TGACACTGTGTCCTGGTACCAACAGGCCCTGGGTCAGGGGCCCCAGTTTATCTTTCAGTATTATGAGGAGGAAGAG
AGACAGAGAGGCAACTTCCCTGATCGATTCTCAGGTCACCAGTTCCCTAACTATAGCTCTGAGCTGAATGTGAACG
CCTTGTTGCTGGGGGACTCGGCCCTCTATCTCTGTGCCAGCAGCTTGAGTATGCGGACAGGGGTAGCGAACACTGA
AGCTTTCTTTGGACAAGGCACCAGACTCACAGTTGTAGAAGATCTGCGGAACGTGACCCCTCCTAAGGTGTCCCTG
TTCGAGCCTAGCAAGGCCGAGATCGCCAACAAGCAGAAAGCCACACTCGTGTGCCTGGCCAGAGGCTTCTTTCCCG
ATCACGTGGAACTGTCTTGGTGGGTCAACGGCAAAGAGGTGCACAGCGGCGTCTGCACAGATCCCCAGGCCTACA
AAGAGAGCAACTACAGCTACTGCCTGAGCAGCAGACTGAGAGTGTCCGCCACCTTCTGGCACAACCCCAGAAACC
ACTTCAGATGCCAGGTGCAGTTTCACGGCCTGAGCGAAGAGGACAAGTGGCCTGAGGGCTCTCCCAAGCCTGTGA
CACAGAATATCTCTGCCGAAGCCTGGGGCAGAGCCGATTGTGGAATTACCAGCGCCAGCTACCAGCAGGGCGTGC
TGTCTGCCACAATCCTGTACGAGATCCTGCTGGGCAAAGCCACTCTGTACGCCGTGCTGGTGTCTACCCTGGTCGTG
ATGGCCATGGTCAAGCGGAAGAACAGCCGGAAGAGAAGA**GGAAGCGGC**GCCACCAATTTCAGCCTGCTGAAACA
GGCTGGCGACGTGGAAGAGAACCCTGGACCTTGGAGCCACCCGCAGTTCGAAAAGATGGCATGCCCTGGCTTCCT
GTGGGCACTTGTGATCTCCACCTGTCTTGAATTTAGCATGGCTCAGACAGTCACTCAGTCTCAACCAGAGATGTCTG
TGCAGGAGGCAGAGACCGTGACCCTGAGCTGCACATATGACACCAGTGAGAGTGATTATTATTTATTCTGGTACAA
GCAGCCTCCCAGCAGGCAGATGATTCTCGTTATTCGCCAAGAAGCTTATAAGCAACAGAATGCAACAGAGAATCGT
TTCTCTGTGAACTTCCAGAAAGCAGCCAAATCCTTCAGTCTCAAGATCTCAGACTCACAGCTGGGGGATGCCGCGA
TGTATTTCTGTGCTTTACTATCTAACTTTGGAAATGAGAAATTAACCTTTGGGACTGGAACAAGACTCACCATCATA
CCCAACATCCAGAATCCTGAGCCTGCCGTGTACCAGCTGAAGGACCCTAGAAGCCAGGACAGCACCCTGTGCCTGT
TCACCGACTTCGACAGCCAGATCAACGTGCCCAAGACCATGGAAAGCGGCACCTTCATCACCGACAAGTGTGTGCT
GGACATGAAGGCCATGGACAGCAAGAGCAACGGCGCCATTGCCTGGTCCAACCAGACCAGCTTCACATGCCAGGA
CATCTTCAAAGAGACAAACGCCACCTATCCTAGCAGCGACGTGCCCTGTGATGCCACACTGACCGAGAAGTCCTTC
GAGACAGACATGAACCTGAACTTCCAGAACCTGAGCGTGATGGGCCTGAGAATCCTGCTGCTGAAGGTGGCCGGC
TTCAACCTGCTGATGACCCTGAGACTGTGGTCCAGCTGATAAGGATCC

**Appendix-Figure 7. The full-length sequences of TCR-EF3.** The sequences were inserted in PHIV-eGFP lentiviral transfer vector. The different gene segments are color coded. The TRBV and TRAV chains were separated by Furin p2A and a streptag. The murine constant alpha and beta was used in the TCR sequences. The XbaI and Bam HI recognition sites are shown in blue and the two stop codons in red.

TCTAGAACCATGGGACAGGAAGTGATCTTGCGCTGTGTCCCCATCTCTAATCACTTATACTTCTATTGGTACAGACA
AATCTTGGGGCAGAAAGTCGAGTTTCTGGTTTCCTTTTATAATAATGAAATCTCAGAGAAGTCTGAAATATTCGAT
GATCAATTCTCAGTTGAAAGGCCTGATGGATCAAATTTCACTCTGAAGATCCGGTCCACAAAGCTGGAGGACTCAG
CCATGTACTTCTGTGCCAGCATGGGACTGAAGGAGACCCAGTACTTCGGGCCAGGCACGCGGCTCCTGGTGCTCG
AAGATCTGCGGAACGTGACCCCTCCTAAGGTGTCCCTGTTCGAGCCTAGCAAGGCCGAGATCGCCAACAAGCAGA
AAGCCACACTCGTGTGCCTGGCCAGAGGCTTCTTTCCCGATCACGTGGAACTGTCTTGGTGGGTCAACGGCAAAG
AGGTGCACAGCGGCGTCTGCACAGATCCCCAGGCCTACAAAGAGAGCAACTACAGCTACTGCCTGAGCAGCAGAC
TGAGAGTGTCCGCCACCTTCTGGCACAACCCCAGAAACCACTTCAGATGCCAGGTGCAGTTTCACGGCCTGAGCG
AAGAGGACAAGTGGCCTGAGGGCTCTCCCAAGCCTGTGACACAGAATATCTCTGCCGAAGCCTGGGGCAGAGCC
GATTGTGGAATTACCAGCGCCAGCTACCAGCAGGGCGTGCTGTCTGCCACAATCCTGTACGAGATCCTGCTGGGC
AAAGCCACTCTGTACGCCGTGCTGGTGTCTACCCTGGTCGTGATGGCCATGGTCAAGCGGAAGAACAGCCGGAAG
AGAAGA**GGAAGCGGC**GCCACCAATTTCAGCCTGCTGAAACAGGCTGGCGACGTGGAAGAGAACCCTGGACCTTG
GAGCCACCCGCAGTTCGAAAAGATGATGAAATCCTTGAGAGTTTTACTGGTGATCCTGTGGCTTCAGTTAAGCTGG
GTTTGGAGCCAACAGAAGGAGGTGGAGCAGGATCCTGGACCACTCAGTGTTCCAGAGGGAGCCATTGTTTCTCTC
AACTGCACTTACAGCAACAGTGCTTTTCAATACTTCATGTGGTACAGACAGTATTCCAGAAAAGGCCCTGAGTTGC
TGATGTACACATACTCCAGTGGTAACAAAGAAGATGGAAGGTTTACAGCACAGGTCGATAAATCCAGCAAGTATA
TCTCCTTGTTCATCAGAGACTCACAGCCCAGTGATTCAGCCACCTACCTCTGTGCAATGAGAGCAGATGACAAGAT
CATCTTTGGAAAAGGGACACGACTTCATATTCTCCCCAACATCCAGAATCCTGAGCCTGCCGTGTACCAGCTGAAG
GACCCTAGAAGCCAGGACAGCACCCTGTGCCTGTTCACCGACTTCGACAGCCAGATCAACGTGCCCAAGACCATG
GAAAGCGGCACCTTCATCACCGACAAGTGTGTGCTGGACATGAAGGCCATGGACAGCAAGAGCAACGGCGCCAT
TGCCTGGTCCAACCAGACCAGCTTCACATGCCAGGACATCTTCAAAGAGACAAACGCCACCTATCCTAGCAGCGAC
GTGCCCTGTGATGCCACACTGACCGAGAAGTCCTTCGAGACAGACATGAACCTGAACTTCCAGAACCTGAGCGTG
ATGGGCCTGAGAATCCTGCTGCTGAAGGTGGCCGGCTTCAACCTGCTGATGACCCTGAGACTGTGGTCCAGCTGA
TAACCCGGG

**Appendix-Figure 8. The full-length sequences of TCR-EF4.** The sequences were inserted in PHIV-eGFP lentiviral transfer vector. The different gene segments are color coded. The TRBV and TRAV chains were separated by Furin p2A and a streptag. The murine constant alpha and beta was used in the TCR sequences. The XbaI and XmaI recognition sites are shown in blue and the two stop codons in red.

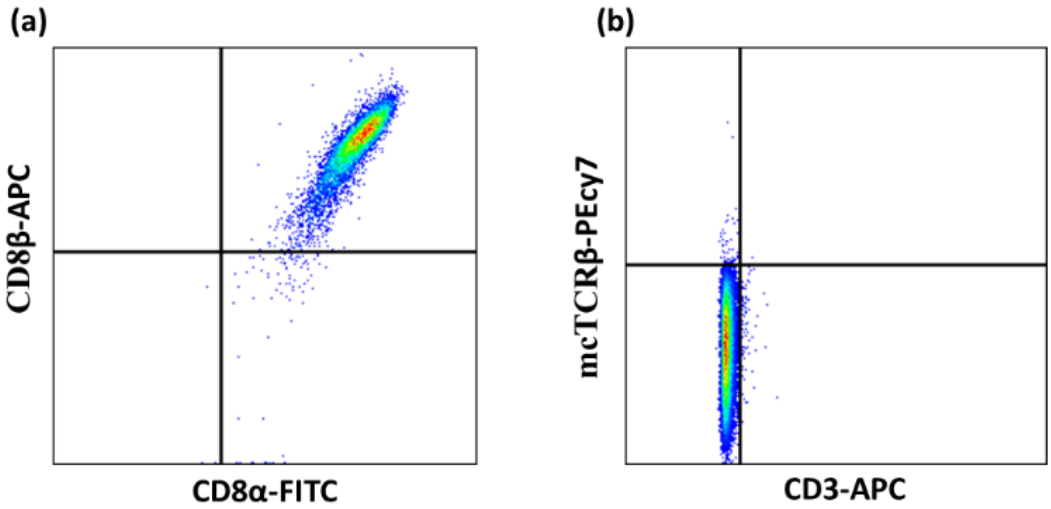


**Appendix-Figure 9. The CD8⁺/TCR deficient JurkatΔ76 cell line.** (a) expression of CD8α and CD8β (b) CD3 and murine constant TCRβ were not expressed on the surface of the JurkatΔ76-CD8 cell line.

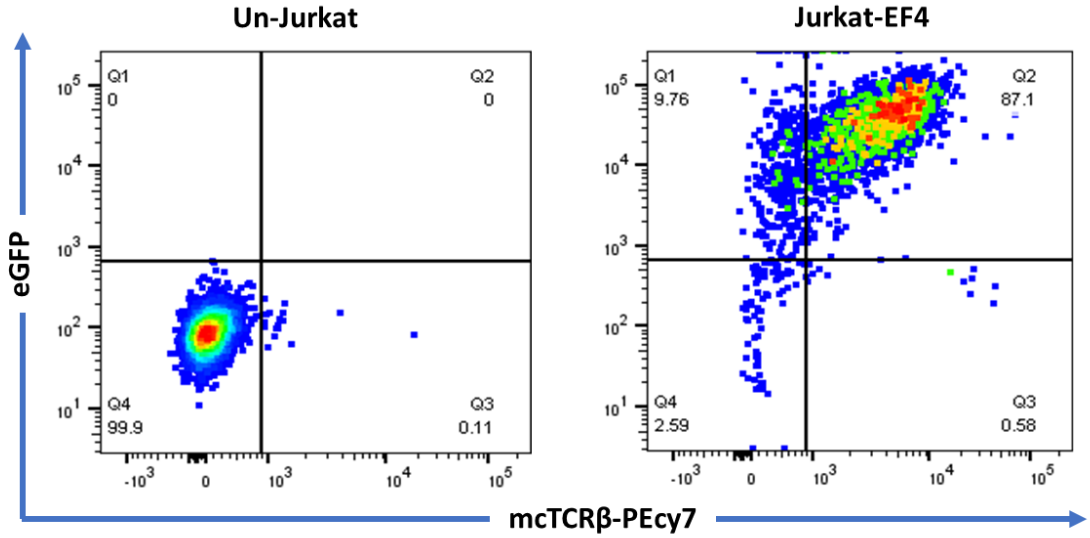


**Appendix-Figure 10. Expression of TCR-EF4 in TCR deficient JurkatΔ76-CD8 cell line.** Around 87 % of the cells were GFP⁺, mcTCRβ⁺. Despite of successful transduction, the Jurkat-EF4 cell lines did not survive.

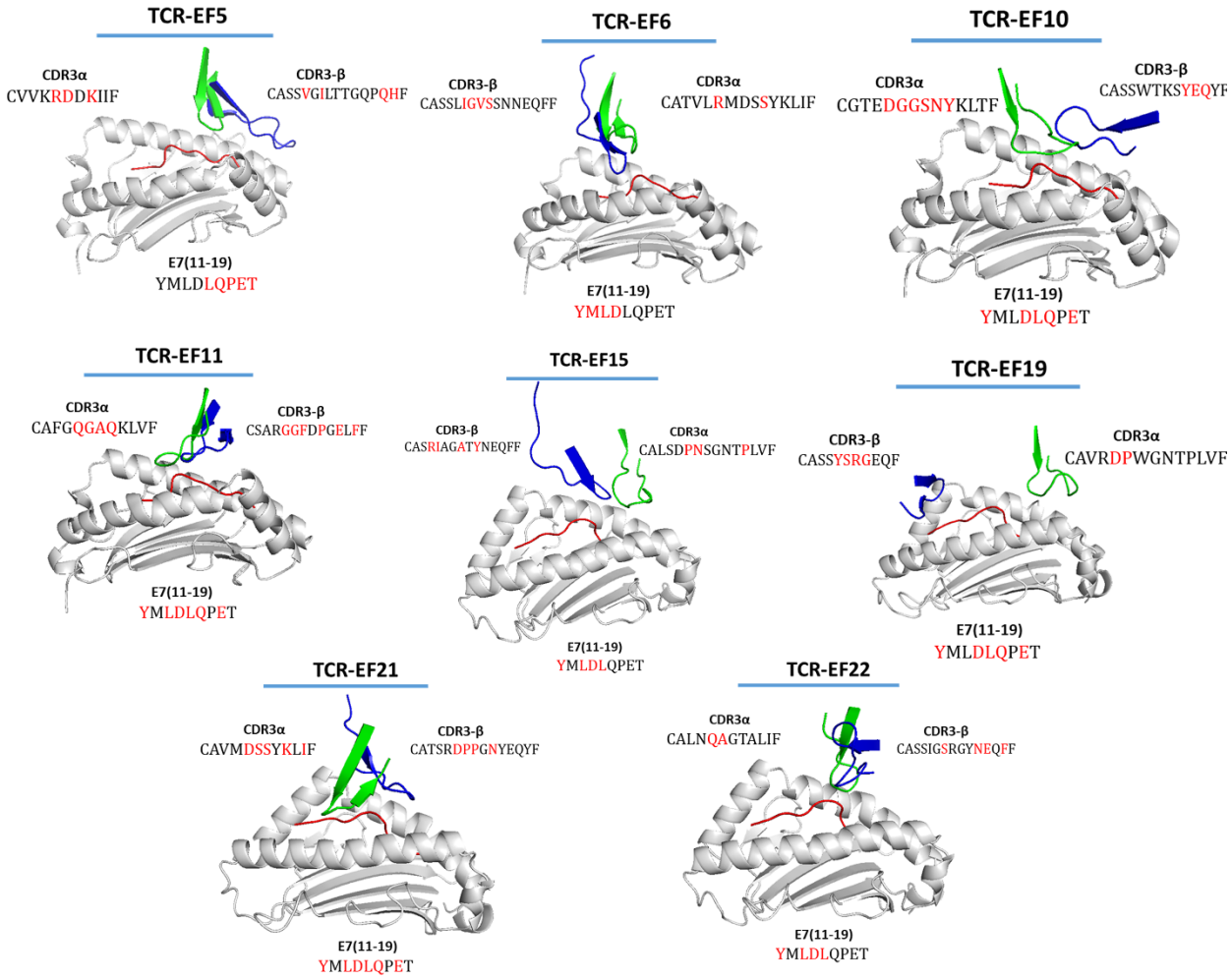


**Appendix-Figure 11. *In silico* analysis of the interaction of candidate TCRs with E7 $_{(11-19)}$- HLA-A*02.** The E7 $_{(11-19)}$ peptide is shown in red and the HLA-A*02 molecule is in white. The CDR3α and CDR3β chains are shown in green and blue, respectively. The interacting residues are depicted in red. Candidate TCRs TCR EF-5, EF6, EF10, EF11, EF15, EF19, EF21 and EF22 did not interact with all essential amino acids of the epitope at position 4-7.

# 6. Publications and presentations

## Journal papers

- **Elham Fakhr**, Ž. Modic, A. Cid-Arregui, Immunotherapy of Cancers Caused by Human Papillomaviruses, *Immunology*, 2021.

- M. Poorebrahim, N. Mohammadkhani, R. Mahmoudi, M. Gholizadeh, **Elham Fakhr**, A.Cid-Arregui, TCR-like CARs and TCR-CARs targeting neoepitopes: an emerging potential, *Cancer gene therapy*, 2021.

- I Quiros-Fernandez, M Poorebrahim, **Elham Fakhr**, A Cid-Arregui, Immunogenic T cell epitopes of SARS-CoV-2 are recognized by circulating memory and naïve CD8 T cells of unexposed individuals, *EbioMedicine*, 2021.

- M.Poorebrahim, S.Sadeghi, **Elham Fakhr**, M. Foad Abazari, V.Poortahmasebi, A.Kheirollahi, H.Askari, A. Rajabzadeh, M. Rastegarpanah, A. Linē, A. Cid-Arregui, Production of GMP-grade CAR T-cells by Lentiviral Vectors: Latest Advances and Future Prospects, Critical reviews in clinical laboratory sciences, 2017.

## Book chapters

- M. Poorebrahim, N. Mohammadkhani, M.F.Abazari, **Elham Fakhr**, I.Quiros-Fernandez, S. Sadeghi and A. Cid-Arregui, CAR-T Cells in Brain Tumors and Autoimmune Diseases – from Basics to the Clinic, *eBook FCDR - CNS and Neurological Disorders: Vol. 8 being published by Bentham eBooks,* 2021.

- M. Poorebrahim, I.Quiros-Fernandez, **Elham Fakhr**, and A. Cid-Arregui. Generation of CAR-T cells using lentiviral vectors, *Methods in Cell Biology*,2021.

## Poster presentations

- **Elham Fakhr**, Angel Cid Arregui, Engineered-TCR T cells: a promising approach for immunotherapy of cervical cancer, 18th Annual KICancer-StratCan Retreat, Djurönäset, Stockholm Archipelago, September 16-17, 2019, Stockholm, Sweden.

- **Elham Fakhr**, Angel Cid Arregui, Engineered-TCR T cells: a promising approach for immunotherapy of cervical cancer, PhD Poster presentation, DKFZ, 18th -22nd Nov, 2019, Heidelberg, Germany.

- **Elham Fakhr**, Angel Cid Arregui, Identification and characterization of T cell receptors reactive to $E7_{(11-19)}$ epitope of HPV-16, DKFZ Virtual PhD retreat, 5-6 July, 2022.

# 7. References


1. Tang D, Kang R, Coyne CB, Zeh HJ, Lotze MT. PAMPs and DAMPs: signal 0s that spur autophagy and immunity. Immunol Rev. 2012;249(1):158-75.
2. Riera Romo M, Perez-Martinez D, Castillo Ferrer C. Innate immunity in vertebrates: an overview. Immunology. 2016;148(2):125-39.
3. Iwasaki A, Medzhitov R. Control of adaptive immunity by the innate immune system. Nat Immunol. 2015;16(4):343-53.
4. Bonilla FA, Oettgen HC. Adaptive immunity. J Allergy Clin Immunol. 2010;125(2 Suppl 2):S33-40.
5. Nutt SL, Hodgkin PD, Tarlinton DM, Corcoran LM. The generation of antibody-secreting plasma cells. Nat Rev Immunol. 2015;15(3):160-71.
6. Crotty S, Felgner P, Davies H, Glidewell J, Villarreal L, Ahmed R. Cutting edge: long-term B cell memory in humans after smallpox vaccination. J Immunol. 2003;171(10):4969-73.
7. Leahy DJ. A structural view of CD4 and CD8. FASEB J. 1995;9(1):17-25.
8. Taniuchi I. CD4 Helper and CD8 Cytotoxic T Cell Differentiation. Annu Rev Immunol. 2018;36:579-601.
9. Collin M, McGovern N, Haniffa M. Human dendritic cell subsets. Immunology. 2013;140(1):22-30.
10. Steinman RM, Cohn ZA. Identification of a novel cell type in peripheral lymphoid organs of mice. I. Morphology, quantitation, tissue distribution. J Exp Med. 1973;137(5):1142-62.
11. Gorelik M, Frischmeyer-Guerrerio PA. Innate and adaptive dendritic cell responses to immunotherapy. Curr Opin Allergy Clin Immunol. 2015;15(6):575-80.
12. Paludan C, Schmid D, Landthaler M, Vockerodt M, Kube D, Tuschl T, et al. Endogenous MHC class II processing of a viral nuclear antigen after autophagy. Science. 2005;307(5709):593-6.
13. Bevan MJ. Cross-priming. Nat Immunol. 2006;7(4):363-5.
14. Hopkins RA, Connolly JE. The specialized roles of immature and mature dendritic cells in antigen cross-presentation. Immunol Res. 2012;53(1-3):91-107.
15. Embgenbroich M, Burgdorf S. Current Concepts of Antigen Cross-Presentation. Front Immunol. 2018;9:1643.
16. Palmowski MJ, Gileadi U, Salio M, Gallimore A, Millrain M, James E, et al. Role of immunoproteasomes in cross-presentation. J Immunol. 2006;177(2):983-90.
17. Li B, Hu L. Cross-presentation of Exogenous Antigens. Transfus Clin Biol. 2019;26(4):346-51.
18. Mogensen TH. Pathogen recognition and inflammatory signaling in innate immune defenses. Clin Microbiol Rev. 2009;22(2):240-73, Table of Contents.
19. Blanco P, Palucka AK, Pascual V, Banchereau J. Dendritic cells and cytokines in human inflammatory and autoimmune diseases. Cytokine Growth Factor Rev. 2008;19(1):41-52.
20. Joffre OP, Segura E, Savina A, Amigorena S. Cross-presentation by dendritic cells. Nat Rev Immunol. 2012;12(8):557-69.
21. Collins M, Ling V, Carreno BM. The B7 family of immune-regulatory ligands. Genome Biol. 2005;6(6):223.
22. Steinman RM. Some interfaces of dendritic cell biology. APMIS. 2003;111(7-8):675-97.
23. Thebeau LG, Morrison LA. B7 costimulation plays an important role in protection from herpes simplex virus type 2-mediated pathology. J Virol. 2002;76(5):2563-6.

24. Vasilevko V, Ghochikyan A, Holterman MJ, Agadjanyan MG. CD80 (B7-1) and CD86 (B7-2) are functionally equivalent in the initiation and maintenance of CD4+ T-cell proliferation after activation with suboptimal doses of PHA. DNA Cell Biol. 2002;21(3):137-49.
25. Fleischer J, Soeth E, Reiling N, Grage-Griebenow E, Flad HD, Ernst M. Differential expression and function of CD80 (B7-1) and CD86 (B7-2) on human peripheral blood monocytes. Immunology. 1996;89(4):592-8.
26. Sansom DM. CD28, CTLA-4 and their ligands: who does what and to whom? Immunology. 2000;101(2):169-77.
27. Hansen W, Westendorf AM, Buer J. Regulatory T cells as targets for immunotherapy of autoimmunity and inflammation. Inflamm Allergy Drug Targets. 2008;7(4):217-23.
28. Li Z, Ju X, Silveira PA, Abadir E, Hsu WH, Hart DNJ, et al. CD83: Activation Marker for Antigen Presenting Cells and Its Therapeutic Potential. Front Immunol. 2019;10:1312.
29. Wang C, Sun W, Ye Y, Bomba HN, Gu Z. Bioengineering of Artificial Antigen Presenting Cells and Lymphoid Organs. Theranostics. 2017;7(14):3504-16.
30. Elgueta R, Benson MJ, de Vries VC, Wasiuk A, Guo Y, Noelle RJ. Molecular mechanism and function of CD40/CD40L engagement in the immune system. Immunol Rev. 2009;229(1):152-72.
31. Liechtenstein T, Dufait I, Bricogne C, Lanna A, Pen J, Breckpot K, et al. PD-L1/PD-1 Co-Stimulation, a Brake for T cell Activation and a T cell Differentiation Signal. J Clin Cell Immunol. 2012;S12.
32. Geisler C, Larsen JK, Plesner T. Identification of alpha beta and gamma delta T cell receptor-positive cells. Scand J Immunol. 1988;28(6):741-5.
33. Lawand M, Dechanet-Merville J, Dieu-Nosjean MC. Key Features of Gamma-Delta T-Cell Subsets in Human Diseases and Their Immunotherapeutic Implications. Front Immunol. 2017;8:761.
34. Famili F, Wiekmeijer AS, Staal FJ. The development of T cells from stem cells in mice and humans. Future Sci OA. 2017;3(3):FSO186.
35. Blanchard L, Girard JP. High endothelial venules (HEVs) in immunity, inflammation and cancer. Angiogenesis. 2021.
36. Porritt HE, Rumfelt LL, Tabrizifard S, Schmitt TM, Zuniga-Pflucker JC, Petrie HT. Heterogeneity among DN1 prothymocytes reveals multiple progenitors with different capacities to generate T cell and non-T cell lineages. Immunity. 2004;20(6):735-45.
37. Dik WA, Pike-Overzet K, Weerkamp F, de Ridder D, de Haas EF, Baert MR, et al. New insights on human T cell development by quantitative T cell receptor gene rearrangement studies and gene expression profiling. J Exp Med. 2005;201(11):1715-23.
38. Kreslavsky T, Garbe AI, Krueger A, von Boehmer H. T cell receptor-instructed alphabeta versus gammadelta lineage commitment revealed by single-cell analysis. J Exp Med. 2008;205(5):1173-86.
39. Parker ME, Ciofani M. Regulation of gammadelta T Cell Effector Diversification in the Thymus. Front Immunol. 2020;11:42.
40. Davis MM, Bjorkman PJ. T-cell antigen receptor genes and T-cell recognition. Nature. 1988;334(6181):395-402.
41. Joglekar AV, Li G. T cell antigen discovery. Nat Methods. 2020.
42. Robins HS, Srivastava SK, Campregher PV, Turtle CJ, Andriesen J, Riddell SR, et al. Overlap and effective size of the human CD8+ T cell receptor repertoire. Sci Transl Med. 2010;2(47):47ra64.
43. La Gruta NL, Gras S, Daley SR, Thomas PG, Rossjohn J. Understanding the drivers of MHC restriction of T cell receptors. Nat Rev Immunol. 2018;18(7):467-78.
44. Lanzarotti E, Marcatili P, Nielsen M. T-Cell Receptor Cognate Target Prediction Based on Paired alpha and beta Chain Sequence and Structural CDR Loop Similarities. Front Immunol. 2019;10:2080.
45. Klein L, Kyewski B, Allen PM, Hogquist KA. Positive and negative selection of the T cell repertoire: what thymocytes see (and don't see). Nat Rev Immunol. 2014;14(6):377-91.

46. Birnbaum ME, Berry R, Hsiao YS, Chen Z, Shingu-Vazquez MA, Yu X, et al. Molecular architecture of the alphabeta T cell receptor-CD3 complex. Proc Natl Acad Sci U S A. 2014;111(49):17576-81.
47. Wucherpfennig KW, Gagnon E, Call MJ, Huseby ES, Call ME. Structural biology of the T-cell receptor: insights into receptor assembly, ligand recognition, and initiation of signaling. Cold Spring Harb Perspect Biol. 2010;2(4):a005140.
48. Wang H, Kadlecek TA, Au-Yeung BB, Goodfellow HE, Hsu LY, Freedman TS, et al. ZAP-70: an essential kinase in T-cell signaling. Cold Spring Harb Perspect Biol. 2010;2(5):a002279.
49. Cibrian D, Sanchez-Madrid F. CD69: from activation marker to metabolic gatekeeper. Eur J Immunol. 2017;47(6):946-53.
50. Schuh K, Twardzik T, Kneitz B, Heyer J, Schimpl A, Serfling E. The interleukin 2 receptor alpha chain/CD25 promoter is a target for nuclear factor of activated T cells. J Exp Med. 1998;188(7):1369-73.
51. von Essen MR, Kongsbak M, Geisler C. Mechanisms behind functional avidity maturation in T cells. Clin Dev Immunol. 2012;2012:163453.
52. Tafuri A, Shahinian A, Bladt F, Yoshinaga SK, Jordana M, Wakeham A, et al. ICOS is essential for effective T-helper-cell responses. Nature. 2001;409(6816):105-9.
53. Nolz JC, Starbeck-Miller GR, Harty JT. Naive, effector and memory CD8 T-cell trafficking: parallels and distinctions. Immunotherapy. 2011;3(10):1223-33.
54. Bouchery T, Kyle R, Ronchese F, Le Gros G. The Differentiation of CD4(+) T-Helper Cell Subsets in the Context of Helminth Parasite Infection. Front Immunol. 2014;5:487.
55. Belizario JE, Brandao W, Rossato C, Peron JP. Thymic and Postthymic Regulation of Naive CD4(+) T-Cell Lineage Fates in Humans and Mice Models. Mediators Inflamm. 2016;2016:9523628.
56. Schmitt E, Klein M, Bopp T. Th9 cells, new players in adaptive immunity. Trends Immunol. 2014;35(2):61-8.
57. Licona-Limon P, Henao-Mejia J, Temann AU, Gagliani N, Licona-Limon I, Ishigame H, et al. Th9 Cells Drive Host Immunity against Gastrointestinal Worm Infection. Immunity. 2013;39(4):744-57.
58. Weaver CT, Hatton RD, Mangan PR, Harrington LE. IL-17 family cytokines and the expanding diversity of effector T cell lineages. Annu Rev Immunol. 2007;25:821-52.
59. Breitfeld D, Ohl L, Kremmer E, Ellwart J, Sallusto F, Lipp M, et al. Follicular B helper T cells express CXC chemokine receptor 5, localize to B cell follicles, and support immunoglobulin production. J Exp Med. 2000;192(11):1545-52.
60. Chen W, Jin W, Hardegen N, Lei KJ, Li L, Marinos N, et al. Conversion of peripheral CD4+CD25- naive T cells to CD4+CD25+ regulatory T cells by TGF-beta induction of transcription factor Foxp3. J Exp Med. 2003;198(12):1875-86.
61. Amarnath S, Costanzo CM, Mariotti J, Ullman JL, Telford WG, Kapoor V, et al. Regulatory T cells and human myeloid dendritic cells promote tolerance via programmed death ligand-1. PLoS Biol. 2010;8(2):e1000302.
62. Schoenberger SP, Toes RE, van der Voort EI, Offringa R, Melief CJ. T-cell help for cytotoxic T lymphocytes is mediated by CD40-CD40L interactions. Nature. 1998;393(6684):480-3.
63. Bennett SR, Carbone FR, Karamalis F, Flavell RA, Miller JF, Heath WR. Help for cytotoxic-T-cell responses is mediated by CD40 signalling. Nature. 1998;393(6684):478-80.
64. Trapani JA, Smyth MJ. Functional significance of the perforin/granzyme cell death pathway. Nat Rev Immunol. 2002;2(10):735-47.
65. Trapani JA, Jans DA, Jans PJ, Smyth MJ, Browne KA, Sutton VR. Efficient nuclear targeting of granzyme B and the nuclear consequences of apoptosis induced by granzyme B and perforin are caspase-dependent, but cell death is caspase-independent. J Biol Chem. 1998;273(43):27934-8.
66. Van Parijs L, Abbas AK. Role of Fas-mediated cell death in the regulation of immune responses. Curr Opin Immunol. 1996;8(3):355-61.

67. Seder RA, Ahmed R. Similarities and differences in CD4+ and CD8+ effector and memory T cell generation. Nat Immunol. 2003;4(9):835-42.
68. Sallusto F, Geginat J, Lanzavecchia A. Central memory and effector memory T cell subsets: function, generation, and maintenance. Annu Rev Immunol. 2004;22:745-63.
69. Doorbar J, Egawa N, Griffin H, Kranjec C, Murakami I. Human papillomavirus molecular biology and disease association. Rev Med Virol. 2015;25 Suppl 1:2-23.
70. Egawa N, Egawa K, Griffin H, Doorbar J. Human Papillomaviruses; Epithelial Tropisms, and the Development of Neoplasia. Viruses. 2015;7(7):3863-90.
71. de Villiers EM, Fauquet C, Broker TR, Bernard HU, zur Hausen H. Classification of papillomaviruses. Virology. 2004;324(1):17-27.
72. Munoz N, Bosch FX, de Sanjose S, Herrero R, Castellsague X, Shah KV, et al. Epidemiologic classification of human papillomavirus types associated with cervical cancer. N Engl J Med. 2003;348(6):518-27.
73. de Martel C, Plummer M, Vignat J, Franceschi S. Worldwide burden of cancer attributable to HPV by site, country and HPV type. Int J Cancer. 2017;141(4):664-70.
74. Gillison ML, Alemany L, Snijders PJ, Chaturvedi A, Steinberg BM, Schwartz S, et al. Human papillomavirus and diseases of the upper airway: head and neck cancer and respiratory papillomatosis. Vaccine. 2012;30 Suppl 5:F34-54.
75. Moscicki AB, Schiffman M, Burchell A, Albero G, Giuliano AR, Goodman MT, et al. Updating the natural history of human papillomavirus and anogenital cancers. Vaccine. 2012;30 Suppl 5:F24-33.
76. Goon P, Sonnex C, Jani P, Stanley M, Sudhoff H. Recurrent respiratory papillomatosis: an overview of current thinking and treatment. Eur Arch Otorhinolaryngol. 2008;265(2):147-51.
77. Ottinger M, Smith JA, Schweiger MR, Robbins D, Powell ML, You J, et al. Cell-type specific transcriptional activities among different papillomavirus long control regions and their regulation by E2. Virology. 2009;395(2):161-71.
78. zur Hausen H, Meinhof W, Scheiber W, Bornkamm GW. Attempts to detect virus-secific DNA in human tumors. I. Nucleic acid hybridizations with complementary RNA of human wart virus. Int J Cancer. 1974;13(5):650-6.
79. Gissmann L, deVilliers EM, zur Hausen H. Analysis of human genital warts (condylomata acuminata) and other genital tumors for human papillomavirus type 6 DNA. Int J Cancer. 1982;29(2):143-6.
80. Gissmann L, Wolnik L, Ikenberg H, Koldovsky U, Schnurch HG, zur Hausen H. Human papillomavirus types 6 and 11 DNA sequences in genital and laryngeal papillomas and in some cervical cancers. Proc Natl Acad Sci U S A. 1983;80(2):560-3.
81. Zachow KR, Ostrow RS, Bender M, Watts S, Okagaki T, Pass F, et al. Detection of human papillomavirus DNA in anogenital neoplasias. Nature. 1982;300(5894):771-3.
82. Woodman CB, Collins SI, Young LS. The natural history of cervical HPV infection: unresolved issues. Nat Rev Cancer. 2007;7(1):11-22.
83. Stanley M. Immunobiology of HPV and HPV vaccines. Gynecol Oncol. 2008;109(2 Suppl):S15-21.
84. Crosbie EJ, Einstein MH, Franceschi S, Kitchener HC. Human papillomavirus and cervical cancer. Lancet. 2013;382(9895):889-99.
85. Johansson C, Schwartz S. Regulation of human papillomavirus gene expression by splicing and polyadenylation. Nat Rev Microbiol. 2013;11(4):239-51.
86. Stanley MA. Epithelial cell responses to infection with human papillomavirus. Clin Microbiol Rev. 2012;25(2):215-22.
87. Zheng ZM, Baker CC. Papillomavirus genome structure, expression, and post-transcriptional regulation. Front Biosci. 2006;11:2286-302.

88. Doorbar J, Quint W, Banks L, Bravo IG, Stoler M, Broker TR, et al. The biology and life-cycle of human papillomaviruses. Vaccine. 2012;30 Suppl 5:F55-70.
89. D'Abramo CM, Archambault J. Small molecule inhibitors of human papillomavirus protein - protein interactions. Open Virol J. 2011;5:80-95.
90. Pyeon D, Pearce SM, Lank SM, Ahlquist P, Lambert PF. Establishment of human papillomavirus infection requires cell cycle progression. PLoS Pathog. 2009;5(2):e1000318.
91. Horvath CA, Boulet GA, Renoux VM, Delvenne PO, Bogers JP. Mechanisms of cell entry by human papillomaviruses: an overview. Virol J. 2010;7:11.
92. Hindmarsh PL, Laimins LA. Mechanisms regulating expression of the HPV 31 L1 and L2 capsid proteins and pseudovirion entry. Virol J. 2007;4:19.
93. Spoden G, Freitag K, Husmann M, Boller K, Sapp M, Lambert C, et al. Clathrin- and caveolin-independent entry of human papillomavirus type 16--involvement of tetraspanin-enriched microdomains (TEMs). PLoS One. 2008;3(10):e3313.
94. Day PM, Lowy DR, Schiller JT. Papillomaviruses infect cells via a clathrin-dependent pathway. Virology. 2003;307(1):1-11.
95. DiMaio D, Petti LM. The E5 proteins. Virology. 2013;445(1-2):99-114.
96. Doorbar J. Molecular biology of human papillomavirus infection and cervical cancer. Clin Sci (Lond). 2006;110(5):525-41.
97. Moody C. Mechanisms by which HPV Induces a Replication Competent Environment in Differentiating Keratinocytes. Viruses. 2017;9(9).
98. Klingelhutz AJ, Roman A. Cellular transformation by human papillomaviruses: lessons learned by comparing high- and low-risk viruses. Virology. 2012;424(2):77-98.
99. Elfgren K, Kalantari M, Moberger B, Hagmar B, Dillner J. A population-based five-year follow-up study of cervical human papillomavirus infection. Am J Obstet Gynecol. 2000;183(3):561-7.
100. Wentzensen N, Vinokurova S, von Knebel Doeberitz M. Systematic review of genomic integration sites of human papillomavirus genomes in epithelial dysplasia and invasive cancer of the female lower genital tract. Cancer Res. 2004;64(11):3878-84.
101. Jones DL, Alani RM, Münger K. The human papillomavirus E7 oncoprotein can uncouple cellular differentiation and proliferation in human keratinocytes by abrogating p21Cip1-mediated inhibition of cdk2. Genes & development. 1997;11(16):2101-11.
102. Scheffner M, Werness BA, Huibregtse JM, Levine AJ, Howley PM. The E6 oncoprotein encoded by human papillomavirus types 16 and 18 promotes the degradation of p53. Cell. 1990;63(6):1129-36.
103. Veldman T, Horikawa I, Barrett JC, Schlegel R. Transcriptional activation of the telomerase hTERT gene by human papillomavirus type 16 E6 oncoprotein. Journal of virology. 2001;75(9):4467-72.
104. Doorbar J. The E4 protein; structure, function and patterns of expression. Virology. 2013;445(1-2):80-98.
105. Steinbach A, Riemer AB. Immune evasion mechanisms of human papillomavirus: An update. Int J Cancer. 2018;142(2):224-9.
106. Matthews K, Leong CM, Baxter L, Inglis E, Yun K, Backstrom BT, et al. Depletion of Langerhans cells in human papillomavirus type 16-infected skin is associated with E6-mediated down regulation of E-cadherin. J Virol. 2003;77(15):8378-85.
107. Guess JC, McCance DJ. Decreased migration of Langerhans precursor-like cells in response to human keratinocytes expressing human papillomavirus type 16 E6/E7 is related to reduced macrophage inflammatory protein-3alpha production. J Virol. 2005;79(23):14852-62.
108. Hasan UA, Bates E, Takeshita F, Biliato A, Accardi R, Bouvard V, et al. TLR9 expression and function is abolished by the cervical cancer-associated human papillomavirus type 16. J Immunol. 2007;178(5):3186-97.

109. Ronco LV, Karpova AY, Vidal M, Howley PM. Human papillomavirus 16 E6 oncoprotein binds to interferon regulatory factor-3 and inhibits its transcriptional activity. Genes Dev. 1998;12(13):2061-72.
110. Rincon-Orozco B, Halec G, Rosenberger S, Muschik D, Nindl I, Bachmann A, et al. Epigenetic silencing of interferon-kappa in human papillomavirus type 16-positive cells. Cancer Res. 2009;69(22):8718-25.
111. Karim R, Meyers C, Backendorf C, Ludigs K, Offringa R, van Ommen GJ, et al. Human papillomavirus deregulates the response of a cellular network comprising of chemotactic and proinflammatory genes. PLoS One. 2011;6(3):e17848.
112. Niebler M, Qian X, Hofler D, Kogosov V, Kaewprag J, Kaufmann AM, et al. Post-translational control of IL-1beta via the human papillomavirus type 16 E6 oncoprotein: a novel mechanism of innate immune escape mediated by the E3-ubiquitin ligase E6-AP and p53. PLoS Pathog. 2013;9(8):e1003536.
113. Evans M, Borysiewicz LK, Evans AS, Rowe M, Jones M, Gileadi U, et al. Antigen processing defects in cervical carcinomas limit the presentation of a CTL epitope from human papillomavirus 16 E6. J Immunol. 2001;167(9):5420-8.
114. Georgopoulos NT, Proffitt JL, Blair GE. Transcriptional regulation of the major histocompatibility complex (MHC) class I heavy chain, TAP1 and LMP2 genes by the human papillomavirus (HPV) type 6b, 16 and 18 E7 oncoproteins. Oncogene. 2000;19(42):4930-5.
115. Hasim A, Abudula M, Aimiduo R, Ma JQ, Jiao Z, Akula G, et al. Post-transcriptional and epigenetic regulation of antigen processing machinery (APM) components and HLA-I in cervical cancers from Uighur women. PLoS One. 2012;7(9):e44952.
116. Ashrafi GH, Haghshenas MR, Marchetti B, O'Brien PM, Campo MS. E5 protein of human papillomavirus type 16 selectively downregulates surface HLA class I. Int J Cancer. 2005;113(2):276-83.
117. Grabowska AK, Riemer AB. The invisible enemy - how human papillomaviruses avoid recognition and clearance by the host immune system. Open Virol J. 2012;6:249-56.
118. Piersma SJ. Immunosuppressive tumor microenvironment in cervical cancer patients. Cancer Microenviron. 2011;4(3):361-75.
119. Kirnbauer R, Booy F, Cheng N, Lowy DR, Schiller JT. Papillomavirus L1 major capsid protein self-assembles into virus-like particles that are highly immunogenic. Proc Natl Acad Sci U S A. 1992;89(24):12180-4.
120. Harper DM, Franco EL, Wheeler C, Ferris DG, Jenkins D, Schuind A, et al. Efficacy of a bivalent L1 virus-like particle vaccine in prevention of infection with human papillomavirus types 16 and 18 in young women: a randomised controlled trial. Lancet. 2004;364(9447):1757-65.
121. Villa LL, Costa RL, Petta CA, Andrade RP, Ault KA, Giuliano AR, et al. Prophylactic quadrivalent human papillomavirus (types 6, 11, 16, and 18) L1 virus-like particle vaccine in young women: a randomised double-blind placebo-controlled multicentre phase II efficacy trial. Lancet Oncol. 2005;6(5):271-8.
122. Joura EA, Giuliano AR, Iversen OE, Bouchard C, Mao C, Mehlsen J, et al. A 9-valent HPV vaccine against infection and intraepithelial neoplasia in women. N Engl J Med. 2015;372(8):711-23.
123. Bray F, Ferlay J, Soerjomataram I, Siegel RL, Torre LA, Jemal A. Global cancer statistics 2018: GLOBOCAN estimates of incidence and mortality worldwide for 36 cancers in 185 countries. CA Cancer J Clin. 2018;68(6):394-424.
124. Fakhr E, Modic Z, Cid-Arregui A. Recent developments in immunotherapy of cancers caused by human papillomaviruses. Immunology. 2021;163(1):33-45.
125. Santin AD, Deng W, Frumovitz M, Buza N, Bellone S, Huh W, et al. Phase II evaluation of nivolumab in the treatment of persistent or recurrent cervical cancer (NCT02257528/NRG-GY002). Gynecol Oncol. 2020;157(1):161-6.

126. Naumann RW, Hollebecque A, Meyer T, Devlin MJ, Oaknin A, Kerger J, et al. Safety and Efficacy of Nivolumab Monotherapy in Recurrent or Metastatic Cervical, Vaginal, or Vulvar Carcinoma: Results From the Phase I/II CheckMate 358 Trial. J Clin Oncol. 2019;37(31):2825-34.
127. Chung HC, Ros W, Delord JP, Perets R, Italiano A, Shapira-Frommer R, et al. Efficacy and Safety of Pembrolizumab in Previously Treated Advanced Cervical Cancer: Results From the Phase II KEYNOTE-158 Study. J Clin Oncol. 2019;37(17):1470-8.
128. Burtness B, Harrington KJ, Greil R, Soulieres D, Tahara M, de Castro G, Jr., et al. Pembrolizumab alone or with chemotherapy versus cetuximab with chemotherapy for recurrent or metastatic squamous cell carcinoma of the head and neck (KEYNOTE-048): a randomised, open-label, phase 3 study. Lancet. 2019;394(10212):1915-28.
129. Zhao Y, Yang W, Huang Y, Cui R, Li X, Li B. Evolving Roles for Targeting CTLA-4 in Cancer Immunotherapy. Cell Physiol Biochem. 2018;47(2):721-34.
130. Khoja L, Atenafu EG, Ye Q, Gedye C, Chappell M, Hogg D, et al. Real-world efficacy, toxicity and clinical management of ipilimumab treatment in metastatic melanoma. Oncol Lett. 2016;11(2):1581-5.
131. D'Angelo SP, Larkin J, Sosman JA, Lebbe C, Brady B, Neyns B, et al. Efficacy and Safety of Nivolumab Alone or in Combination With Ipilimumab in Patients With Mucosal Melanoma: A Pooled Analysis. J Clin Oncol. 2017;35(2):226-35.
132. Callahan MK, Odunsi K, Sznol M, Nemunaitis JJ, Ott PA, Dillon PM, et al. Phase 1 study to evaluate the safety and tolerability of MEDI4736 (durvalumab, DUR)+ tremelimumab (TRE) in patients with advanced solid tumors. American Society of Clinical Oncology; 2017.
133. Chabeda A, Yanez RJR, Lamprecht R, Meyers AE, Rybicki EP, Hitzeroth, II. Therapeutic vaccines for high-risk HPV-associated diseases. Papillomavirus Res. 2018;5:46-58.
134. Lin K, Doolan K, Hung CF, Wu TC. Perspectives for preventive and therapeutic HPV vaccines. J Formos Med Assoc. 2010;109(1):4-24.
135. Huh WK, Dizon DS, Powell MA, Leath CA, Landrum LM, Tanner E, et al. ADXS11-001 immunotherapy in squamous or non-squamous persistent/recurrent metastatic cervical cancer: Results from stage I of the phase II GOG/NRG0265 study. American Society of Clinical Oncology; 2016.
136. Basu P, Mehta A, Jain M, Gupta S, Nagarkar RV, John S, et al. A Randomized Phase 2 Study of ADXS11-001 Listeria monocytogenes-Listeriolysin O Immunotherapy With or Without Cisplatin in Treatment of Advanced Cervical Cancer. Int J Gynecol Cancer. 2018;28(4):764-72.
137. Safran H, Leonard KL, DiPetrillo TA, Klipfel A, Schechter S, Oldenburg N, et al. ADXS11-001 Lm-LLO Immunotherapy, Mitomycin, 5-fluorouracil (5-FU) and Intensity-modulated radiation therapy (IMRT) for Anal Cancer. American Society of Clinical Oncology; 2017.
138. Ghamande SA, Platt D, Wheatley D, Rungruang BJ, Janik JE, Khleif S. Phase I study evaluating high-dose treatment with ADXS11-001, a Listeria monocytogenes-listeriolysin O (Lm-LLO) immunotherapy, in women with cervical cancer. American Society of Clinical Oncology; 2016.
139. Cohen EE, Moore KN, Slomovitz BM, Chung CH, Anderson ML, Morris SR, et al. Phase I/II study of ADXS11-001 or MEDI4736 immunotherapies alone and in combination, in patients with recurrent/metastatic cervical or human papillomavirus (HPV)-positive head and neck cancer. Journal for ImmunoTherapy of Cancer. 2015;3(Suppl 2).
140. Le Tourneau C, Delord J-P, Cassier P, Loirat D, Tavernaro A, Bastien B, et al. Phase Ib/II trial of TG4001 (Tipapkinogene sovacivec), a therapeutic HPV-vaccine, and Avelumab in patients with recurrent/metastatic (R/M) HPV-16+ cancers. Annals of Oncology. 2019;30:v494-v5.
141. Trimble CL, Peng S, Kos F, Gravitt P, Viscidi R, Sugar E, et al. A phase I trial of a human papillomavirus DNA vaccine for HPV16+ cervical intraepithelial neoplasia 2/3. Clin Cancer Res. 2009;15(1):361-7.

142. Maldonado L, Teague JE, Morrow MP, Jotova I, Wu TC, Wang C, et al. Intramuscular therapeutic vaccination targeting HPV16 induces T cell responses that localize in mucosal lesions. Sci Transl Med. 2014;6(221):221ra13.
143. Kumar S, Biswas M, Jose T. HPV vaccine: Current status and future directions. Med J Armed Forces India. 2015;71(2):171-7.
144. Massarelli E, William W, Johnson F, Kies M, Ferrarotto R, Guo M, et al. Combining Immune Checkpoint Blockade and Tumor-Specific Vaccine for Patients With Incurable Human Papillomavirus 16-Related Cancer: A Phase 2 Clinical Trial. JAMA Oncol. 2019;5(1):67-73.
145. Gerritsen AE, Witter DJ, Creugers NHJ. Long-term follow-up indicates unimpaired oral health-related quality of life for people having shortened dental arches. J Dent. 2017;65:41-4.
146. Greenfield WW, Stratton SL, Myrick RS, Vaughn R, Donnalley LM, Coleman HN, et al. A phase I dose-escalation clinical trial of a peptide-based human papillomavirus therapeutic vaccine with Candida skin test reagent as a novel vaccine adjuvant for treating women with biopsy-proven cervical intraepithelial neoplasia 2/3. Oncoimmunology. 2015;4(10):e1031439.
147. Su JH, Wu A, Scotney E, Ma B, Monie A, Hung CF, et al. Immunotherapy for cervical cancer: Research status and clinical potential. BioDrugs. 2010;24(2):109-29.
148. Vici P, Pizzuti L, Mariani L, Zampa G, Santini D, Di Lauro L, et al. Targeting immune response with therapeutic vaccines in premalignant lesions and cervical cancer: hope or reality from clinical studies. Expert Rev Vaccines. 2016;15(10):1327-36.
149. Yang A, Farmer E, Wu TC, Hung CF. Perspectives for therapeutic HPV vaccine development. J Biomed Sci. 2016;23(1):75.
150. Choi YJ, Hur SY, Kim T-J, Hong SR, Lee JK, Cho C-H, et al. A phase II, prospective, randomized, multicenter, open-label study of GX-188E, an HPV DNA vaccine, in patients with cervical intraepithelial neoplasia 3. Clinical Cancer Research. 2020;26(7):1616-23.
151. Hillemanns P, Petry KU, Woelber L, Böhmer G, Stubsrud E, Skjørestad I, et al. Abstract CT209: Safety, efficacy and immunogenicity of VB10. 16, a therapeutic DNA vaccine targeting human papillomavirus (HPV) 16 E6 and E7 proteins for high grade cervical intraepithelial neoplasia (CIN 2/3): 6-month data from an exploratory open-label phase I/2a trial. AACR; 2019.
152. Yu L, Hu Z, Gao C, Feng B, Wang L, Tian X, et al. deletion of HPV18 E6 and E7 genes using dual sgRNA-directed CRISPR/Cas9 inhibits growth of cervical cancer cells. Int J Clin Exp Med. 2017;10(6):9206-13.
153. Hu Z, Ding W, Zhu D, Yu L, Jiang X, Wang X, et al. TALEN-mediated targeting of HPV oncogenes ameliorates HPV-related cervical malignancy. J Clin Invest. 2015;125(1):425-36.
154. Ding W, Hu Z, Zhu D, Jiang X, Yu L, Wang X, et al. Zinc finger nucleases targeting the human papillomavirus E7 oncogene induce E7 disruption and a transformed phenotype in HPV16/18-positive cervical cancer cells. Clin Cancer Res. 2014;20(24):6495-503.
155. Stevanovic S, Draper LM, Langhan MM, Campbell TE, Kwong ML, Wunderlich JR, et al. Complete regression of metastatic cervical cancer after treatment with human papillomavirus-targeted tumor-infiltrating T cells. J Clin Oncol. 2015;33(14):1543-50.
156. Ramos CA, Narala N, Vyas GM, Leen AM, Gerdemann U, Sturgis EM, et al. Human papillomavirus type 16 E6/E7-specific cytotoxic T lymphocytes for adoptive immunotherapy of HPV-associated malignancies. J Immunother. 2013;36(1):66-76.
157. Stevanovic S, Helman SR, Wunderlich JR, Langhan MM, Doran SL, Kwong MLM, et al. A Phase II Study of Tumor-infiltrating Lymphocyte Therapy for Human Papillomavirus-associated Epithelial Cancers. Clin Cancer Res. 2019;25(5):1486-93.
158. Baruch EN, Berg AL, Besser MJ, Schachter J, Markel G. Adoptive T cell therapy: An overview of obstacles and opportunities. Cancer. 2017;123(S11):2154-62.

159. Draper LM, Kwong ML, Gros A, Stevanovic S, Tran E, Kerkar S, et al. Targeting of HPV-16+ Epithelial Cancer Cells by TCR Gene Engineered T Cells Directed against E6. Clin Cancer Res. 2015;21(19):4431-9.
160. Doran SL, Stevanovic S, Adhikary S, Gartner JJ, Jia L, Kwong MLM, et al. T-Cell Receptor Gene Therapy for Human Papillomavirus-Associated Epithelial Cancers: A First-in-Human, Phase I/II Study. J Clin Oncol. 2019;37(30):2759-68.
161. Jin BY, Campbell TE, Draper LM, Stevanovic S, Weissbrich B, Yu Z, et al. Engineered T cells targeting E7 mediate regression of human papillomavirus cancers in a murine model. JCI Insight. 2018;3(8).
162. Nagarsheth NB, Norberg SM, Sinkoe AL, Adhikary S, Meyer TJ, Lack JB, et al. TCR-engineered T cells targeting E7 for patients with metastatic HPV-associated epithelial cancers. Nat Med. 2021;27(3):419-25.
163. Quiros-Fernandez I, Poorebrahim M, Fakhr E, Cid-Arregui A. Immunogenic T cell epitopes of SARS-CoV-2 are recognized by circulating memory and naive CD8 T cells of unexposed individuals. EBioMedicine. 2021;72:103610.
164. Scholten KB, Turksma AW, Ruizendaal JJ, van den Hende M, van der Burg SH, Heemskerk MH, et al. Generating HPV specific T helper cells for the treatment of HPV induced malignancies using TCR gene transfer. J Transl Med. 2011;9:147.
165. Schreurs MW, Scholten KB, Kueter EW, Ruizendaal JJ, Meijer CJ, Hooijberg E. In vitro generation and life span extension of human papillomavirus type 16-specific, healthy donor-derived CTL clones. J Immunol. 2003;171(6):2912-21.
166. Hoffmann TK, Arsov C, Schirlau K, Bas M, Friebe-Hoffmann U, Klussmann JP, et al. T cells specific for HPV16 E7 epitopes in patients with squamous cell carcinoma of the oropharynx. Int J Cancer. 2006;118(8):1984-91.
167. Riemer AB, Keskin DB, Zhang G, Handley M, Anderson KS, Brusic V, et al. A conserved E7-derived cytotoxic T lymphocyte epitope expressed on human papillomavirus 16-transformed HLA-A2+ epithelial cancers. J Biol Chem. 2010;285(38):29608-22.
168. Chen G, Yang X, Ko A, Sun X, Gao M, Zhang Y, et al. Sequence and Structural Analyses Reveal Distinct and Highly Diverse Human CD8(+) TCR Repertoires to Immunodominant Viral Antigens. Cell Rep. 2017;19(3):569-83.
169. Nilges K, Hohn H, Pilch H, Neukirch C, Freitag K, Talbot PJ, et al. Human papillomavirus type 16 E7 peptide-directed CD8+ T cells from patients with cervical cancer are cross-reactive with the coronavirus NS2 protein. J Virol. 2003;77(9):5464-74.
170. Garcia-Bates TM, Kim E, Concha-Benavente F, Trivedi S, Mailliard RB, Gambotto A, et al. Enhanced Cytotoxic CD8 T Cell Priming Using Dendritic Cell-Expressing Human Papillomavirus-16 E6/E7-p16INK4 Fusion Protein with Sequenced Anti-Programmed Death-1. J Immunol. 2016;196(6):2870-8.
171. Sallusto F, Lanzavecchia A. Efficient presentation of soluble antigen by cultured human dendritic cells is maintained by granulocyte/macrophage colony-stimulating factor plus interleukin 4 and downregulated by tumor necrosis factor alpha. J Exp Med. 1994;179(4):1109-18.
172. Wilkins MR, Gasteiger E, Bairoch A, Sanchez JC, Williams KL, Appel RD, et al. Protein identification and analysis tools in the ExPASy server. Methods Mol Biol. 1999;112:531-52.
173. Ko J, Park H, Seok C. GalaxyTBM: template-based modeling by building a reliable core and refining unreliable local regions. BMC Bioinformatics. 2012;13:198.
174. Heo L, Park H, Seok C. GalaxyRefine: Protein structure refinement driven by side-chain repacking. Nucleic Acids Res. 2013;41(Web Server issue):W384-8.
175. Torchala M, Moal IH, Chaleil RA, Fernandez-Recio J, Bates PA. SwarmDock: a server for flexible protein-protein docking. Bioinformatics. 2013;29(6):807-9.

176. Xue LC, Rodrigues JP, Kastritis PL, Bonvin AM, Vangone A. PRODIGY: a web server for predicting the binding affinity of protein-protein complexes. Bioinformatics. 2016;32(23):3676-8.
177. Lang Kuhs KA, Lin SW, Hua X, Schiffman M, Burk RD, Rodriguez AC, et al. T cell receptor repertoire among women who cleared and failed to clear cervical human papillomavirus infection: An exploratory proof-of-principle study. PLoS One. 2018;13(1):e0178167.
178. Verstraete K, Vandriessche G, Januar M, Elegheert J, Shkumatov AV, Desfosses A, et al. Structural insights into the extracellular assembly of the hematopoietic Flt3 signaling complex. Blood. 2011;118(1):60-8.
179. Kyte J, Doolittle RF. A simple method for displaying the hydropathic character of a protein. J Mol Biol. 1982;157(1):105-32.
180. Gasteiger E, Hoogland C, Gattiker A, Wilkins MR, Appel RD, Bairoch A. Protein identification and analysis tools on the ExPASy server. The proteomics protocols handbook. 2005:571-607.
181. Zhang SQ, Ma KY, Schonnesen AA, Zhang M, He C, Sun E, et al. High-throughput determination of the antigen specificities of T cell receptors in single cells. Nat Biotechnol. 2018.
182. Lee JU, Kim LK, Choi JM. Revisiting the Concept of Targeting NFAT to Control T Cell Immunity and Autoimmune Diseases. Front Immunol. 2018;9:2747.
183. Lang Kuhs-TCR cervical HPV 2018 [Available from: https://doi.org/10.21417/B7X067.
184. Guruprasad K, Reddy BV, Pandit MW. Correlation between stability of a protein and its dipeptide composition: a novel approach for predicting in vivo stability of a protein from its primary sequence. Protein Eng. 1990;4(2):155-61.
185. Hung CF, Hsu KF, Cheng WF, Chai CY, He L, Ling M, et al. Enhancement of DNA vaccine potency by linkage of antigen gene to a gene encoding the extracellular domain of Fms-like tyrosine kinase 3-ligand. Cancer Res. 2001;61(3):1080-8.
186. Cueto FJ, Sancho D. The Flt3L/Flt3 Axis in Dendritic Cell Biology and Cancer Immunotherapy. Cancers (Basel). 2021;13(7).
187. Zhang S, Broxmeyer HE. Flt3 ligand induces tyrosine phosphorylation of gab1 and gab2 and their association with shp-2, grb2, and PI3 kinase. Biochem Biophys Res Commun. 2000;277(1):195-9.
188. Li J, Chen S, Ge J, Lu F, Ren S, Zhao Z, et al. A novel therapeutic vaccine composed of a rearranged human papillomavirus type 16 E6/E7 fusion protein and Fms-like tyrosine kinase-3 ligand induces CD8(+) T cell responses and antitumor effect. Vaccine. 2017;35(47):6459-67.
189. Kim SW, Choi SM, Choo YS, Kim IK, Song BW, Kim HS. Flt3 ligand induces monocyte proliferation and enhances the function of monocyte-derived dendritic cells in vitro. J Cell Physiol. 2015;230(8):1740-9.
190. Silveira GF, Wowk PF, Machado AM, Duarte dos Santos CN, Bordignon J. Immature dendritic cells generated from cryopreserved human monocytes show impaired ability to respond to LPS and to induce allogeneic lymphocyte proliferation. PLoS One. 2013;8(7):e71291.
191. Drake DR, 3rd, Ream RM, Lawrence CW, Braciale TJ. Transient loss of MHC class I tetramer binding after CD8+ T cell activation reflects altered T cell effector function. J Immunol. 2005;175(3):1507-15.
192. Liu H, Rhodes M, Wiest DL, Vignali DA. On the dynamics of TCR:CD3 complex cell surface expression and downmodulation. Immunity. 2000;13(5):665-75.
193. Wolfl M, Kuball J, Ho WY, Nguyen H, Manley TJ, Bleakley M, et al. Activation-induced expression of CD137 permits detection, isolation, and expansion of the full repertoire of CD8+ T cells responding to antigen without requiring knowledge of epitope specificities. Blood. 2007;110(1):201-10.
194. Spindler MJ, Nelson AL, Wagner EK, Oppermans N, Bridgeman JS, Heather JM, et al. Massively parallel interrogation and mining of natively paired human TCRalphabeta repertoires. Nat Biotechnol. 2020;38(5):609-19.

195. Kaech SM, Ahmed R. Memory CD8+ T cell differentiation: initial antigen encounter triggers a developmental program in naive cells. Nat Immunol. 2001;2(5):415-22.
196. van Stipdonk MJ, Lemmens EE, Schoenberger SP. Naive CTLs require a single brief period of antigenic stimulation for clonal expansion and differentiation. Nat Immunol. 2001;2(5):423-9.
197. Mercado R, Vijh S, Allen SE, Kerksiek K, Pilip IM, Pamer EG. Early programming of T cell populations responding to bacterial infection. J Immunol. 2000;165(12):6833-9.
198. Dash P, Fiore-Gartland AJ, Hertz T, Wang GC, Sharma S, Souquette A, et al. Quantifiable predictive features define epitope-specific T cell receptor repertoires. Nature. 2017;547(7661):89-93.
199. Glanville J, Huang H, Nau A, Hatton O, Wagar LE, Rubelt F, et al. Identifying specificity groups in the T cell receptor repertoire. Nature. 2017;547(7661):94-8.
200. Greenshields-Watson A, Attaf M, MacLachlan BJ, Whalley T, Rius C, Wall A, et al. CD4(+) T Cells Recognize Conserved Influenza A Epitopes through Shared Patterns of V-Gene Usage and Complementary Biochemical Features. Cell Rep. 2020;32(2):107885.
201. Kumar M, Keller B, Makalou N, Sutton RE. Systematic determination of the packaging limit of lentiviral vectors. Hum Gene Ther. 2001;12(15):1893-905.
202. Amirache F, Levy C, Costa C, Mangeot PE, Torbett BE, Wang CX, et al. Mystery solved: VSV-G-LVs do not allow efficient gene transfer into unstimulated T cells, B cells, and HSCs because they lack the LDL receptor. Blood. 2014;123(9):1422-4.
203. Hemmi H, Takeuchi O, Sato S, Yamamoto M, Kaisho T, Sanjo H, et al. The roles of two IkappaB kinase-related kinases in lipopolysaccharide and double stranded RNA signaling and viral infection. J Exp Med. 2004;199(12):1641-50.
204. Perry AK, Chow EK, Goodnough JB, Yeh WC, Cheng G. Differential requirement for TANK-binding kinase-1 in type I interferon responses to toll-like receptor activation and viral infection. J Exp Med. 2004;199(12):1651-8.
205. Li L, Gao Y, Srivastava R, Wang W, Xiong Q, Fang Z, et al. Lentiviral delivery of combinatorial CAR/CRISPRi circuit into human primary T cells is enhanced by TBK1/IKKvarepsilon complex inhibitor BX795. J Transl Med. 2020;18(1):363.
206. Castellanos Mdel C, Lopez-Giral S, Lopez-Cabrera M, de Landazuri MO. Multiple cis-acting elements regulate the expression of the early T cell activation antigen CD69. Eur J Immunol. 2002;32(11):3108-17.
207. Stefanova I, Hemmer B, Vergelli M, Martin R, Biddison WE, Germain RN. TCR ligand discrimination is enforced by competing ERK positive and SHP-1 negative feedback pathways. Nat Immunol. 2003;4(3):248-54.
208. Plas DR, Johnson R, Pingel JT, Matthews RJ, Dalton M, Roy G, et al. Direct regulation of ZAP-70 by SHP-1 in T cell antigen receptor signaling. Science. 1996;272(5265):1173-6.
209. Bhattacharyya ND, Feng CG. Regulation of T Helper Cell Fate by TCR Signal Strength. Front Immunol. 2020;11:624.
210. Kiani A, Garcia-Cozar FJ, Habermann I, Laforsch S, Aebischer T, Ehninger G, et al. Regulation of interferon-gamma gene expression by nuclear factor of activated T cells. Blood. 2001;98(5):1480-8.
211. Teixeira LK, Fonseca BP, Vieira-de-Abreu A, Barboza BA, Robbs BK, Bozza PT, et al. IFN-gamma production by CD8+ T cells depends on NFAT1 transcription factor and regulates Th differentiation. J Immunol. 2005;175(9):5931-9.
212. Pachulec E, Neitzke-Montinelli V, Viola JP. NFAT2 Regulates Generation of Innate-Like CD8(+) T Lymphocytes and CD8(+) T Lymphocytes Responses. Front Immunol. 2016;7:411.
213. Macian F, Lopez-Rodriguez C, Rao A. Partners in transcription: NFAT and AP-1. Oncogene. 2001;20(19):2476-89.
214. Sun XN, Li C, Liu Y, Du LJ, Zeng MR, Zheng XJ, et al. T-Cell Mineralocorticoid Receptor Controls Blood Pressure by Regulating Interferon-Gamma. Circ Res. 2017;120(10):1584-97.

215. Zhong S, Malecek K, Johnson LA, Yu Z, Vega-Saenz de Miera E, Darvishian F, et al. T-cell receptor affinity and avidity defines antitumor response and autoimmunity in T-cell immunotherapy. Proc Natl Acad Sci U S A. 2013;110(17):6973-8.
216. Valitutti S, Lanzavecchia A. Serial triggering of TCRs: a basis for the sensitivity and specificity of antigen recognition. Immunol Today. 1997;18(6):299-304.
217. Rachmilewitz J, Lanzavecchia A. A temporal and spatial summation model for T-cell activation: signal integration and antigen decoding. Trends Immunol. 2002;23(12):592-5.
218. Gonzalez PA, Carreno LJ, Cespedes PF, Bueno SM, Riedel CA, Kalergis AM. Modulation of tumor immunity by soluble and membrane-bound molecules at the immunological synapse. Clin Dev Immunol. 2013;2013:450291.
219. Yu K, Shi J, Lu D, Yang Q. Comparative analysis of CDR3 regions in paired human alphabeta CD8 T cells. FEBS Open Bio. 2019;9(8):1450-9.
220. Nguyen P, Liu W, Ma J, Manirarora JN, Liu X, Cheng C, et al. Discrete TCR repertoires and CDR3 features distinguish effector and Foxp3+ regulatory T lymphocytes in myelin oligodendrocyte glycoprotein-induced experimental allergic encephalomyelitis. J Immunol. 2010;185(7):3895-904.
221. Mason D. A very high level of crossreactivity is an essential feature of the T-cell receptor. Immunol Today. 1998;19(9):395-404.
222. Frank SA. Immunology and Evolution of Infectious Disease. Princeton (NJ)2002.
223. Lee CH, Salio M, Napolitani G, Ogg G, Simmons A, Koohy H. Predicting Cross-Reactivity and Antigen Specificity of T Cell Receptors. Front Immunol. 2020;11:565096.